PALEOSEISMOLOGY OF UTAH, VOLUME 25

HISTORY OF LATE HOLOCENE EARTHQUAKES AT THE WILLOW CREEK SITE AND ON THE NEPHI SEGMENT, WASATCH FAULT ZONE, UTAH

by Anthony J. Crone, Stephen F. Personius, Christopher B. DuRoss, Michael N. Machette, and Shannon A. Mahan

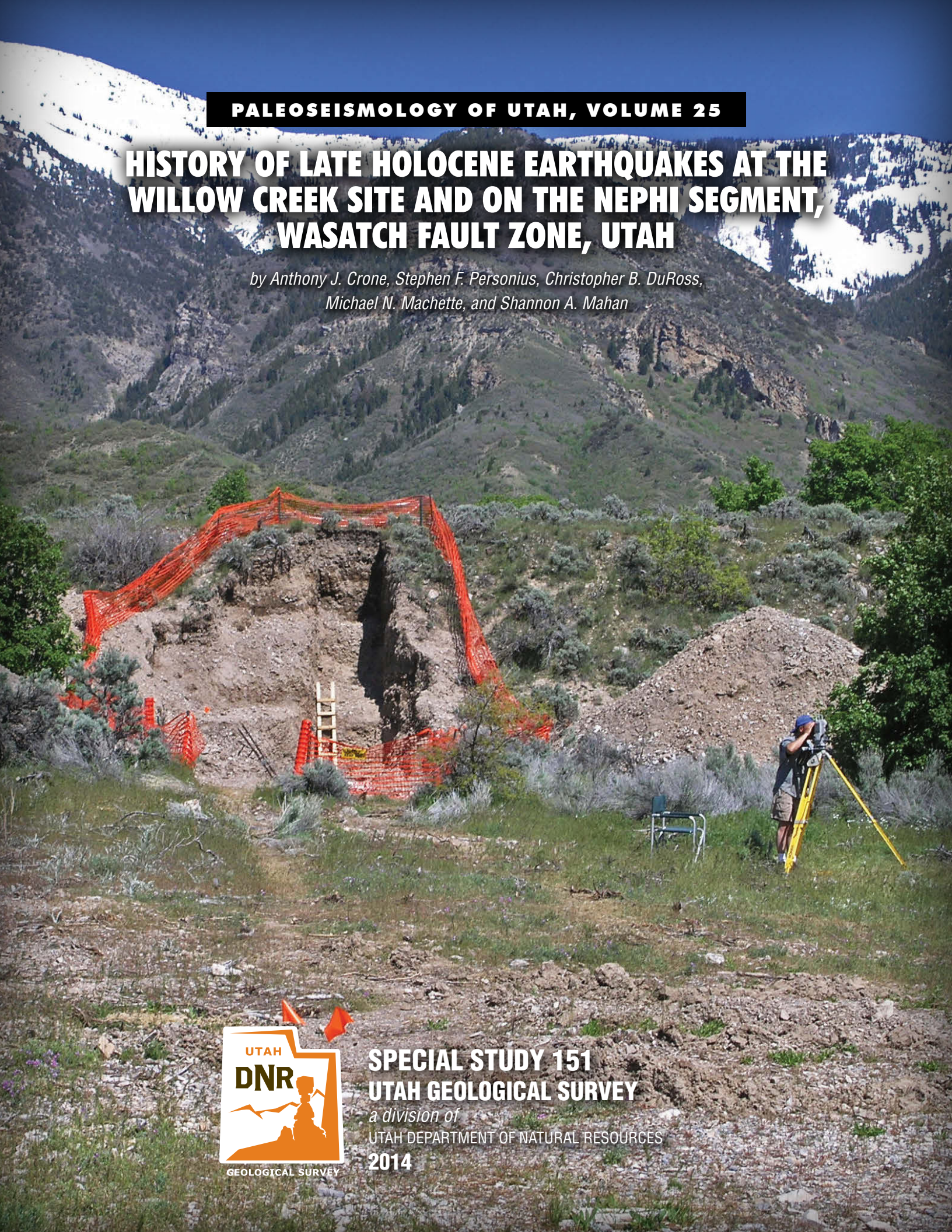

UTAH DNR GEOLOGICAL SURVEY

SPECIAL STUDY 151
UTAH GEOLOGICAL SURVEY
a division of
UTAH DEPARTMENT OF NATURAL RESOURCES
2014

PALEOSEISMOLOGY OF UTAH, VOLUME 25

HISTORY OF LATE HOLOCENE EARTHQUAKES AT THE WILLOW CREEK SITE AND ON THE NEPHI SEGMENT, WASATCH FAULT ZONE, UTAH

by Anthony J. Crone[1], Stephen F. Personius[2], Christopher B. DuRoss[3], Michael N. Machette[4], and Shannon A. Mahan[5]

[1] *U.S. Geological Survey retired, Boulder, Colorado, 80304*

[2] *Geologic Hazards Science Center, U.S. Geological Survey, Denver, Colorado, 80225-0046*

[3] *Utah Geological Survey, P.O. Box 146100, Salt Lake City, Utah, 84114-6100*

[4] *U.S. Geological Survey retired, Port Townsend, Washington, 98368*

[5] *Crustal Imaging and Characterization Science Center, U.S. Geological Survey, Denver, Colorado, 80225-0046*

Cover photo: *View looking east toward the Willow Creek South Trench. Photo by Stephen F. Personius.*

ISBN: 978-1-55791-894-9

SPECIAL STUDY 151
UTAH GEOLOGICAL SURVEY
a division of
UTAH DEPARTMENT OF NATURAL RESOURCES
2014

STATE OF UTAH
Gary R. Herbert, Governor

DEPARTMENT OF NATURAL RESOURCES
Michael Styler, Executive Director

UTAH GEOLOGICAL SURVEY
Richard G. Allis, Director

PUBLICATIONS
contact
Natural Resources Map & Bookstore
1594 W. North Temple
Salt Lake City, UT 84114
telephone: 801-537-3320
toll-free: 1-888-UTAH MAP
website: mapstore.utah.gov
email: geostore@utah.gov

UTAH GEOLOGICAL SURVEY
contact
1594 W. North Temple, Suite 3110
Salt Lake City, UT 84114
telephone: 801-537-3300
website: geology.utah.gov

FOREWORD

This Utah Geological Survey Special Study, *History of Late Holocene Earthquakes at the Willow Creek Site and on the Nephi Segment, Wasatch Fault Zone, Utah*, is the twenty-fifth report in the Paleoseismology of Utah series. This series makes the results of paleoseismic investigations in Utah available to geoscientists, engineers, planners, public officials, and the general public. These studies provide critical paleoseismic information such as earthquake timing, recurrence, displacement, slip rate, fault geometry, and segmentation, which can be used to characterize potential seismic sources and evaluate the long-term seismic hazard of Utah's Quaternary faults.

This report presents new data from the Willow Creek site that provides well-defined and narrow bounds on the times of the three youngest earthquakes on the southern strand of the Nephi segment, Wasatch fault zone, and refines the time of the youngest earthquake to about 200 years ago. This is the youngest surface rupture on the entire Wasatch fault zone, which occurred about a century or less before European settlers arrived in Utah. Two trenches at the Willow Creek site (WCN and WCS) exposed three scarp-derived colluvial wedges that are evidence of three paleoearthquakes (WC1, WC2, and WC3). The three wedges are younger than the 2.4 ± 0.2 ka Willow Creek alluvial fan at the WCS trench site. Stratigraphic relations in the WCN trench indicate that a fourth earthquake (WC4) (and possibly others) occurred prior to 2.4 ka and is younger than the 6.2-ka faulted alluvial fan at the WCN site. OxCal modeling of ages from Willow Creek indicate that paleoearthquake WC1 occurred at 0.2 ± 0.1 ka, WC2 occurred at 1.2 ± 0.1 ka, and WC3 occurred at 1.9 ± 0.6 ka (all 2σ uncertainty). Stratigraphic constraints on the time of paleoearthquake WC4 are extremely poor, so OxCal modeling only yields a broadly constrained age of 4.7 ± 1.8 ka.

Results from the Willow Creek site significantly refine the times of late Holocene earthquakes on the southern strand of the Nephi segment, and this result, when combined with a reanalysis of the stratigraphic and chronologic information from previous investigations at North Creek and Red Canyon, yield a stronger basis for correlating individual earthquakes between all three sites. An OxCal model used to develop a segment-wide chronology for the last three surface-rupturing earthquakes on the southern strand showed the time of earthquake N1 (N denotes an earthquake recognized at all three trench sites) is 0.2 ± 0.1 ka (210 ± 90 yr B.P.), the time of N2 is 1.2 ± 0.1 ka (1230 ± 100 yr B.P.), and the time of N3 is 2.0 ± 0.4 ka (2000 ± 390 yr B.P.) (all 2σ uncertainty). Using the two intervals between the best-constrained earthquakes (N3–N1), the mean late Holocene recurrence for the southern strand is 0.9 ± 0.2 kyr.

The frequency of earthquakes combined with the amount of associated vertical displacement indicates an anomalously high, post-middle Holocene slip rate for the southern strand of the Nephi segment. The high rate is attributed to a cluster of late Holocene earthquakes because the high short-term rate is at least a factor of 10 greater than the rates for mid-Pleistocene and longer periods of time. The cumulative paleoseismic data from all sites on the Nephi segment and from the southern part of the adjacent Provo segment suggest a complex pattern of Holocene surface ruptures. However, details of the interaction between the two segments remain unclear and require a longer and more complete paleoseismic record for both the northern and southern strands of the Nephi segment in order to make a more rigorous comparison with the history of earthquakes on the Provo segment.

The new data from the Willow Creek site and the resulting segment-wide history of earthquake ruptures provide insight into the interaction of the two Nephi-segment fault strands and between the Nephi and adjacent Provo segment to the north. Developing a greater understanding of the paleoseismic parameters of the Holocene-active Nephi segment is critical for developing better models of probabilistic ground shaking; refining probabilistic earthquake-hazard assessments; and improving earthquake-hazard evaluations for the Wasatch Front, all of which help reduce earthquake risks to the region's residents.

William Lund, Editor
Paleoseismology of Utah Series

PALEOSEISMOLOGY OF UTAH SERIES PUBLICATIONS

UGS publications produced as part of the Paleoseismology of Utah series may be found online at http://geology.utah.gov/ghp/consultants/paleoseismic_series.htm and with the links given for each publication below.

1. Fault behavior and earthquake recurrence on the Provo segment of the Wasatch fault zone at Mapleton, Utah County, Utah—Paleoseismology of Utah, Volume 1, 1991, by Lund, W.R., Schwartz, D.P., Mulvey, W.E., Budding, K.E., and Black, B.D.: Utah Geological Survey Special Study 75, 41 p., available online at http://ugspub.nr.utah.gov/publications/special_studies/SS-75.pdf.

2. Paleoseismic analysis of the Wasatch fault zone at the Brigham City trench site, Brigham City, Utah and the Pole Patch trench site, Pleasant View, Utah—Paleoseismology of Utah, Volume 2, 1991, by Personius, S.F.: Utah Geological Survey Special Study 76, 39 p., available online at http://ugspub.nr.utah.gov/publications/special_studies/SS-76.pdf.

3. The number and timing of paleoseismic events on the Nephi and Levan segments, Wasatch fault zone, Utah—Paleoseismology of Utah, Volume 3, 1991, by Jackson, M.: Utah Geological Survey Special Study 78, 23 p., 3 plates, available online at http://ugspub.nr.utah.gov/publications/special_studies/SS-78.pdf.

4. Seismotectonics of north-central Utah and southwestern Wyoming—Paleoseismology of Utah, Volume 4, 1994, by West, M.W.: Utah Geological Survey Special Study 82, 93 p., 5 plates, scale 1:100,000, available online at http://ugspub.nr.utah.gov/publications/special_studies/SS-82.pdf.

5. Neotectonic deformation along the East Cache fault zone, Cache County, Utah—Paleoseismology of Utah, Volume 5, 1994, by McCalpin, J.P.: Utah Geological Survey Special Study 83, 37 p., available online at http://ugspub.nr.utah.gov/publications/special_studies/ss-83.pdf.

6. The Oquirrh fault zone, Tooele County, Utah—surficial geology and paleoseismicity—Paleoseismology of Utah, Volume 6, 1996, by Lund, W.R., editor: Utah Geological Survey Special Study 88, 64 p., 2 plates, scale 1:24,000, available online at http://ugspub.nr.utah.gov/publications/special_studies/SS-88.pdf.

7. Paleoseismic investigation on the Salt Lake City segment of the Wasatch fault zone at the South Fork Dry Creek and Dry Gulch sites, Salt Lake County, Utah—Paleoseismology of Utah, Volume 7, 1996, by Black, B.D., Lund, W.R., Schwartz, D.P., Gill, H.E., and Mayes, B.H.: Utah Geological Survey Special Study 92, 22 p., 1 plate, available online at http://ugspub.nr.utah.gov/publications/special_studies/SS-92.pdf.

8. Paleoseismic investigation at Rock Canyon, Provo segment, Wasatch fault zone, Utah County, Utah—Paleoseismology of Utah, Volume 8, 1998, by Lund, W.R., and Black, B.D.: Utah Geological Survey Special Study 93, 21 p., 2 plates, available online at http://ugspub.nr.utah.gov/publications/special_studies/SS-93.pdf.

9. Paleoseismic investigation of the Clarkston, Junction Hills, and Wellsville faults, West Cache fault zone, Cache County, Utah—Paleoseismology of Utah, Volume 9, 2000, by Black, B.D., Giraud, R.E., and Mayes, B.H.: Utah Geological Survey Special Study 98, 23 p., 1 plate, available online at http://ugspub.nr.utah.gov/publications/special_studies/SS-98.pdf.

10. Post-Bonneville paleoearthquake chronology of the Salt Lake City segment, Wasatch fault zone, from the 1999 “mega-trench” site—Paleoseismology of Utah, Volume 10, 2002, by McCalpin, J.P.: Utah Geological Survey Miscellaneous Publication 02-7, 38 p., available online at http://ugspub.nr.utah.gov/publications/misc_pubs/MP-02-7WFZ-SLC.pdf.

11. Post-Provo paleoearthquake chronology of the Brigham City segment, Wasatch fault zone, Utah—Paleoseismology of Utah, Volume 11, 2002, by McCalpin, J.P., and Forman, S.L.: Utah Geological Survey Miscellaneous Publication 02-9, 46 p., available online at http://ugspub.nr.utah.gov/publications/misc_pubs/MP-02-9WFZ-BrigCity.pdf.

12. Neotectonics of Bear Lake Valley, Utah and Idaho; a preliminary assessment—Paleoseismology of Utah, Volume 12, 2003, by McCalpin, J.P.: Utah Geological Survey Miscellaneous Publication 03-4, 43 p., available online at http://ugspub.nr.utah.gov/publications/misc_pubs/MP-03-4.pdf.

13. Holocene earthquake history of the northern Weber segment of the Wasatch fault zone, Utah—Paleoseismology of Utah, Volume 13, 2006, by Nelson, A.R., Lowe, M., Personius, S., Bradley, L., Forman, S.L., Klauk, R., and Garr, J.: Utah Geological Survey Miscellaneous Publication 05-8, 39 p., 2 plates, available online at http://ugspub.nr.utah.gov/publications/misc_pubs/MP-05-8.pdf.

14. Paleoseismic investigation and long-term slip history of the Hurricane fault in southwestern Utah—Paleoseismology of Utah, Volume 14, 2007, by Lund, W.R., Hozik, M.J., and Hatfield, S.C.: Utah Geological Survey Special Study 119, 81 p., CD, available online at http://ugspub.nr.utah.gov/publications/special_studies/SS-119.pdf.

15. Surficial-geologic reconnaissance and scarp profiling on the Collinston and Clarkston Mountain segments of the Wasatch fault zone, Box Elder County, Utah—paleoseismic inferences, implications for adjacent segments and issues for diffusion-equation scarp-age modeling—Paleoseismology of Utah, Volume 15, 2007, by Hylland, M.D.: Utah Geological Survey Special Study 121, 18 p., CD, available online at http://ugspub.nr.utah.gov/publications/special_studies/SS-121.pdf.

16. Paleoseismic reconnaissance of the Sevier fault, Kane and Garfield Counties, Utah—Paleoseismology of Utah, Volume 16, 2008, by Lund, W.R, Knudsen, T.R., and Vice, G.S.: Utah Geological Survey Special Study 122, 31 p., CD, available online at http://ugspub.nr.utah.gov/publications/special_studies/SS-122.pdf.

17. Paleoseismic investigation of the northern strand of the Nephi segment of the Wasatch fault zone at Santaquin, Utah—Paleoseismology of Utah, Volume 17, 2008, by DuRoss, C.B., McDonald, G.N., and Lund, W.R.: Utah Geological Survey Special Study 124, 33 p., 1 plate, available online at http://geology.utah.gov/online/ss/ss-124.pdf.

18. Paleoseismic investigation of the northern Weber segment of the Wasatch fault zone at Rice Creek trench site, North Ogden, Utah—Paleoseismology of Utah, Volume 18, 2009, by DuRoss, C.B., Personius, S.F., Crone, A.J., McDonald, G.N., and Lidke, D.J.: Utah Geological Survey Special Study 130, 37 p., 2 plates, CD, available online at http://geology.utah.gov/online/ss/ss-130.pdf.

19. Late Quaternary faulting in East Canyon Valley, Northern Utah—Paleoseismology of Utah, Volume 19, 2010, by Piety, L.A., Anderson, L.W., and Ostenaa, D.A.: Utah Geological Survey Miscellaneous Publication 10-5, 40 p., CD, available online at http://geology.utah.gov/online/mp/mp10-05/mp10-05.pdf.

20. Compilation of U.S. Bureau of Reclamation Seismotectonic Studies in Utah, 1982-1999—Paleoseismology of Utah, Volume 20, 2011, compiled by Lund, W.R., Bowman, S.D., and Piety, L.A.: Utah Geological Survey Miscellaneous Publication 11-2, variously paginated, CD, available online at http://geology.utah.gov/online/mp/mp11-02/mp11-2.pdf.

21. Compilation of 1982-83 seismic safety investigation reports of eight SCS dams in southwestern Utah (Hurricane and Washington fault zones) and low-sun-angle aerial photography, Washington and Iron Counties, Utah, and Mohave County, Arizona — Paleoseismology of Utah, Volume 21, 2011, by Bowman, S.D., Young, B.W., and Unger, C.D.: Utah Geological Survey Open-File Report 583, 4 p., 2 plates, 6 DVD set, available online at http://geology.utah.gov/online/ofr/ofr-583/ofr-583.pdf.

22. Late Holocene earthquake history of the Brigham City segment of the Wasatch fault zone at the Hansen Canyon, Kotter Canyon, and Pearsons Canyon trench sites, Box Elder County, Utah —Paleoseismology of Utah, Volume 22, 2012, by DuRoss, C.B., Personius, S.F., Crone, A.J., McDonald, G.N., and Briggs, R., 2012,: Utah Geological Survey Special Study 142, 28 p., 3 plates, 5 appendices, available online at http://geology.utah.gov/online/ss/ss-142/ss-142.pdf.

23. Compilation of U.S. Geological Survey National Earthquake Hazards Reduction Program Final Technical Reports for Utah, 2013, compiled by Bowman, S.D., and Lund, W.R.: Utah Geological Survey Miscellaneous Publication 13-3, 9 p. + 56 reports, available online at http://geology.utah.gov/online/mp/mp13-03/mp13-03.pdf.

24. Evaluating surface faulting chronologies of graben-bounding faults in Salt Lake Valley, Utah—New paleoseismic data from the Salt Lake City segment of the Wasatch fault zone and the West Valley fault zone—Paleoseismology of Utah, Volume 24, 2014, by DuRoss, C.B., and Hylland, M.D.: Utah Geological Survey Special Study 149, 76 p. + 14 appendices, 2 plates, CD, available online at http://geology.utah.gov/online/ss/ss-149/ss-149.pdf.

CONTENTS

FIGURES

TABLES

HISTORY OF LATE HOLOCENE EARTHQUAKES AT THE WILLOW CREEK SITE AND ON THE NEPHI SEGMENT, WASATCH FAULT ZONE, UTAH

by Anthony J. Crone, Stephen F. Personius, Christopher B. DuRoss, Michael N. Machette, and Shannon A. Mahan

ABSTRACT

The 42-km-long Nephi segment is the southernmost part of the Wasatch fault zone that has evidence of multiple Holocene surface ruptures; it is composed of two strands, a 25-km-long southern strand and a 17-km-long northern strand. We excavated two large trenches (Willow Creek North and Willow Creek South) and a smaller subsidiary trench across fault scarps on the Willow Creek alluvial fan, which is about 10 km north of Nephi, Utah, on the southern strand. The Willow Creek North trench crossed a 6.7-m-high scarp, and the Willow Creek South trench crossed a 6.0-m-high scarp. We exposed evidence of three surface-rupturing earthquakes in both trenches. Time-stratigraphic OxCal models using luminescence and radiocarbon ages constrain the times of three prehistoric earthquakes to be 0.2 ± 0.1 ka (2σ), 1.2 ± 0.1 ka (2σ), and 1.9 ± 0.6 ka (2σ). Stratigraphic relations provide evidence of at least one additional surface rupture at the Willow Creek site since deposition of a 6.2-ka alluvial fan; this is the first evidence of more than three Holocene earthquakes on the Nephi segment. The short-term vertical slip rate at Willow Creek is about 2.6–3.4 mm/yr for the past 2.5 kyr, and vertical displacement is 2.3–2.4 m per earthquake.

We evaluated the earthquake-timing data from earlier paleoseismic studies at the North Creek and Red Canyon sites and combined them with our Willow Creek chronology to develop a southern-strand chronology of earthquakes, assuming that the entire strand ruptures during large earthquakes. Earthquake N1 occurred at 0.2 ± 0.1 ka (2σ), N2 occurred at 1.2 ± 0.1 ka (2σ), N3 occurred at 2.0 ± 0.4 ka (2σ), and N4 occurred at 4.7 ± 1.8 ka (2σ). These times yield open and closed recurrence intervals; using the three youngest and best-constrained earthquakes, the closed-interval recurrence time between N1 and N3 is 0.9 ± 0.2 kyr and the open-interval recurrence since 6.2 ka is about 1.6 kyr. N1 apparently postdates the only well-documented earthquake on the northern strand, which occurred at about 0.5 ka and produced about 3 m of vertical displacement based on a paleoseismic study near Santaquin. Earlier earthquakes at the Santaquin site predate alluvial-fan deposits exposed in the trench and occurred prior to 1.5 ka, and likely prior to 6.9 ka, based on charcoal radiocarbon ages. The frequency of earthquakes within a well-constrained time interval at the Willow Creek site combined with the amount of vertical displacement indicates an anomalously high, post-middle Holocene slip rate for the southern strand of the Nephi segment. We attribute this high rate to a cluster of late Holocene earthquakes because the high short-term rate is at least a factor of 10 greater than the rates for mid-Pleistocene and longer periods of time.

Our comparison of the rupture histories on both strands of the Nephi segment and the adjacent Provo segment to the north indicates a complex interaction between these three parts of the Wasatch fault zone. Earthquake chronologies for the three parts of the fault zone indicate that the southern strand likely ruptures as an independent seismic source, but the current data are inadequate to resolve questions about the interaction of the northern strand with the adjacent Provo segment. These questions can only be resolved by acquiring longer and more complete paleoseismic records for the northern and southern strands of the Nephi segment.

INTRODUCTION

Overview

The 343-km-long Wasatch fault zone (WFZ) in central Utah (figure 1) is one of the most thoroughly studied normal faults in the world. More than a century ago, famed geologist G.K. Gilbert recognized the fresh-looking scarps along the fault and concluded that multiple surface-rupturing earthquakes had occurred on the fault since the adjacent basin had been occupied by Lake Bonneville in the late Pleistocene. He also recognized that a long history of repeated movements on the WFZ was responsible for the precipitous western front of the Wasatch Range (summarized in Gilbert, 1928). Since Gilbert's initial investigations, the Wasatch Front has been the focus of intense urbanization, and at present, about 2.1 million people or about 75 percent of Utah's population lives within a short distance of the fault zone. Although no historical earthquakes have produced surface rupture on the WFZ since European settlers first arrived in Utah in 1847, geological studies confirm that large surface-faulting earthquakes have ruptured

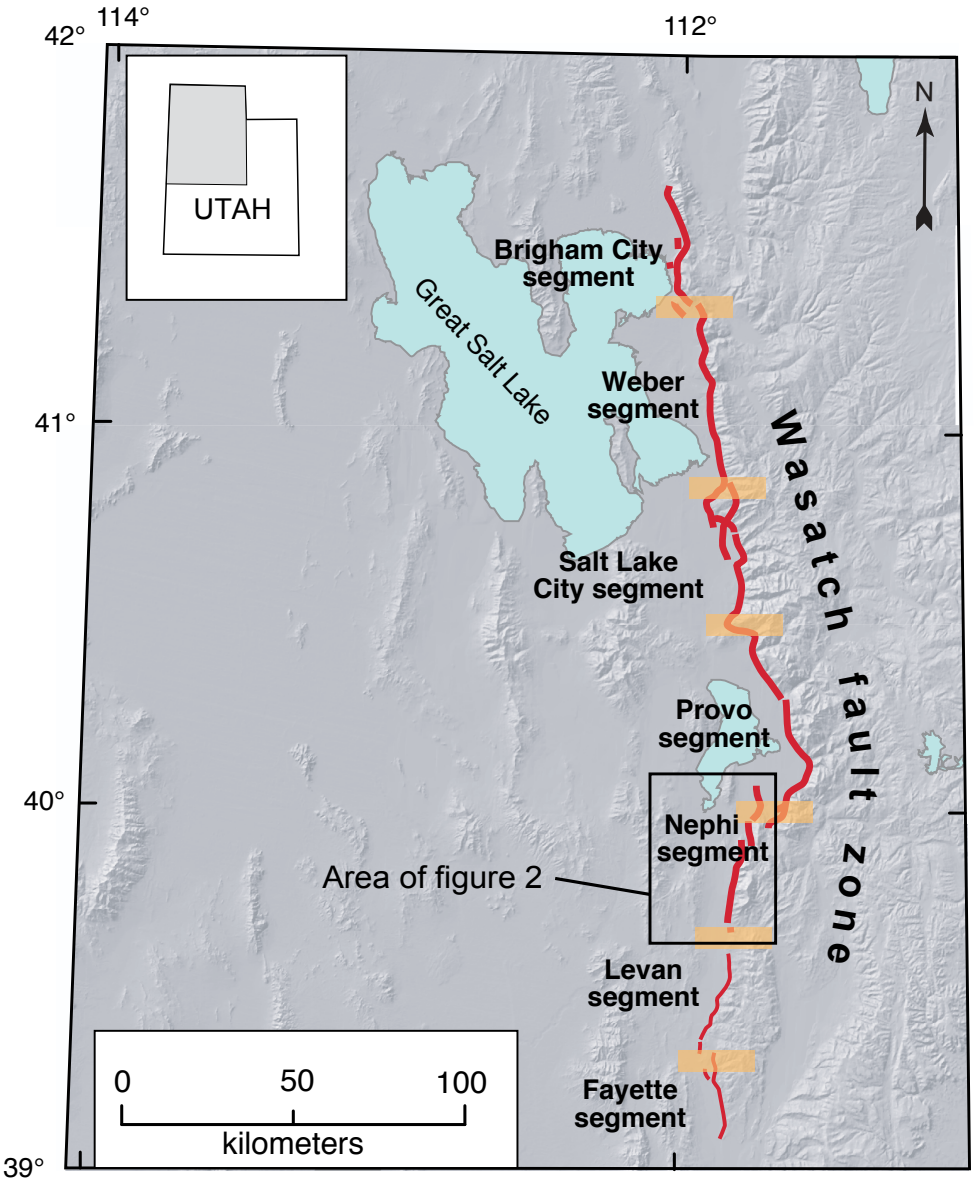

Figure 1. *Shaded-relief map showing segments of the Wasatch fault zone that have ruptured in Holocene time. Thicker red lines have multiple Holocene ruptures and thin red lines have only one Holocene surface rupture. Fault segments are defined by the geometry of fault traces and the geomorphology of scarps on individual segments. Orange bands show segment boundaries.*

six and likely seven segments of the fault zone in the Holocene (Machette and others, 1992; Hylland and Machette, 2008; also summarized in Lund, 2005), and five of those segments, the Brigham City, Weber, Salt Lake City, Provo, and Nephi segments, have ruptured multiple times in the Holocene. Given this history of Holocene earthquakes, the WFZ poses a serious hazard to much of Utah's population and the associated infrastructure.

Starting in the 1970s and continuing into the early 1990s, at least 14 paleoseismic studies defined the basic Holocene rupture history for the six central fault segments (Lund, 2005; Bowman and Lund, 2013). Subsequently, eight additional fault-related studies since the early 1990s have help refine the times of surface ruptures on the segments and extended the paleoseismic record farther back in time.

In recent years, the Utah Geological Survey (UGS) has convened the Utah Quaternary Fault Parameters Working Group (UQFPWG) annually to systematically evaluate paleoseismic data in Utah to better understand the level of seismic hazard statewide (Lund, 2005; also http://geology.utah.gov/ghp/workgroups/uqfpwg.htm). Through this process, in 2004 the UGS designated the Nephi segment as one of the highest priority targets for additional paleoseismic research, in part because of ambiguities in its earthquake history and in part because southward expansion of urbanization could both destroy potential study sites and increase seismic risk on the

segment. In response to this designation, we embarked on an effort to better define the times of prehistoric earthquakes on the Nephi segment, which is along the southern part of the WFZ (figure 1). We focused our effort on at a site on the Willow Creek alluvial fan, which is at the foot of Mt. Nebo, the highest peak in the Wasatch Range (figure 2).

Here we interpret the results of our paleoseismic study at the Willow Creek site and integrate those results with earthquake histories from other study sites to develop an updated, segment-wide earthquake history. We document the occurrence of at least four surface-faulting earthquakes on the Nephi segment since mid-Holocene time, which indicates an unusually

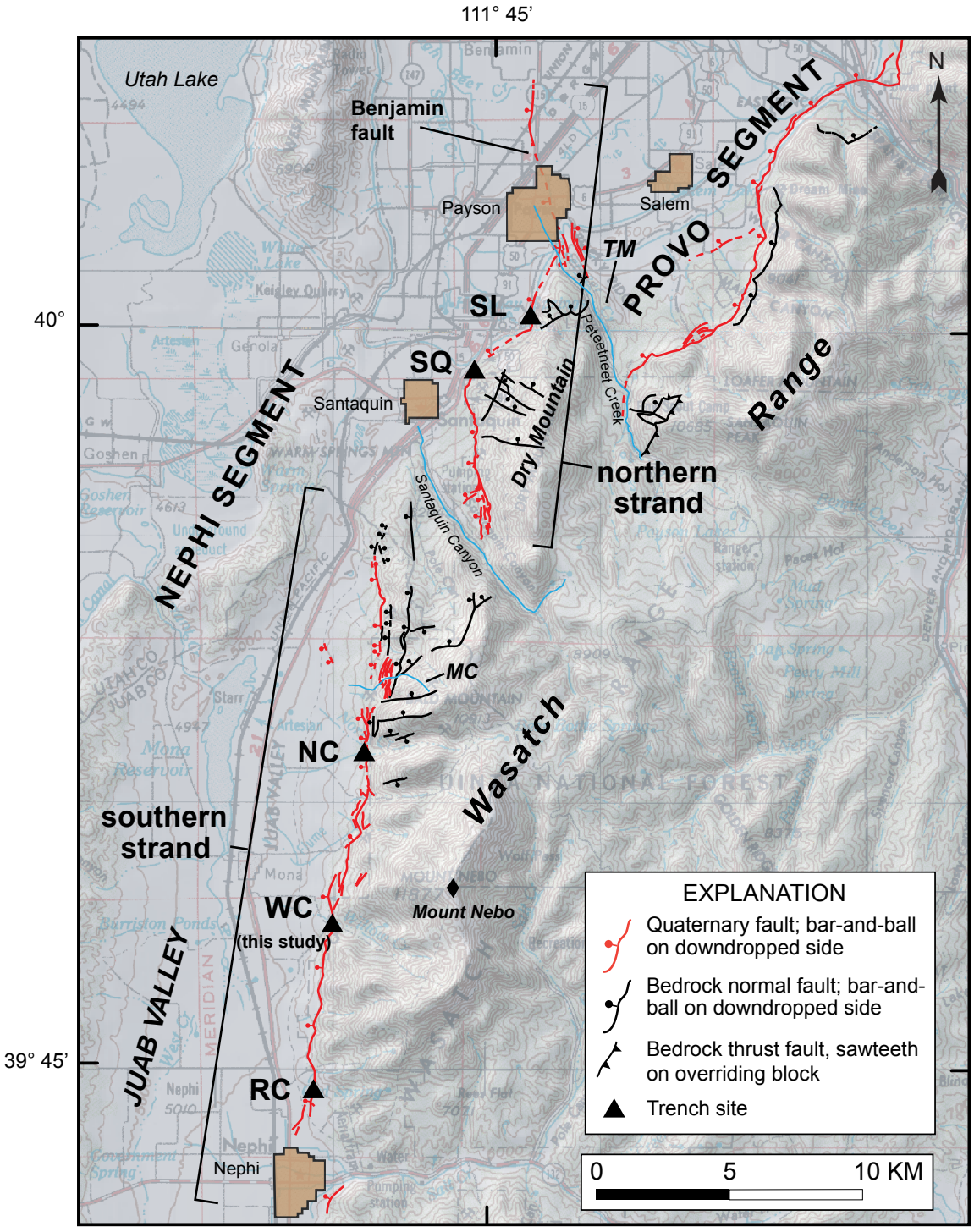

Figure 2. *Nephi segment and southern part of the Provo segment of the Wasatch fault. Generalized traces of faults and trench sites are discussed in the text. Scarps on Quaternary deposits are shown in red, and faults in Tertiary through Precambrian rocks are shown in black. The segment is divided into southern and northern strands at a 4-km-wide step between the strands. Abbreviations: MC, Mendenhall Creek;* NC, *North Creek;* RC, *Red Canyon;* SL, *Spring Lake;* SQ, *Santaquin; TM, Tithing Mountain;* WC, *Willow Creek. Modified from Machette (1992) and Harty and others (1997).*

high short-term slip rate compared to estimates of long-term rates for the segment. We interpret this difference in slip rates to be evidence of earthquake clustering. Our segment-wide history of earthquake ruptures provides insight into the interaction of the two Nephi-segment fault strands and between the Nephi and adjacent Provo segment to the north. Collectively, a greater understanding of the temporal and spatial distribution of surface ruptures on the fault zone contributes to better models of probabilistic ground shaking and thus aids in assessing the seismic hazard that affects the majority of Utah's citizens.

The Nephi Segment

Paleoseismic studies of the Nephi segment are valuable because the segment is a structurally complex part of the Wasatch fault system that is composed of two distinct, overlapping strands and a large part of the segment overlaps with the adjacent Provo segment (figure 2). Furthermore, it is possible that the overlapping sections of these west-dipping normal faults may converge and intersect at depth (Machette and others, 1992). Accordingly, paleoseismic data can provide valuable evidence regarding the interaction between these parts of the fault zone during large-slip earthquakes and thus help characterize the seismic hazard in Utah, as well as provide insight into the behavior of segment boundaries on normal faults.

The 42-km-long Nephi segment extends from near the town of Nephi, northward to beyond the town of Payson in Utah Valley (figure 2). The geometry of the segment indicates that it is composed of two strands, a 25-km-long southern strand (western strand of Machette and others, 1992) that bounds the steep range front between Nephi and near the town of Santaquin (Harty and others, 1997), and the 17-km-long northern strand (eastern strand of Machette and others, 1992) that extends from Santaquin Canyon into Utah Valley and includes the Benjamin fault (Machette, 1992; Machette and others, 1992; DuRoss and Bruhn, 2004). The two strands are linked by a bedrock fault that cuts through a promontory in the Wasatch Range (Machette and others, 1992; Harty and others, 1997).

At its northern end, the Nephi segment is separated from the adjacent 60-km-long Provo segment by the Payson salient (Wheeler and Krystinik, 1988), which is a 7.5–9 km right step across Dry Mountain (Machette and others, 1992; DuRoss and Bruhn, 2004). At the Nephi segment's southern end, prominent Quaternary fault scarps die out near Interstate I-15, about 2–3 km north of the town of Nephi (Harty and others, 1997). A 6-km-long gap separates the southernmost scarps on the Nephi segment from scarps on the 33-km-long Levan segment to the south (DuRoss and Bruhn, 2004; Hylland and Machette, 2008).

THE WILLOW CREEK TRENCH SITE

Objectives and Site Characteristics

Much of the range-front along the Nephi segment was incorporated into the Mount Nebo Wilderness area in 1984, which severely limited options for trench sites. Fortunately, a small section of fault scarps on the upper part of the Willow Creek alluvial fan on U.S. Forest Service (USFS) administered land is outside the wilderness area and was available for study. We had two study objectives: 1) to refine the times of the youngest and preceding surface-rupturing earthquakes, and 2) to determine the times of as many older earthquakes as possible.

The Willow Creek site is about 3.7 km east-southeast of Mona, Utah, and about 9.8 km north of Nephi, Utah, near the middle of the southern strand of the Nephi segment (figure 2). It is essentially equidistant between the previously studied Red Canyon (6.3 km to the south) and the North Creek sites (6.5 km to the north). Fault scarps are steep, high, and continuous along this part of the fault, and multiple surface ruptures have vertically displaced alluvial-fan deposits about 6–7 m at Willow Creek (figures 3, 4, 5, and 6; Machette and others, 2007).

We excavated two large trenches and one smaller subsidiary trench at the site in 2005: the Willow Creek North (WCN) trench was about 150 m north of the USFS Willow Creek road, and the Willow Creek South (WCS) trench was about 55 m north of the road (figure 5B). At the WCS site, the surface faulting is expressed as a single scarp, but to the north, it divides into two splays. At the WCN site, the eastern splay coincides with the large scarp, and the western splay coincides with a small scarp (figure 5B).

Our trenches had maximum depths of 4–5 m and exposed sequences of fluvial sand and gravel, debris-flow deposits, and stacked colluvial wedges. We interpreted evidence of three surface ruptures in each trench and used acceleration mass spectrometry (AMS) radiocarbon (^{14}C) and optically stimulated luminescence (OSL) dating to determine the age of the deposits and to bracket the times of the surface-rupturing earthquakes (table 1). Radiocarbon samples of charcoal and A-horizon soil material were first analyzed to identify the nature of the plant material, such as herbaceous twigs, and individual charcoal fragments (appendix A). This information allowed us to date specific types of burnt wood (charcoal) and charred plant material that were local to the trench site and thus reduce the likelihood of dating reworked material (Puseman and Cummings, 2005). We used quartz for OSL dating to estimate the age of fine-grained eolian and colluvial sediment (Duller, 2004).

Radiocarbon ages are commonly reported in calibrated years before present (cal yr B.P., where present is A.D. 1950), and luminescence ages are commonly reported in kiloannum (ka).

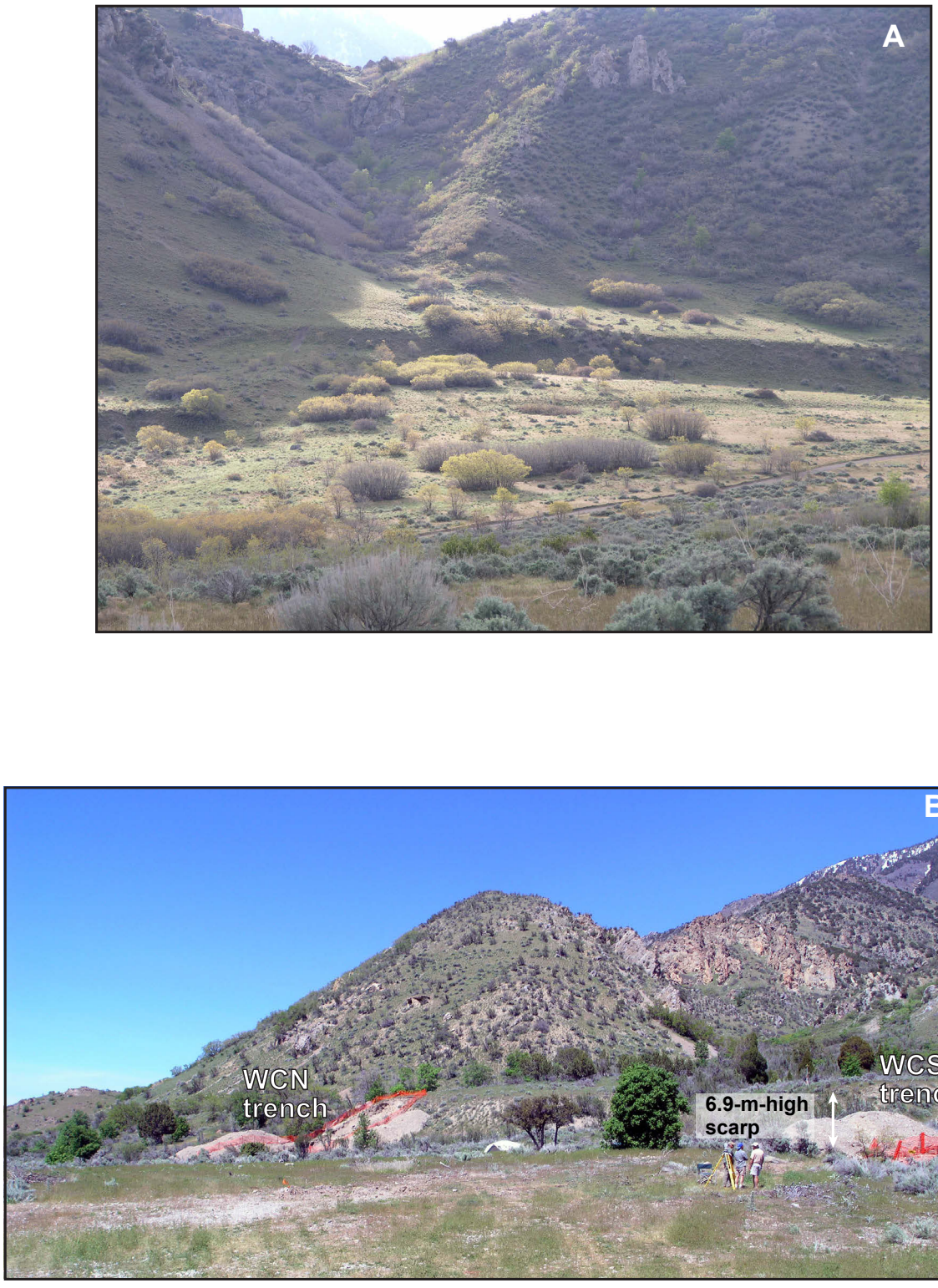

Figure 3. *Fault scarps near the Willow Creek alluvial fan. Scarps are typically more than 5 m high. A: Fault scarp about 450 m north of the Willow Creek site that has a steep face and sharp crest that are evidence of multiple young surface ruptures. View is to the east; see figure 4 for location. B: View to the north of the Willow Creek site. Light-colored spoil piles are from the Willow Creek North (WCN) and Willow Creek South (WCS) trenches. White arrow shows approximate location of 6.9-m-high fault scarp at the WCS site. See figure 5B for map of site. Photographs by S.F. Personius, May 2005.*

Figure 4. *Oblique aerial view of the Willow Creek alluvial fan and fault scarp on the Nephi segment. View is to the east. Willow Creek drains the large valley in the upper right of the view. About 1.1 km north of the Willow Creek fan, the fault scarps are difficult to trace because the fault zone extends into a large landslide in the Carboniferous Manning Canyon Shale. Small islands of possible landslide deposits are surrounded by younger deposits of the Willow Creek alluvial fan; two examples are outlined by white dashed lines. White arrows show the scarp in figure 3A and locations of Willow Creek North (WCN) and Willow Creek South (WCS) trenches. Photograph by C.B. DuRoss, 2005.*

For consistency throughout this report, we present both calibrated radiocarbon and luminescence ages in ka and round the ages to the nearest century. For example, a calibrated ^{14}C age of 670 ± 60 cal yr B.P. is rounded to 0.7 ± 0.1 ka, and an OSL age of 1.24 ± 0.16 yr is rounded to 1.2 ± 0.2 ka. In table 1, we list the ^{14}C and OSL ages relevant to the Willow Creek site. In discussing the OSL ages, we report the ages in thousands of calendar years (ka) before the date when we developed the OxCal models (2010), and do not specifically adjust for the 60-year difference between the time when the models were constructed versus the reference standard for ^{14}C (1950). This difference is modest compared to many of the OSL-age uncertainties, which generally range from one to several hundred years at 2σ uncertainty. Furthermore, the 60-year time difference is accounted for in the probability density functions (PDFs) generated by the OxCal modeling of earthquake times.

Detailed maps of the site and large-format maps of the trench walls, as well as related analytical information, were presented by Machette and others (2007) and are included in this report as appendix B. Here, we interpret those data to define the history of earthquakes at the site.

We found evidence of minor monoclinal tilting of the fan deposits on the hanging-wall block in both Willow Creek trenches as shown by slightly steeper westward dips of the hanging-wall units. Much of this tilting could be related to the ductile behavior of landslide deposits of Manning Canyon Shale, which may be locally present beneath the Willow Creek fan. The tops of these landslide deposits are exposed as small islands of landslide debris surrounded by Holocene fan alluvium downslope from our study area (figures 4 and 5A; M.N. Machette, unpublished mapping, 1984). The ductile nature of the Manning Canyon landslide deposits might explain the expression of the fault scarps several hundred meters north of the Willow Creek site, where they are subtle and difficult to trace in the landslide (figures. 4 and 5A). We speculate that this style of ductile deformation could be responsible for some of the tilting at the Willow Creek site.

Willow Creek North Trench

Setting and General Stratigraphy

The WCN trench was at the northern margin of the Willow Creek drainage where the alluvium is not derived from the

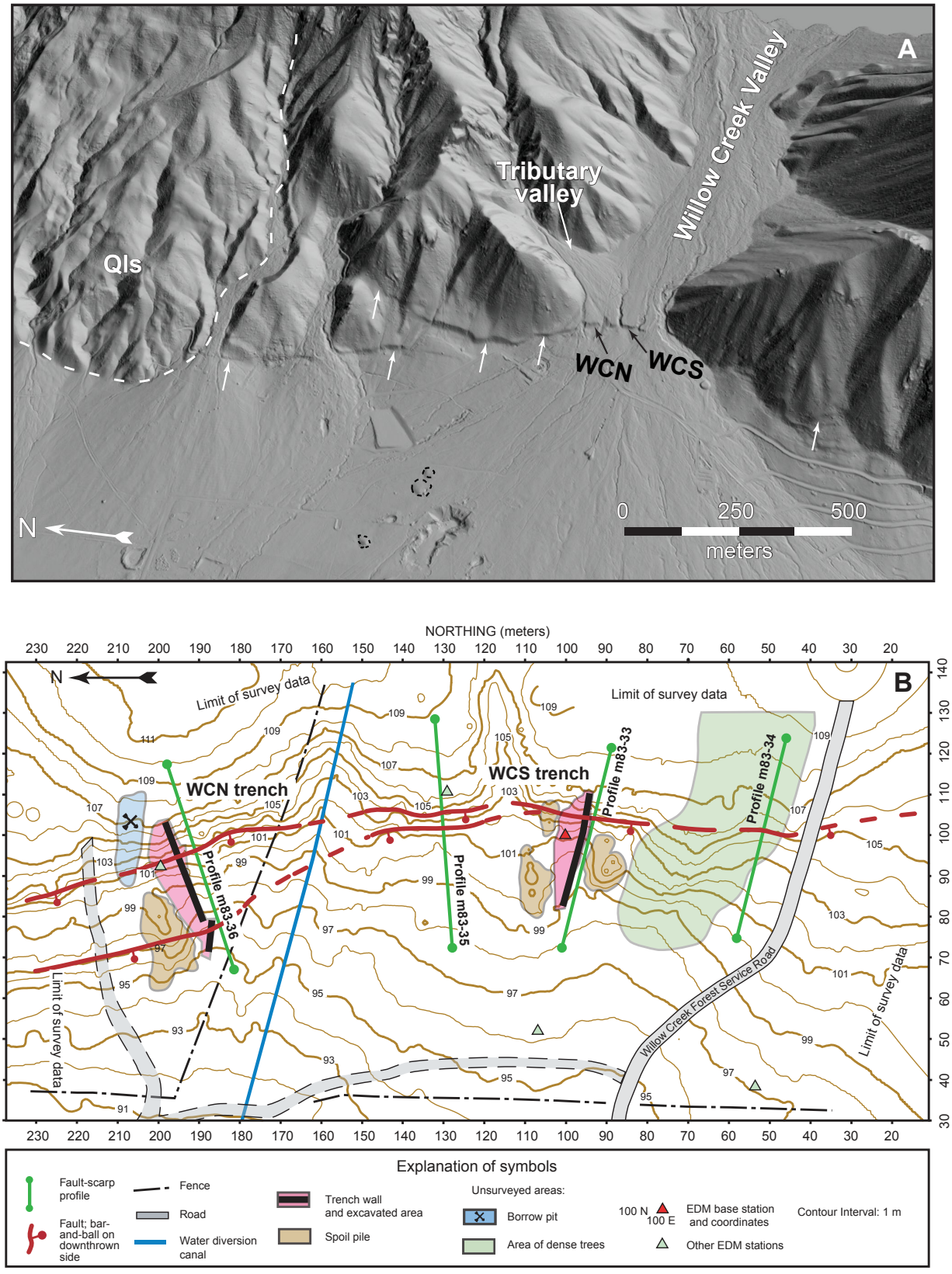

Figure 5. *Shaded-relief and topographic maps of the Willow Creek alluvial fan and trench site. A: View to the east of the fan, adjacent range front, and landslide in Carboniferous Manning Canyon Shale (Qls). Areas outlined in black dots on Willow Creek fan are blocks of ancient landslide debris that have not been completely buried by younger alluvium. Shaded-relief map (illumination from the east) generated from LiDAR data that are available at http://www.opentopography.org. Data set is EarthScope Intermountain Seismic Belt LiDAR Project. B: Topographic map shows fault traces and locations of trenches and scarp profiles. Elevations on map are relative to an arbitrary datum. The scarp profiles adjacent to the trenches are shown on figure 6. Modified from Machette and others (2007).*

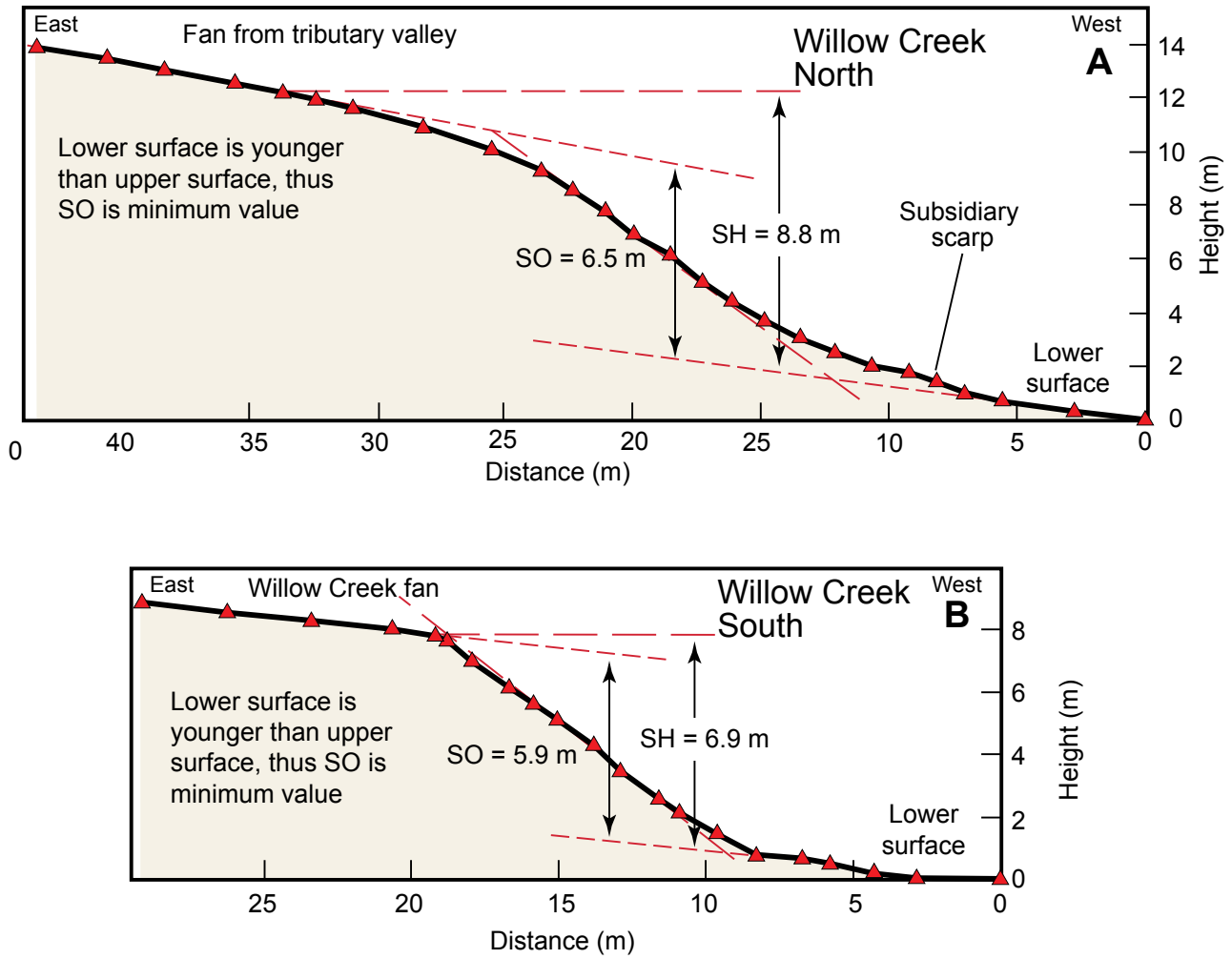

Figure 6. *Profiles of the fault scarp at the Willow Creek site. A is adjacent to the Willow Creek North trench and is profile m83-36 of Machette and others (2007). B is adjacent to the Willow Creek South trench and is profile m83-33 of Machette and others (2007). Abbreviations: SH, scarp height; SO, surface offset (after Bucknam and Anderson, 1979). Reanalysis of the profiles yielded slightly revised values of surface offset and scarp height. Scarp profiles in the vicinity of the Willow Creek site (shown on figure 5) have a range in height of 6.3–8.8 m and minimum surface offsets of 5.2–6.7 m. See figure 5B for site map and location of profiles.*

main drainage basin of Willow Creek, but from a southwestward-draining tributary valley (figure 5). Machette and others (2007) indicate a total scarp height of 8.7 m with a surface offset of 6.7 m from a scarp profile at the WCN trench (their profile m83-36 in appendix B), but we have reanalyzed the original profile data and slightly modify these values to yield a scarp height of 8.8 m and a surface offset of 6.5 m (figure 6A).

In the WCN trench, we exposed a sequence of gently west-dipping, massive to moderately stratified debris-flow deposits, and gravelly to sandy fluvial deposits (unit 5) in the footwall east of the main fault zone (figure 7A; see also Machette and others [2007] in appendix B for details of the stratigraphy). This sequence contains thin silty layers that are likely composed largely of loess. Unit 5 also contains a thin but distinct burn layer (unit 5–6, figure 7A), from which we collected charcoal and plant material. A radiocarbon age from a sample of monocot or herbaceous dicot (flowering plant) stems from this layer yielded a ^{14}C age of 5420 ± 35 yr, which has a rounded calibrated age of 6.2 ± 0.1 ka (WCN-R1, table 1). These delicate plant fragments could not have been transported long distances nor would they have survived on the surface for a long time before burial, so their radiocarbon age is likely an accurate date for deposition of part of the WCN fan alluvium, which was not exposed in the fault hanging wall in the trench.

Deposits in the hanging wall west of the main fault zone consist of a sequence of interbedded massive, cobbley debris-flow deposits and massive to moderately stratified sandy to pebbly fluvial gravel (unit 4, figure 7A). Although similar in lithology to the sediments in the footwall, the hanging-wall deposits are considerably younger based on an OSL age of 1.2 ± 0.2 ka (WCN-L03) from unit 3-1 exposed in the subsidiary trench (figure 7B). Thus, we did not expose correlative units across the fault zone.

Evidence of Prehistoric Earthquakes

The fault zone in the WCN trench is marked by an approximately 1.5-m-wide main zone that contains a main eastern strand (F1 on figure 7A), several subsidiary strands (F2), and a prominent antithetic strand (F3) that bounds the western side of a 2-m-wide graben. This zone accommodates most of the vertical displacement associated with the scarp. About 8–9 m west of the main fault zone, a steep, east-dipping reverse fault vertically displaces stratigraphic units about 0.6 m (F4), up to the east. Farther to the west near the toe of the large scarp (figure 7B), a subsidiary, down-to-the-west normal fault (S1) and antithetic fault (S2) coincide with a subtle, 1-m-high scarp. At the main fault zone, the debris-flow deposits and the fluvial gravel of unit 4 are overlain by three colluvial wedges (figure 7A). We identified individual wedges on the basis of distinctive changes in clast sizes and sorting, imbrication of clasts and stone lines, changes in texture of the colluvium, and the upward extent of fault strands. The lack of prominent soil horizons and oxidation between the wedges show that the length of time between individual surface ruptures was short enough to preclude the development of distinct soil profiles. Soil organic matter was locally slightly concentrated near the tops of wedges, but commonly, it was generally disseminated throughout the wedges.

Unit Cw1 is the unfaulted colluvial deposit shed from the scarp following the youngest earthquake at Willow Creek (WC1). The upper part of unit Cw1 buries the eroded free face on the easternmost main fault strand. Unit Cw2 directly

Table 1. *Summary of radiocarbon (^{14}C), optically stimulated luminescence (OSL), and thermoluminescence (TL) age estimates for samples from the Nephi segment, Wasatch fault zone.*

Willow Creek Radiocarbon and Luminescence Ages

Sample ID[1]	^{14}C age (1σ)[2]	cal yr B.P. (2σ)[2]	Rounded age (2σ)[2]	Comment[3]
WCN-R1	5420 ± 35	6230 ± 80	6.2 ± 0.1	Unit 5-6; in footwall
WCN-R2	Not dated	—	—	Unit 5-6; in footwall
WCN-R3	1275 ± 35	1220 ± 80	1.2 ± 0.1	At top of unit Cw2
WCN-R4	725 ± 35	670 ± 60	0.7 ± 0.1	At top of unit Cw2
WCN-R5	265 ± 35	320 ± 180	0.3 ± 0.2	At top of unit Cw3; too young
WCN-R6	Not dated	—	—	At top of unit 3-1; subsidiary trench
WCN-R7	330 ± 30	390 ± 100	0.4 ± 0.1	At top of unit 2; subsidiary trench
WCS-R1	210 ± 35	180 ± 200	0.2 ± 0.2	At top of unit Cw1
WCS-R2	230 ± 35	210 ± 220	0.2 ± 0.2	At top of unit 3-1a
WCS-R3	310 ± 45	380 ± 120	0.4 ± 0.1	At top of unit 3-1a
WCS-R4	2965 ± 35	3140 ± 120	3.1 ± 0.1	At top of unit 4-9; in footwall
WCS-R5	3000 ± 35	3200 ± 140	3.2 ± 0.1	At top of unit 4-9; in footwall
WCS-R6	500 ± 60	540 ± 120	0.5 ± 0.1	At top of unit 2; too young
WCS-R7	205 ± 35	180 ± 200	0.2 ± 0.2	At top of unit Cw2; too young
Sample ID	OSL age (1σ)[2]	Rounded age (2σ)[2]	Comment[3]	
WCN-L01	5.13 ± 0.32	5.1 ± 0.6	At top of unit Cw3; too old	
WCN-L02	1.04 ±0.07	1.0 ± 0.1	At top of unit Cw2	
WCN-L03	1.24 ± 0.08	1.2 ± 0.2	At top of unit 3-1; subsidiary trench	
WCS-L01	2.32 ±0.17	2.3 ± 0.3	In unit 3-3	
WCS-L02	2.57 ± 0.12	2.6 ± 0.2	In unit 3-3	
WCS-L03	4.94 ± 0.21	4.9 ± 0.4	In unit 4-7; in footwall	
WCS-L04	2.50 ± 0.19	2.5 ± 0.4	In unit 4-2; in footwall	
WCS-L05	3.05 ± 0.15	3.1 ± 0.3	In unit Cw3	

[1] WCN, Willow Creek north trench; WCS, Willow Creek south trench.
[2] Laboratory-reported ^{14}C ages are listed as ^{14}C age in years before A.D. 1950, calibrated radiocarbon ages are listed as cal yr B.P. Radiocarbon ages were calibrated using OxCal v4.1.7 online program. Rounded ages are in ka and are rounded to the nearest century. Luminescence ages are reported in ka. See Machette and others (2007; presented in appendix B of this report) for details of age analyses.
[3] Cw, colluvial wedge.

Table 1. *Continued*

North Creek Radiocarbon Ages

Sample ID[1]	^{14}C age (1σ)[2]	cal yr B.P. (2σ)[2]	Rounded age (2σ)[2]	Comment
WC-12-80-2 (A)	300 ± 300	360 ± 460	0.4 ± 0.5	Charcoal from buried A horizon on scarp colluvium.
WC-12-80-3 (A)	2180 ± 80	2180 ± 200	2.2 ± 0.2	From buried soil A horizon on North Creek alluvium.
WC-12-80-3 (C)	4500 ± 300	5130 ± 760	5.1 ± 0.8	Same as above.
WC-12-80-4 (A)	250 ± 300	340 ± 440	0.3 ± 0.4	From burn layer at base of historical mudflow.
WC-12-80-5 (C)	1350 ±70	1260 ± 140	1.3 ± 0.1	Charcoal from sandy silt alluvium.
WC-12-80-5 (A)	1550 ± 300	1520 ± 660	1.5 ± 0.7	Same as above.
WC-12-80-6 (C)	1110 ± 60	1030 ± 140	1.0 ± 0.1	Charcoal from buried soil A horizon on faulted alluvium.
WC-12-80-6 (A)	700 ± 250	690 ± 460	0.7 ± 0.5	Same as above.
WC-12-80-7 (C)	3640 ± 75	3970 ± 220	4.0 ± 0.2	From buried soil on scarp colluvium from second oldest earthquake.
WC-12-80-7 (A)	3850 ± 400	4320 ± 1060	4.3 ± 1.1	Same as above.
WC-12-80-7 (A)	1700 ± 300	1680 ± 660	1.7 ± 0.7	Same as above.
WC-12-80-8 (A)	1200 ± 300	1150 ± 580	1.2 ± 0.6	Detrital charcoal from buried soil on alluvium.
WC-12-80-9 (A)	1350 ± 250	1280 ± 520	1.3 ± 0.5	Charcoal from same deposit as WC-12-80-7.
WC-12-80-10 (A)	0 ± 300	250 ± 360	0.3 ± 0.4	Detrital charcoal from unfaulted mudflow deposit.
WC-12-80-11 (A)	4000 ± 400	4510 ± 1060	4.5 ± 1.1	Detrital charcoal from North Creek alluvial-fan deposit.
USGSW-4057 (C)	4580 ± 250	5230 ± 620	5.2 ± 0.6	From North Creek alluvial-fan deposit in footwall.

[1] WC-12-80 samples are from the North Creek site as reported by Hanson and others (1981, 1982). "A" suffix for sample numbers indicates AMS determination; "C" suffix indicates conventional radiocarbon determination.
[2] Laboratory-reported ^{14}C ages are listed as ^{14}C age in years before A.D. 1950, calibrated radiocarbon ages are listed as cal yr B.P. Radiocarbon ages were calibrated using OxCal v4.1.7 online program. Rounded ages are in ka and are rounded to the nearest century. Luminescence ages are reported in ka.

Red Canyon Radiocarbon Ages[1]

Sample ID	^{14}C age (1σ)	MRTC[1] (years)	cal yr B.P. (2σ)[3]	Rounded age (2σ)[4]	Comment
B25185	3550 ± 150	200	3600 ± 800	3.6 ± 0.8	From bottom of unit 4.
B24186	1380 ± 120	100	1300 +400/ -600	1.3 ± 0.5	From top of unit 4.
B25402	2900 ± 90	100	2900 +600/ -400	2.9 ± 0.5	From top of unit 3 at main fault.
B25184	3690 ± 170	100	3900 +1000/ -800	3.9 ± 0.9	From top of unit 4 near main fault.

Red Canyon Thermoluminescence Age Estimates

Sample ID	Reported TL age (1σ)	Rounded age (2σ)[4]	Comment
ITL-48	14,600 ± 1200	14.6 ± 1.2	Not discussed by Jackson or shown on figure 15.
ITL-66	1700 ± 200	1.7 ± 0.2	From top of unit 4.
ITL-67	1500 ± 400	1.5 ± 0.4	From top of unit 3.
ITL-88	1300 ± 500	1.3 ± 0.5	From top of unit 3 at main fault.
ITL-90	7000 ± 800	7.0 ± 0.8	From top of unit 4 near main fault.

[1] Red Canyon data are from Jackson (1991).
[2] Mean residence time correction (MRTC) for organic material in soil A horizon.
[3] Calibrated ages are taken directly from Jackson (1991) and are not recalibrated using OxCal v4.1.7. Jackson (1991) reported an uncertainty of 1σ, but the value listed here is increased to 2σ to be consistent with other values in the table.
[4] Rounded ages are in ka and are rounded to the nearest century.

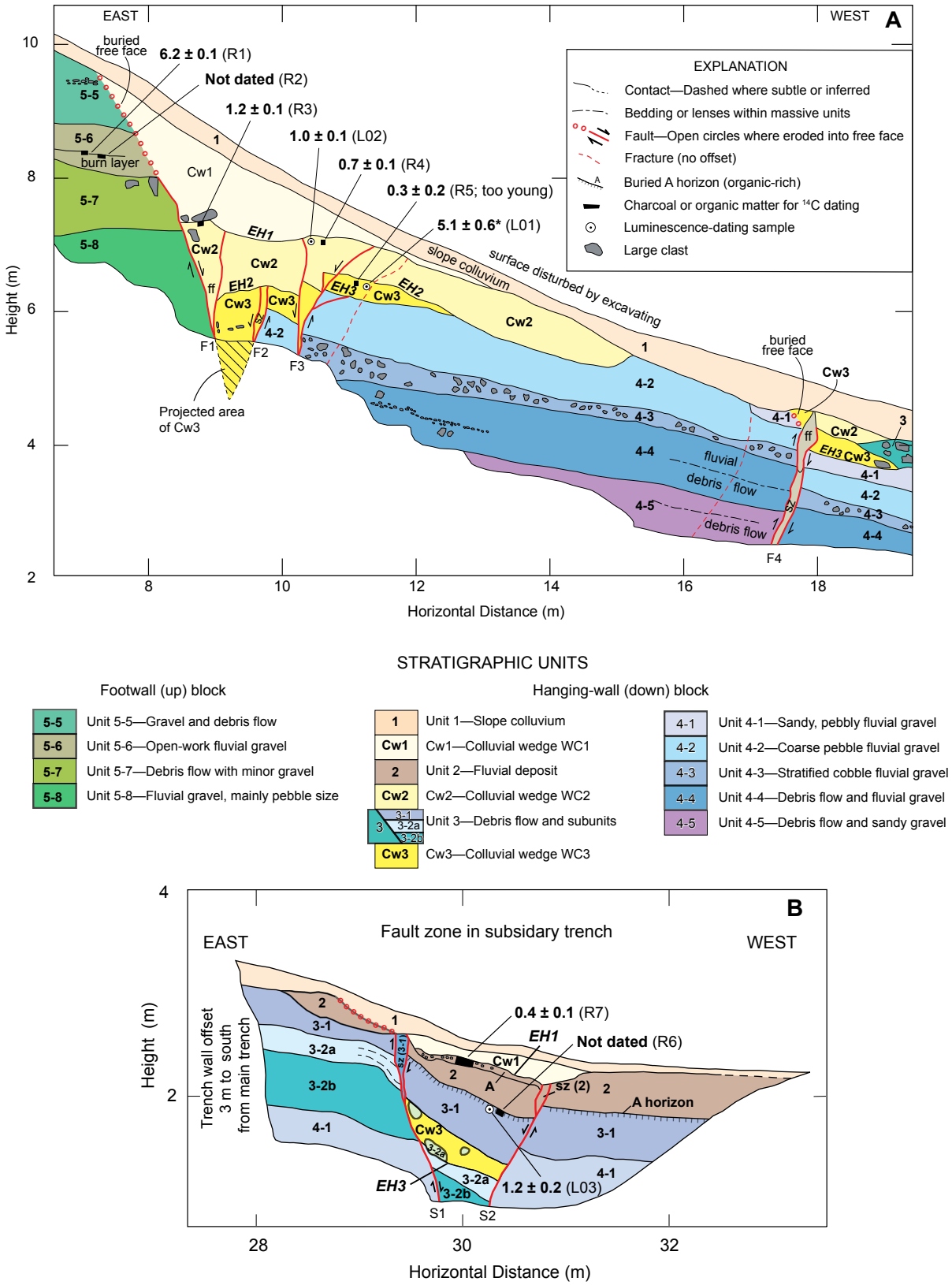

Figure 7. *Schematic diagrams of stratigraphy and faults in the Willow Creek North (WCN) trench. Modified from Machette and others (2007); see Machette and others (2007) for large-scale maps of the trench wall (included as appendix B of this report). Radiocarbon ages (^{14}C) from Machette and others (2007) have been recalibrated for this study. Ages are rounded to the nearest 100 years and are in kiloannum (ka). Ages labeled with "R" indicate radiocarbon ages, "L" indicate luminescence ages; see table 1 for list of ages. A: Stratigraphic relations across the main fault zone (F1 to F3). Deposits in the hanging wall and footwall do not correlate across the main fault. Asterisk next to age determination indicates that the age was not used in the OxCal model for the Willow Creek site because of suspected inheritance of signal or contamination. See text for discussion. B: Stratigraphic relations across the fault zone associated with small scarp in the subsidiary trench. Abbreviations: EH, earthquake horizon; ff, fissure fill; sz, shear zone. Numbers of units in this trench do not correlate with similar-numbered units in the Willow Creek South trench (figure 8).*

beneath unit Cw1 is the colluvial deposit resulting from the preceding surface-rupturing earthquake (WC2). We mapped three fault strands that extend through unit Cw2 colluvium, and therefore, those strands moved during the most recent earthquake. Unit Cw2 buries the third colluvial wedge (Cw3) that was deposited following the third oldest earthquake at Willow Creek (WC3). We were unable to expose the entire colluvial wedge from earthquake WC3 because part of it had been down dropped in a narrow graben between faults F1 and F2, below the depth that we could excavate the trench (figure 7A).

Even though we did not expose the lower part of unit Cw3, we can estimate a minimum downward extent and area, shown by the crosshatched area on figure 7A. The total area of unit Cw3 is only about two-thirds to one-half the area of units Cw2 or Cw1. The smaller area (volume) of unit Cw3 may be evidence that the fault scarp from earthquake WC3 was smaller than the scarps from earthquakes WC2 and WC1. This size difference could be interpreted as evidence that either earthquake WC3 had a smaller amount of throw than the younger earthquakes, or that a substantial amount of the surface deformation from earthquake WC3 was accommodated by distributed deformation and warping.

A steep, east-dipping reverse fault (F4) is associated with only two colluvial wedges, units Cw2 and Cw3 (figure 7A). Unit 3, a debris-flow deposit, buries the toe of the lower wedge (unit Cw3) and is, in turn, buried by the upper wedge (unit Cw2). Downslope, the debris flow (unit 3) increases in thickness, and we were able to subdivide it into subunits. At the subsidiary scarp, the debris-flow subunits are faulted by faults S1 and S2 to form a graben (figure 7B), and in the graben, colluvial-wedge deposit Cw3 is interstratified in unit 3, which shows that the earthquake occurred during deposition of the lower part of unit 3. An OSL sample from an A horizon formed on unit 3-1 (pebbly to bouldery debris-flow deposit) yielded a rounded age of 1.2 ± 0.2 ka (WCN-L03). Based on the correlation of stratigraphic units and the age of this faulted, buried soil (discussed in the following section), we interpret the colluvial wedge in the graben to indicate movement on the graben-bounding faults during earthquake WC3 (figure 7B). At reverse fault F4, the colluvial wedge (unit Cw3) that is buried by the upper part of unit 3 must be related to earthquake WC3, and the wedge that is on top of unit 3 (unit Cw2) is likely related to earthquake WC2. Both of these wedges are buried by modern slope colluvium (unit 1).

In the trench across the small, subsidiary scarp, a thin colluvial wedge (unit Cw1) near the surface buries a weak soil that is formed on fluvial gravel (unit 2). A charcoal fragment from sagebrush in the soil had a ^{14}C age that is rounded to 0.4 ± 0.1 ka (WCN-R7). The colluvial wedge is unfaulted and is buried by a thin veneer of modern slope colluvium. These relations indicate that this colluvial deposit is associated with earthquake WC1.

We also have evidence of one or more older earthquake(s), WC4, based on the absence of correlative deposits in the footwall and hanging wall. Thus, at least one, and possibly more, earthquakes must pre-date WC3 to down drop the 6.2 ± 0.1 ka fan gravel (unit 5) in the footwall well below the exposed level of unit 4 in the bottom of our WCN trench exposures.

Times of Earthquakes

Radiocarbon and OSL ages as reported by Machette and others (2007) (appendix B) and listed in table 1 place limits on the times of the three earthquakes in the WCN trench. All three surface-rupturing earthquakes are younger than the 6.2 ± 0.1 ka age of the fan gravel in the footwall (WCN-R1). However, in both this trench and the WCS trench, several ^{14}C samples yielded anomalously young ages relative to their stratigraphic position, which indicates that young carbon has been locally mixed into these colluvial deposits by burrowing animals, insects, plants and other sources of sample contamination.

The only constraints that we have on the time of the oldest earthquake, WC4 (and possibly other earthquakes), are that it is older than earthquake WC3 and younger than the 6.2-ka age of the footwall fan gravel. We did not expose any stratigraphic units that are directly related to this earthquake.

The minimum age of earthquake WC3 is unconstrained in the WCN trench because a ^{14}C age and an OSL age from unit Cw3 yielded contradictory results. The ^{14}C age of 0.3 ± 0.2 ka (WCN-R5) from this wedge is clearly too young, so the sample is likely contaminated with young carbon from an unrecognized krotovina (animal burrow). The OSL sample from the same deposit yielded an age estimate of 5.1 ± 0.6 ka (WCN-L01), but we consider this age to be too old (because of incomplete bleaching of the sediment before burial) based on the age constraints for earthquake WC3 in the WCS trench; data from the WCS trench indicates that earthquake WC3 is younger than about 2.5 ka (discussed below).

Three samples from colluvial-wedge unit Cw2 establish a minimum limit on the age of earthquake WC2 in the WCN trench. A ^{14}C sample (WCN-R4) that yielded an age of 0.7 ± 0.1 ka is in the same stratigraphic position as another ^{14}C and an OSL sample (figure 7A). The second ^{14}C age from a charred fragment of sagebrush and the OSL sample from the upper part of unit Cw2 yielded similar ages of 1.2 ± 0.1 ka (WCN-R3) and 1.0 ± 0.1 ka (WCN-L02), respectively. The 0.7-ka ^{14}C age may be contaminated by younger carbon from bioturbation. Based on these samples, earthquake WC2 is somewhat older than these ages, or older than about 1.0–1.2 ka.

The maximum age of earthquake WC1 is defined by the above ages from the underlying Cw2 deposit at the main fault, and by a ^{14}C age of 0.4 ± 0.1 ka (WCN-R7) from a buried soil beneath the Cw1 deposit between subsidiary faults S1 and S2

(figure 7B). Based on this age, earthquake WC1 is younger than 0.4 ± 0.1 ka. We have no minimum constraint on the time of WC1 in the WCN trench.

Willow Creek South Trench

Setting and General Stratigraphy

We excavated the WCS trench across a scarp formed on fan alluvium from the Willow Creek drainage. The scarp height is 6.9 m and the surface offset is 5.9 m (figure 6B). The height of this scarp is almost 2 m less than that at the WCN site.

The WCS trench exposed a sequence of alternating fluvial, debris-flow, and loess deposits, all largely conformable with parallel bedding (figure 8; see also Machette and others (2007) in appendix B for details of the stratigraphy). The trench exposed contemporaneous deposits on both sides of the fault, as shown by similar-age sediments in the upper footwall and lower hanging wall of the main fault zone (figure 8). In the footwall east of the main fault zone, we exposed a 7-m-thick section of fan deposits from which we have two ^{14}C and two OSL ages. An OSL sample from silt-rich unit 4-2 about 2 m below the crest of the scarp has an age of 2.5 ± 0.4 ka (figure 8, WCS-L04 in table 1). Downward in this section, we have an OSL age of 4.9 ± 0.4 ka (WCS-L03), and a pair of ^{14}C ages from oak charcoal fragments in a burn layer, which yielded ages of 3.1 ± 0.1 ka and 3.2 ± 0.1 ka (WCS-R4, WCS-R5). The older 4.9-ka OSL age is from a deposit of colluvium mixed with loess, and is out of stratigraphic order with the other two ages. We dismiss the older OSL age because it likely contains sediment grains that were not exposed to sunlight long enough during transport to fully bleach the preexisting luminescence signal. The other ages indicate that the faulted sediments (unit 4) in the WCS trench are in the range of 2.5–3 ka, which is about half the age of the fan sediments in the WCN trench.

In the hanging wall, two OSL ages from an interbedded sequence of fluvial gravel and silty to cobbley debris-flow deposits (units 3-1 through 3-5) confirm that we exposed age-correlative deposits on both sides of the fault. The overall character of the hanging-wall deposits was similar to those in the footwall, but because of the nature of alluvial-fan deposition, facies changes within distances of a few meters make it impossible to directly correlate individual units across the main fault zone. Two OSL samples from a loess-rich debris-flow deposit (unit 3-3) yielded similar ages of 2.6 ± 0.2 ka (WCS-L02) and 2.3 ± 0.3 ka (WCS-L01). The debris-flow deposit could be as young as 2.0 ka (OSL age of 2.3 ka minus 0.3 ka) or as old as 2.8 ka (OSL age of 2.6 ka plus 0.2 ka). These ages are essentially the same as the 2.5 ± 0.4 ka age from the stratigraphically highest part of the footwall section.

Evidence of Prehistoric Earthquakes

The WCS trench exposed the main fault zone and an east-dipping reverse fault about 8 m west of the main fault (figure 8). The main fault zone is composed of a down-to-the-west normal fault with fissure fill against fault planes F1 and F2, and an east-dipping antithetic fault that contains several splays (F3). The fan deposits between the main and antithetic faults are down dropped into a shallow, 4-m-wide graben.

Similar to the WCN trench, we mapped three discrete colluvial wedges, each corresponding to a surface-faulting earthquake. The oldest wedge (unit Cw3) is the smallest, but much of the deposit that is mapped as unit Cw3 on figure 8 is fissure fill adjacent to the main fault. The relatively small size of Cw3 colluvium may be evidence that earthquake WC3 was associated with both broad tilting in the footwall block and only a modest amount of brittle faulting.

Unit Cw2 is the colluvial wedge resulting from earthquake WC2. The Cw2 wedge sits directly on top of the Cw3 wedge. The lack of a distinct soil or notable oxidation in the upper part of unit Cw3 suggests that the older wedge was not exposed at the surface very long before being buried by unit Cw2. This implies that the time between earthquakes WC3 and WC2 was likely less than a thousand years.

The lenticular Cw1 deposit from the youngest earthquake has a well-defined basal contact marked by several aligned flat clasts. The eastern margin of unit Cw1 was deposited against the eroded free face of the fault plane. Similar to the contact between units CW3 and CW2, the upper part of the Cw2 wedge lacks a soil or notable oxidation indicating that the time between stabilization of the Cw2 wedge and burial by the overlying Cw1 wedge was also likely less than a thousand years. The upper part of unit Cw1 grades into the slope colluvium (unit 1) that mantles the modern scarp.

The reverse fault (F4, figure 8) splays upward into several strands near the surface, and transports unit 3-1 horizontally about 0.8 m over the pre-faulting ground surface. Fault F4 is capped by a small but distinct colluvial wedge (unit Cw1), which buries a soil A horizon formed on the alluvial-fan deposits of unit 3-1a. The wedge is, in turn, buried by fluvial deposits (unit 1-2) and modern slope colluvium (unit 1). Most of the displacement on this reverse fault occurred during earthquake WC1, but a small amount of movement may have occurred during an earlier earthquake because the easternmost splay of fault F4 in the bottom of the trench extends upward to the top of unit 3-4a, but does not extend into the overlying stratigraphic units.

Times of Earthquakes

Radiocarbon and OSL ages from the WCS trench further constrain the times of earthquakes at the site (Machette and oth-

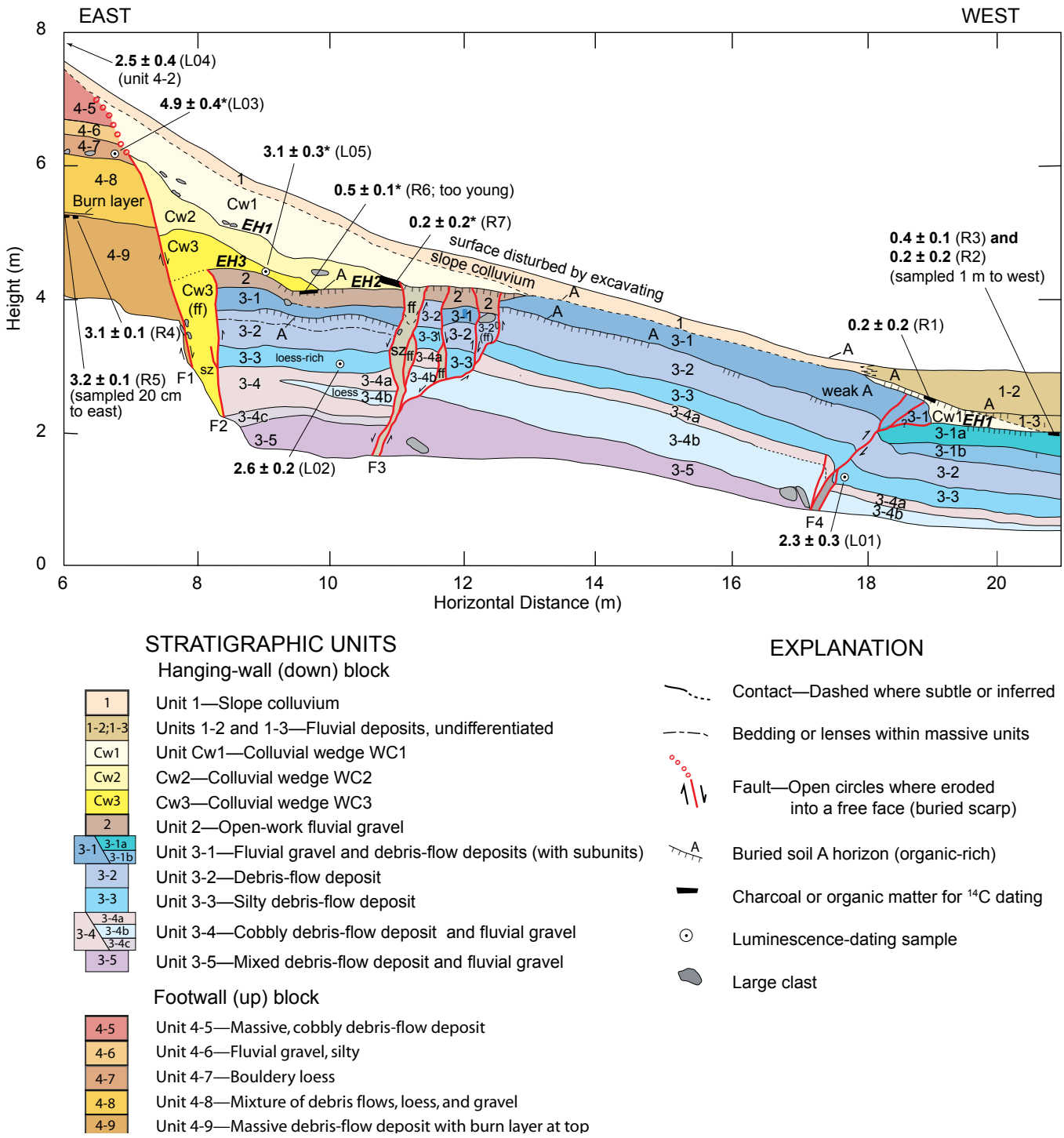

STRATIGRAPHIC UNITS

Hanging-wall (down) block

- Unit 1—Slope colluvium
- Units 1-2 and 1-3—Fluvial deposits, undifferentiated
- Unit Cw1—Colluvial wedge WC1
- Cw2—Colluvial wedge WC2
- Cw3—Colluvial wedge WC3
- Unit 2—Open-work fluvial gravel
- Unit 3-1—Fluvial gravel and debris-flow deposits (with subunits)
- Unit 3-2—Debris-flow deposit
- Unit 3-3—Silty debris-flow deposit
- Unit 3-4—Cobbly debris-flow deposit and fluvial gravel
- Unit 3-5—Mixed debris-flow deposit and fluvial gravel

Footwall (up) block

- Unit 4-5—Massive, cobbly debris-flow deposit
- Unit 4-6—Fluvial gravel, silty
- Unit 4-7—Bouldery loess
- Unit 4-8—Mixture of debris flows, loess, and gravel
- Unit 4-9—Massive debris-flow deposit with burn layer at top

EXPLANATION

- Contact—Dashed where subtle or inferred
- Bedding or lenses within massive units
- Fault—Open circles where eroded into a free face (buried scarp)
- Buried soil A horizon (organic-rich)
- Charcoal or organic matter for ^{14}C dating
- Luminescence-dating sample
- Large clast

Figure 8. *Schematic diagram of stratigraphy and faults in the Willow Creek South (WCS) trench. Modified from Machette and others (2007); see Machette and others (2007) for large-scale map of the trench wall (appendix B). Radiocarbon ages from Machette and others (2007) have been recalibrated for this study. Ages are rounded to the nearest 100 years and are in kiloannum (ka). Ages labeled with "R" indicate radiocarbon ages, "L" indicate luminescence ages; see table 1 for details. Abbreviations are: EH, earthquake horizon; ff, fissure fill; sz, shear zone in a specific unit. Asterisk next to age indicates that the age was not used in the OxCal model for the Willow Creek site.*

ers, 2007; appendix B). Two OSL ages of 2.6 ± 0.2 ka and 2.3 ± 0.3 ka from the alluvial-fan deposit (unit 3-3) in the hanging wall establish a maximum time for all three earthquakes. Conversely, the minimum time since earthquake WC3 is poorly constrained in the trench. An OSL sample from unit Cw3 yielded an age of 3.1 ± 0.3 ka (WCS-L05), but this age is older than the underlying fan deposits, so this sample probably retained an inherited luminescence signal before burial. The ^{14}C sample of a tiny fragment (0.007 g) of maple charcoal from the buried soil formed on the alluvial fan (unit 2) beneath the Cw3 wedge has an age of 0.5 ± 0.1 ka (WCS-R6), which is too young considering its stratigraphic position. The poor results from these two samples leave us with no valid constraints on the minimum time since earthquake WC3 in this trench.

We have only one sample from the WCS trench that establishes a minimum limit on the time of earthquake WC2. A charred monocot stem (WCS-R7) from the top of unit Cw2 has a ^{14}C age of 0.2 ± 0.2 ka, which is a minimum constraint for earthquake WC2 and a maximum limit for earthquake WC1.

Three ^{14}C samples near the reverse fault put tight time limits on earthquake WC1. Two samples (WCS-R2 and WCS-R3) from the buried soil that had formed on the alluvial fan (unit 3-1a) immediately adjacent to unit Cw1 and beneath fluvial gravel unit 1-3 define the maximum time for the earthquake (along with the previously noted age of 0.2 ± 0.2 ka). Charred woody twigs from sample WCS-R3 yielded an age of 0.4 ± 0.1 ka and similar twigs from sample WCS-R2, collected 1 m to the west, yielded an age of 0.2 ± 0.2 ka. Furthermore, sample WCN-R7 from the subsidiary trench at the WCN site is in the same stratigraphic position (beneath Cw1) as WCS-R1 and WCS-R2, and it has an age of 0.4 ± 0.1 ka. Collectively, these samples indicate that the most recent earthquake at the Willow Creek site occurred not more than about 400 years ago.

At the reverse fault, a weakly developed, organic-rich soil on the Cw1 deposit provides a minimum time constraint on earthquake WC1. Charred woody twigs from this soil yielded an age of 0.2 ± 0.2 ka (WCS-R1). On the basis of this age and the previously discussed maximum limits, WC1 occurred about 200 to 400 years ago, or shortly before European settlers arrived in Utah in 1847.

Model for Times of Prehistoric Earthquakes

The ^{14}C and OSL ages from both Willow Creek trenches establish important new constraints on the times of three late Holocene surface-rupturing earthquakes along the southern strand of the Nephi segment (figure 9; see also Machette and others (2007) in appendix B). To better refine the times of those earthquakes, we developed an OxCal model (version 4.1.7) to integrate the ^{14}C and OSL ages from our Willow Creek trenches into an internally consistent and coherent model that estimates the times of the prehistoric surface ruptures and calculates recurrence intervals based on available numerical ages and stratigraphic constraints. The OxCal program is a statistically rigorous way to calibrate ^{14}C ages and estimate the times (and associated uncertainties) of the paleoearthquakes (Bronk Ramsey, 2001, 2008; Lienkaemper and Bronk Ramsey, 2009). The OxCal analysis uses Bayesian statistics to generate probability density functions (PDFs) of the earthquake times. The broad or narrow nature of a PDF is dictated by the rigor with which the chronological and stratigraphic information estab-

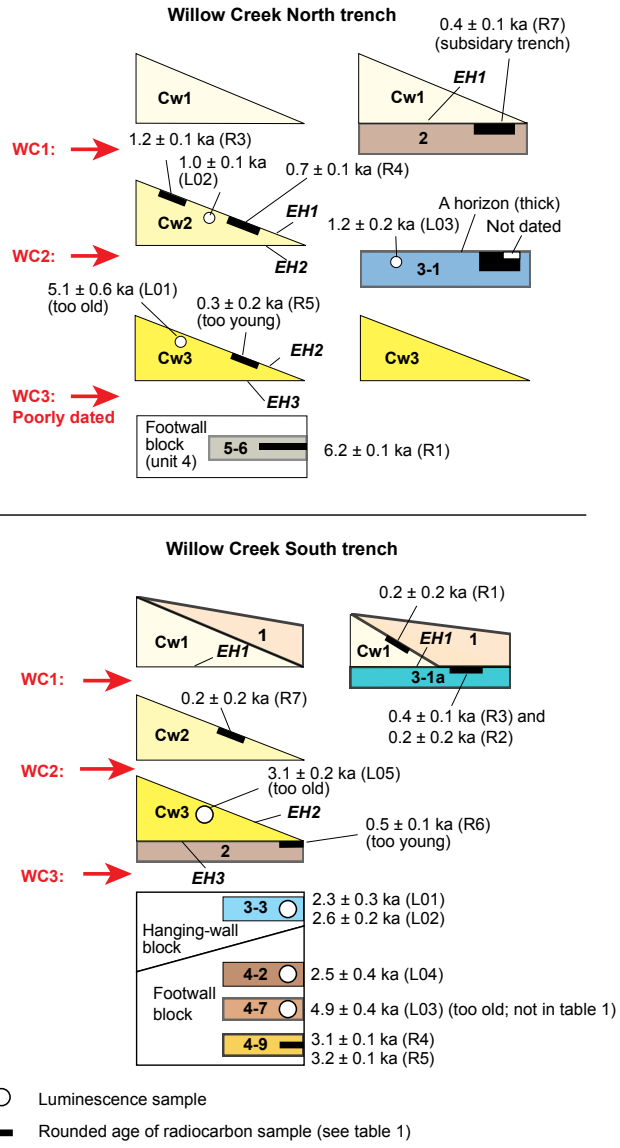

Figure 9. *Diagram showing stratigraphic relations and age constraints for times of prehistoric earthquakes in the Willow Creek North (WCN) and Willow Creek South (WCS) trenches. Column on the left for the WCN trench shows constraints from the main, large trench (figure 7A); column on right shows constraints from the subsidiary trench (figure 7B). Unit 3-1 in the WCN trench is considered to be older than the colluvial wedge from earthquake WC2 (unit Cw2) on the basis of its thick soil A horizon and its position between units Cw2 and Cw3 at the 18-m mark in the trench (figure 7A). Open circles denote sample locations for luminescence ages, and black boxes denote sample locations for radiocarbon ages. EH, earthquake horizon.*

lish bounds for the earthquake times. We used a combination of 15 ^{14}C and OSL ages to define the chronology of depositional phases and surface ruptures at Willow Creek (figures 9 and 10).

To develop the OxCal models discussed in this report, we followed the OxCal command procedure described by DuRoss and others (2011) and used the "Boundary" command to define the times of individual earthquakes. For earthquake WC3, we paired the Boundary with a "Zero Boundary" command, which skews the time distribution (PDF) for the earthquake toward either the minimum or maximum ages. The resulting earthquake PDF more accurately reflects the geological relations based on trench stratigraphy, but still allows the earthquake to occur within the full time range of the constraining ages. See DuRoss and others (2011) for details.

In the following discussion, we assess the times of faulting from the oldest surface rupture (earthquake WC4) to the youngest rupture (earthquake WC1) at the Willow Creek site. We also report the first indirect evidence of earthquake(s) WC4, the fourth Holocene-age earthquake on the Nephi segment. Unfortunately, our constraints on the time of earthquake WC4 are very broad, which is reflected by the wide, flat PDF for this earthquake (figure 10). We can only establish that earthquake WC4 predates earthquake WC3 and is younger than the 6.2 ka age of the footwall fan deposits in the WCN trench. With such broad constraints, the OxCal model yields a mean of 4700 ± 1760 cal yr B.P. for earthquake WC4 (2σ uncertainty); we round this to 4.7 ± 1.8 ka.

The age constraints for earthquake WC3 are also broad, but based on the age of the alluvial-fan deposits in the footwall of the WCS trench, it must be younger than about 2.2–2.6 ka. We are unable to constrain the minimum time of earthquake WC3 because of erroneous ages for samples that included either burrowed (R5 and L1) or partially bleached (L05) sediment. The OxCal model yields an age of 1930 ± 560 cal yr B.P. for earthquake WC3 (rounded to 1.9 ± 0.6 ka). Given the lack of a minimum constraint on the time of unit CW3, we consider it more likely that this event occurred closer to the maximum limiting ages rather than the time of unit CW2, which is a minimum constraint in the OxCal model.

Our OxCal model yields an age of 1220 ± 120 cal yr B.P. for earthquake WC2 (rounded to 1.2 ± 0.1 ka). The time of earthquake WC3 (~1.9 ka) provides only a broad maximum limit for earthquake WC2, whereas ^{14}C ages of ~1.0–1.2 ka for charcoal derived from the top of the CW2 colluvial wedge (WCN trench) provide a closer minimum limit.

Finally, the OxCal model yields a time of 210 ± 80 cal yr B.P. (rounded to 0.2 ± 0.1 ka) for earthquake WC1, which suggests that the most recent surface rupture occurred less than one century before European settlement in Utah in 1847. The age of unit Cw1 is well constrained by maximum limiting ages of ~0.2–0.4 ka for soil A horizons that predate the earthquake and the uppermost part of unit Cw2 colluvium, and a 0.2-ka minimum age for a soil developed on unit Cw1. The youthfulness of this earthquake is consistent with the geomorphic expression of the most recent rupture along the range front north of Nephi. There, between Red Canyon and Little Birch Creek, the youngest rupture along the western face of the foothills is largely unvegetated and has a very fresh appearance. It is also consistent with Machette's (1984) observation that the most recent earthquake on the Nephi segment is young based on the steep maximum slope-angles for the scarps.

Displacement Per Earthquake at Willow Creek

Accurately measuring or estimating the vertical displacement associated with an individual surface rupture is complex and subject to multiple sources of uncertainty. Various methods have been applied to estimate the displacement per earthquake including total vertical stratigraphic displacement, measurements of surface offset, colluvial-wedge thickness, and trench retrodeformation, but each approach has its strengths and shortcomings (DuRoss, 2008). In the simplest model of fault-scarp degradation on a gently sloping alluvial fan, the maximum thickness of a colluvial wedge is about one-half of the initial size of the surface rupture, so doubling the wedge thickness is a first-order approximation of the earthquake's vertical displacement (Ostenaa, 1984; McCalpin, 2009). However, in cases where multiple colluvial wedges are stacked upon each other, the geometry of individual wedges deviates from the simple triangular cross section because successive wedges are usually deposited on progressively steeper sloping surfaces. As a result, in a sequence of stacked wedges, the younger wedges tend to have a more lenticular cross-sectional shape rather than the triangular shape of an idealized, single-earthquake wedge (for example, see Nelson, 1992). Because of this progressive change in cross-sectional shape, it is difficult to measure the thicknesses of individual wedges that truly represent the vertical displacement for each earthquake. Furthermore in both Willow Creek trenches, the geometry and dimensions of the oldest wedge have been greatly distorted by shearing and the formation of fissures during subsequent earthquakes. Given these circumstances, we follow the precedent of DuRoss (2008) and simply divide the estimated net vertical offset by the number of earthquakes to estimate the average displacement per earthquake.

To determine cumulative net vertical displacement, we use data from scarp profiles and stratigraphic information from the trenches. Scarp profiles near the WCN and WCS trenches (figure 6) show surface offsets of 6.5 m and 5.9 m, respectively. These values are first-order estimates of the net vertical displacement, but as noted previously, the hanging wall at both trench sites is buried by younger alluvium, so these surface offsets are minimum values.

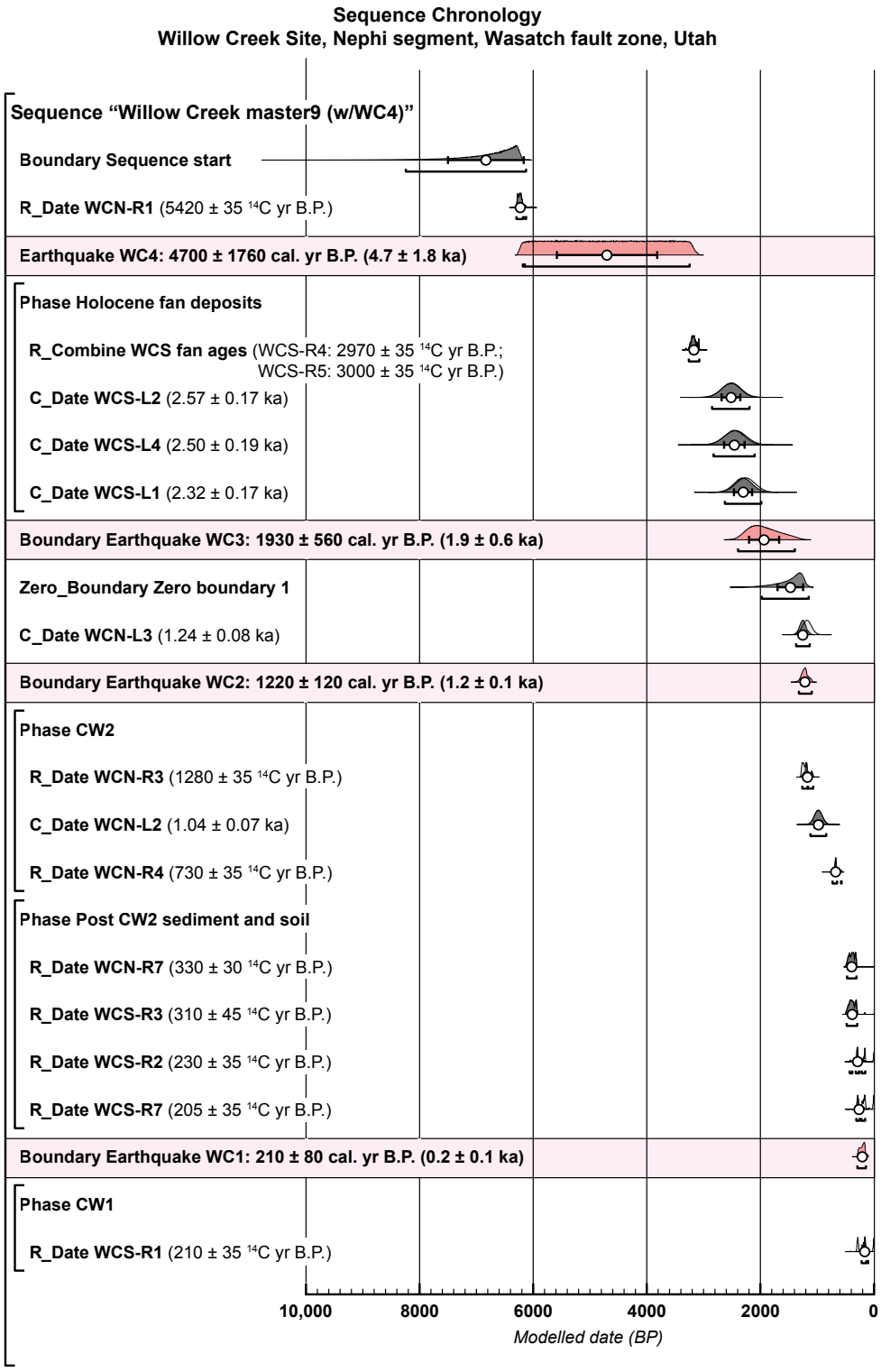

OxCal v4.1.7 Bronk Ramsey (2010); r:5 Atmospheric data from Reimer and others (2009)

Figure 10. *Results of final OxCal model for the Willow Creek trenches. Model name is "Willow Creek master9 (w/WC4)." It was generated using OxCal v4.1.7 (Bronk Ramsey, 2001, 2008, 2010), and it shows the chronology of depositional phases and surface-faulting earthquakes based on data from the trenches. WCN refers to units and samples from the Willow Creek North trench and WCS from the Willow Creek South trench; samples labeled with "R" are radiocarbon ages (referenced to AD 1950), samples labeled with "L" are luminescence ages (referenced to 2010). Historic constraint is based on the lack of large earthquakes since European settlement of the Wasatch Front in 1847 (http://historytogo.utah.gov/facts/brief_history/mormonsettlement.html) and in the town of Nephi in 1851 (http://www.uen.org/utah_history_encyclopedia/n/NEPHI.html). Ages are listed in a sequence (they are in stratigraphic order with no depth constraints) and in one phase (stratigraphic order of the samples is unknown). Light gray areas of probability density functions (PDFs) are distribution of calibrated radiocarbon and luminescence ages before modeling, and dark gray areas are PDFs resulting from OxCal modeling (Bayesian analysis) to determine time constraints of specific earthquakes. White dots are weighted means; brackets are 2σ uncertainties. See table 1 for details of age analyses. OxCal code is in appendix C.*

To better estimate the minimum tectonic throw, we merge the scarp profile near the WCN trench (profile m83-36 of Machette and others, 2007; appendix B) with stratigraphic information in the trench (figure 7A). The scarp profile shows that the alluvial-fan surface on the footwall has a slope of about 11°, which is comparable to the 11.7° dip on beds in the hanging wall (figure 11A). If we project the 11° fan-surface slope to the fault zone and also project an 11° dip of beds from the deepest part of the subsidiary trench (because units 4-1 to 3-1 in this trench postdate earthquakes WC1–3) back to the fault zone, we measure a surface offset of 8.1 m. Thus the actual vertical offset of the mid-Holocene (6.2 ka) deposits in the WCN trench must be greater than 8.1 m.

We use a similar approach to measure the net vertical displacement at the WCS trench, where our revised analysis of profile m83-33 (Machette and others, 2007; appendix B) indicates a surface offset of about 5.9 m (figure 6B). In this trench, we exposed age-correlative deposits on both sides of the fault (figures 8 and 11B). However, the surface of the hanging wall has been buried by young fluvial sand and gravel from recent deposits of Willow Creek (units 1-2 and 1-3, figure 8; channel fill in figure 11B). We exposed at least 1.5 m of this deposit in the WCS trench.

Our best estimate of the net vertical displacement at the WCS site is based on projecting the 5° fan-surface slope on the footwall and the top of the buried fan surface beneath the channel fill in the hanging wall, which has a dip of about 6°. This dip is similar to the 6.5° dip of the bedding and to the 5° slope of the footwall alluvial-fan surface. Extending these projections to the fault zone yields a vertical stratigraphic displacement of 7.1 m with an estimated uncertainty of ± 0.2 m.

If we divide the vertical displacement by the number of earthquakes, we get a displacement-per-earthquake of >2.0 m (8.1

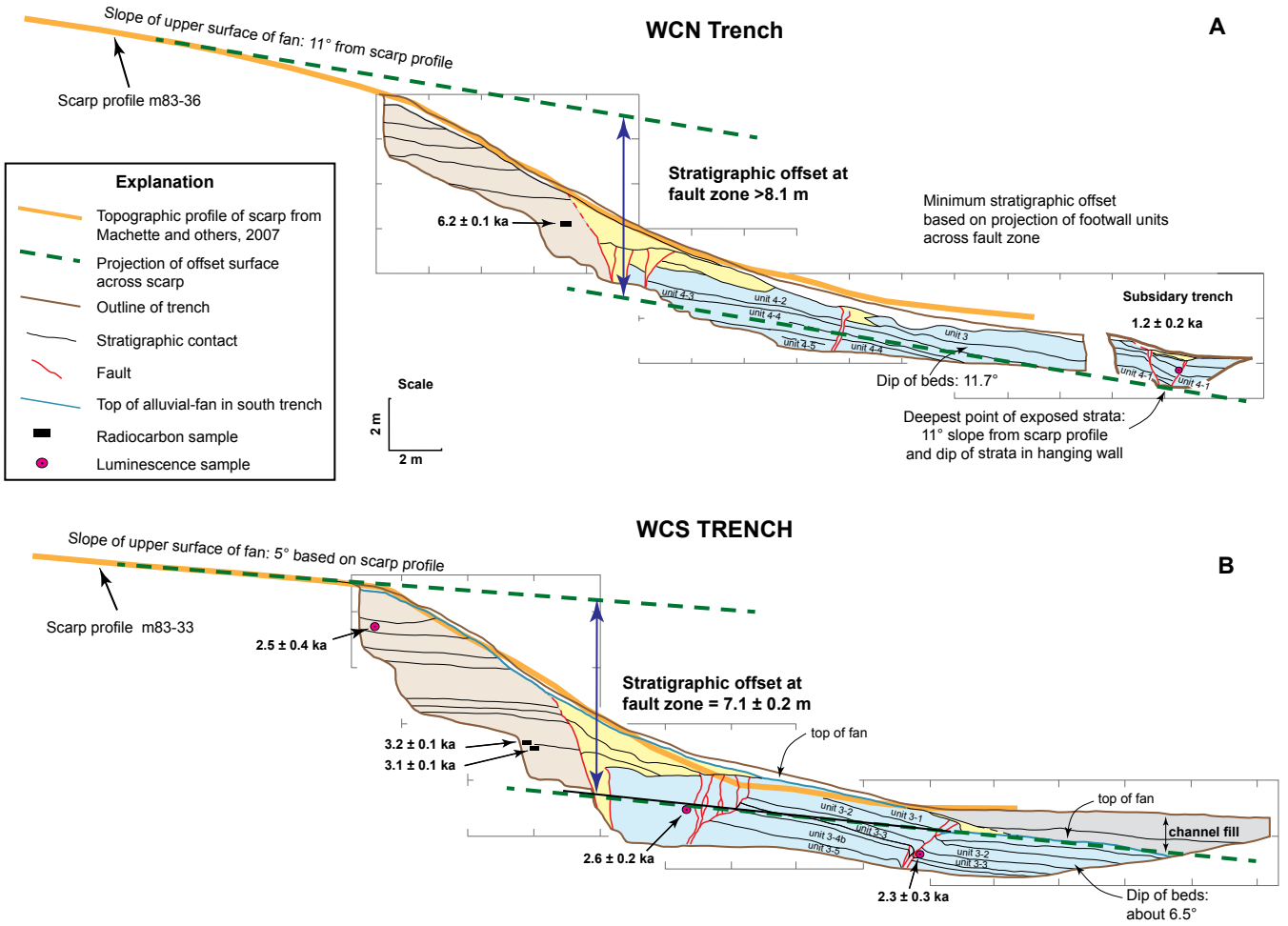

Figure 11. *Simplified diagrams of the Willow Creek trenches showing stratigraphic relations used to estimate the vertical displacement across the fault zone. See Machette and others (2007) for detailed maps of these trench exposures (included as appendix B of this report). In the Willow Creek North (WCN) trench (A), stratigraphic units in the footwall were not exposed in the hanging wall, so our measured vertical stratigraphic displacement is a minimum value. In the Willow Creek South (WCS) trench (B), the age of stratigraphic units in the hanging wall and footwall are largely contemporaneous, so the vertical stratigraphic displacement is a realistic estimate of the tectonic displacement at the fault zone.*

m/4 earthquakes) from the WCN trench, and a value of 2.4 m (7.1 m/3 earthquakes) from the WCS trench. These values are comparable to the average value of 2.0 ± 0.6 m per earthquake estimated by DuRoss (2008) for the Nephi segment. Our preferred value of 2.4 m per earthquake is similar to the range of vertical displacements from other paleoseismic studies on the Nephi segment and is essentially the same as the preferred displacement values from the North Creek site, which is also in the central part of the southern strand (table 2).

Late Holocene Vertical Slip Rate at Willow Creek

Estimating a vertical slip rate relies on accurate measures of the vertical tectonic displacement during a specified time interval. Our best measures of vertical displacement and stratigraphic age are from the WCS trench, where we document 7.1 m of vertical displacement in alluvial-fan deposits that have an age in the range of 2.6 ± 0.2 ka to 2.3 ± 0.3 ka (L02 and L01 in figure 8); thus they could be as young as 2.0 ka and could be as old as 2.8 ka. If we use a mean age of about 2.5 ka, then the late Holocene slip rate is 2.8 mm/yr with a range of 2.5–3.6 mm/yr. Note that in this discussion we use open-interval slip rates, which span the time interval from the age of the faulted deposit to the present. With sufficiently detailed data on the times of past earthquakes, it is possible to determine closed-interval slip rates, which span the time between the oldest dated earthquake and the youngest dated earthquake. We use the open-interval rates here, in part, because it is a commonly used way to cite slip rates.

The slip rate estimated at the WCN trench is a based on a minimum vertical displacement of 8.1 m on 6.2-ka fan deposits. This yields a minimum slip rate of 1.3 mm/yr because the actual vertical displacement on the fan deposits must be greater than 8.1 m.

Our best-constrained slip rate is from the WCS site, and is considerably higher than the preferred rate of 1.1 mm/yr estimated by the UQFPWG (Lund, 2005). Our maximum rate of 3.6 mm/yr exceeds the group's 3.0 mm/yr upper bound for a slip rate (Lund, 2005). DuRoss and Bruhn (2004) report a slip rate of 0.5–0.7 mm/yr since the mid-Holocene based on the chronology of inferred earthquakes that they derived from a morphological analysis of fault scarps along the entire Nephi segment. Using the data of Jackson (1991), Mattson and Bruhn (2001) reported a short-term (since 4.3 ka) slip rate of 1.3 mm/yr at the Red Canyon site, where the average size of scarps at the southern end is smaller than elsewhere on the segment. Machette and others (1992) reported an average mid-Holocene slip rate of 0.8–1.0 mm/yr at Gardner Creek near Nephi, and Harty and others (1997) reported a slip rate of 0.7–1.0 mm/yr at Willow Creek (assuming a middle Holocene

Table 2. *Summary of vertical displacements at paleoseismic study sites on the Nephi segment.*

Site Name[1]	Earthquake name	NVTD[2]	Displacement[2]			Reference (s)	Comments
			Average	Preferred	Range		
SQ	SQ1	2.2–3.3	2.2–3.3	3.0 ± 0.2	—	DuRoss and others (2008)	Only one earthquake at site.
NC		7.0 ± 0.2	2.2–3.8	—	—	Hanson and others (1981); Schwartz and Coppersmith (1984)	From profile of fault scarp.
	NC1			2.0–2.2	1.0–4.5		From fault displacements.
	NC2			2.0–2.5			From colluvium thickness.
	NC3			2.6			From height of strath terrace.
WC		7.1 ± 0.2	2.4			This report	Based on stratigraphic throw in WCS trench.
	WC1			2.4			One-third of NVTD.
	WC2			2.4			One-third of NVTD.
	WC3			2.4			One-third of NVTD.
RC		5.4 ± 0.3				Jackson (1991)	Based on stratigraphic throw measured in trench.
	RC1			1.4 ± 0.3			From colluvium thickness.
	RC2			1.5 ± 0.2			From colluvium thickness.
	RC3			1.7 ± 0.3			From colluvium thickness and fault displacements.

[1] Site names are: Santaquin, SQ; North Creek, NC; Willow Creek, WC; Red Canyon, RC.
[2] NVTD, net vertical tectonic displacement. All displacement values are in meters.

age for the faulted alluvial fan) and a range of 0.5–1.2 mm/yr for the entire segment.

The wide range in reported slip-rate values for the Nephi segment largely reflects the poor age control for the faulted deposits (table 3). At Willow Creek, we have internally consistent and well-defined ages for the faulted deposits, so our rate of 2.5–3.6 mm/yr for the past 2.5 ka is based on well-dated deposits. However, we recognize that this slip rate spans a very short time interval, whereas other reported slip rates span up to tens of thousands of years. The sequence of three surface-faulting earthquakes in the past 2.5 kyr at Willow Creek may be evidence of earthquake clustering, which was suggested by Machette and others (1992), McCalpin and Nishenko (1996), and Friedrich and others (2003) for the entire WFZ. We discuss the subject of clustering later in this report.

PREVIOUS STUDIES OF PREHISTORIC RUPTURES ON THE NEPHI SEGMENT

Other than our study at Willow Creek, information about prehistoric ruptures on the Nephi segment is currently based on data from three sites: North Creek and Red Canyon, which were studied in the late 1970s and early 1980s, and Santaquin, which was studied contemporaneously with our work at Willow Creek (figure 2). An additional site near Spring Lake near the northern end of the segment has been recently studied, but the only pub-

Table 3. *Site-specific measurements of vertical displacement and inferred slip rate on the Nephi segment. Sites with asterisk (*) are on northern strand of segment; all other sites are on southern strand.*

Site name	Location (Lat., long.)[1]	VD (m)[2]	Deposit age (ka)	Inferred slip rate (mm/yr)	Comment[2]	Reference(s)
Spring Lake area*	40.00228, 111.73368	SH: 4 m; SO: 3 m	afy (Holocene to uppermost Pleistocene)[3]	0.5	NW flank of Dry Mtn., S of Payson, UT	Machette, 1992
Santaquin*	39.98159, 111.76126	3.0 ± 0.2	6.8–7.0	0.4–0.5	VD is SO across scarp	DuRoss and others, 2008
Santaquin*	39.98159, 111.76126	9.0	16.8	0.5	VD of Bonneville shoreline	DuRoss and others, 2008
North Creek	39.85550, 111.80445	4.3	4.8–5.5	0.8–1.2	Rate for closed interval between earthquakes NC3 and NC1	Harty and others, 1997
North Creek	39.85550, 111.80445	7.0 ± 0.5 NVTD	5.2 ± 0.3[4]	1.2–1.5	Rate for open interval between age of faulted gravel and present	Hanson and others, 1981, 1982
Willow Creek North	39.79844, 111.81855	>8.1 STRAT	6.2 ± 0.1	>1.3	STRAT from figure 15A; time from figure 13.	This report
Willow Creek South	39.79758, 111.81839	7.1 STRAT	2.4 ± 0.2	2.6–3.4	STRAT from figure 15B; time from figure 13.	This report
Gardner Creek	39.74759, 111.08265	2.6[5]	4–6	0.7–1.0	Closed interval between MRE and third earthquake	Harty and others, 1997
Gardner Creek	39.74759, 111.08265	30	250	0.12	Long-term, pre-Bonneville slip	Harty and others, 1997; Machette, 1984.
Red Canyon	39.74134, 111.82688	2.9 ± 0.5	3.0–5.5	0.6–0.8[6]	Closed interval rate between RC3 and RC1	Harty and others, 1997
Red Canyon	39.74134, 111.82688	3.6 ± 0.2	3.0–5.5	0.7–1.0[7]	Closed interval rate between RC3 and RC1	Harty and others, 1997
Red Canyon	39.74134, 111.82688	5.4 ± 0.3 NVTD	4.0–4.5	1.1–1.4	Open interval rate from time of RC3 to present	Jackson, 1991

[1] Location is north latitude and west longitude in degrees (WGS84 datum).
[2] Abbreviations: SH, scarp height; SO, surface offset; NVTD, net-vertical tectonic displacement; STRAT, stratigraphic displacement; VD, vertical displacement; MRE, most recent earthquake.
[3] Machette (1992) applied the label of afy to young alluvial-fan deposits "where the specific age of Holocene deposits has not been determined." For purposes of this calculation, we use a general age of 6.2 ka based on the age of the dated fan gravel at the Willow Creek North site.
[4] Based on OxCal calibration of a radiocarbon age of 4580 ± 250 yr B.P. collected by R.C. Bucknam from alluvium of North Creek fan and reported in Hanson and others (1982).
[5] Assumes earthquake times are the same as at North Creek and uses NVTD value equal to two-thirds of the 3.9 m of surface offset.
[6] Values reported as Red Canyon A site in table 1 of Harty and others (1997).
[7] Values reported as Red Canyon B site in table 1 of Harty and others (1997).

lished information from this work is in an abstract (Horns and others, 2009); detailed results have yet to be published.

Paleoseismology of the North Creek Site

The first study to identify prehistoric earthquakes on the Nephi segment was conducted at North Creek along the north-central part of the segment (figure 2), and the results were reported by Hanson and others (1981, 1982), Schwartz and others (1983), and Schwartz and Coppersmith (1984). These pioneering studies reported evidence for three Holocene surface ruptures, but were only able to establish broad bounds for the times of each rupture. The three trenches at North Creek exposed colluvial deposits from two surface-faulting earthquakes, and a third earthquake was inferred from an inset stream terrace that is preserved on the upthrown side of the fault (figure 12).

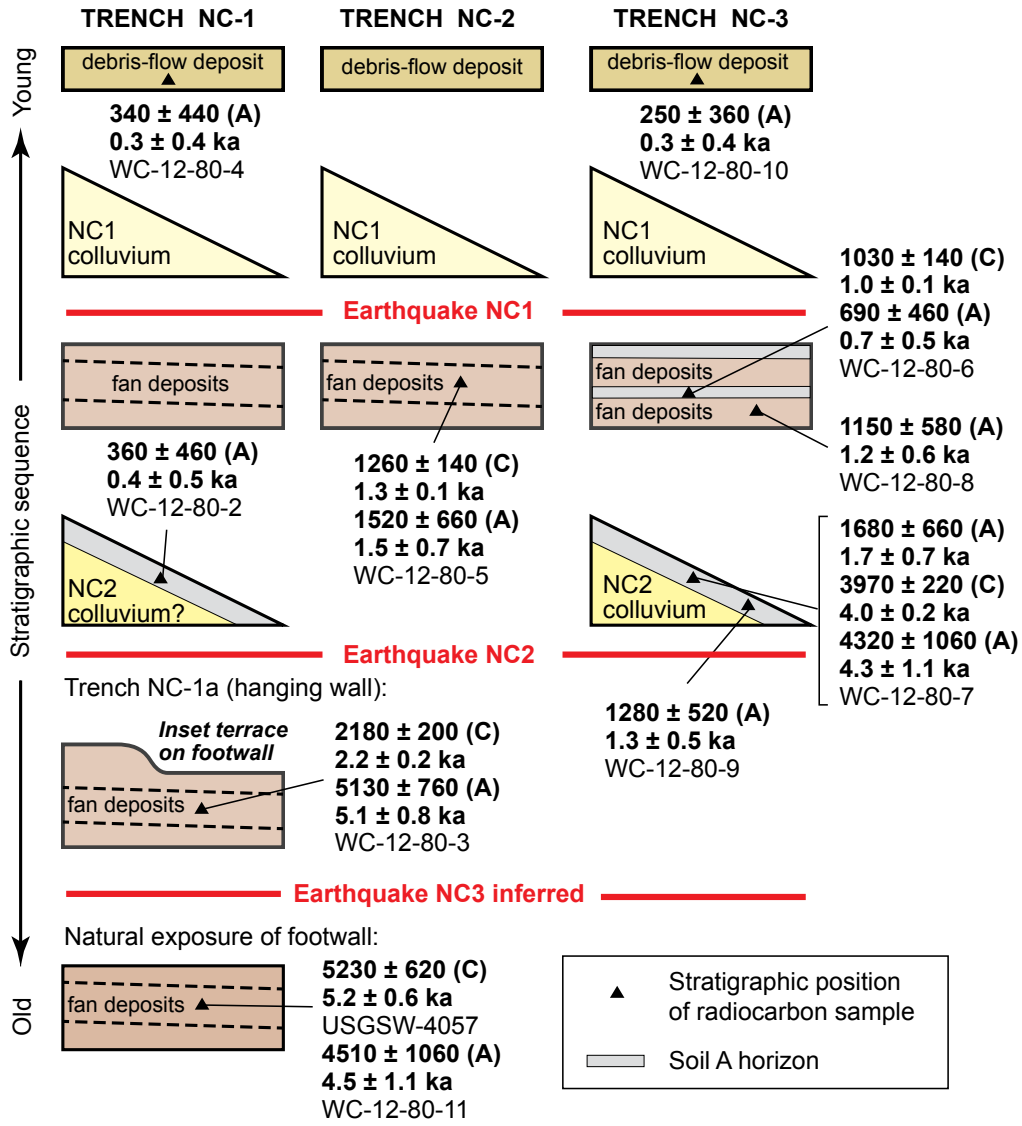

Figure 12. *Schematic diagram showing the stratigraphic relations of radiocarbon ages at the North Creek site; modified from Hanson and others (1981, 1982). Bold numbers are calibrated ages (cal yr B.P.) using OxCal v4.1.7, and non-bold type denotes sample identification names. Ages determined using conventional (proportional counting) radiocarbon techniques are indicated by "C"; ages determined by accelerator mass spectrometry are indicated by "A." The suite of radiocarbon ages between colluvial units NC1 and NC2 permit two interpretations. An "older" interpretation is that NC2 colluvium is in the age range of about 3–4 ka, whereas the "younger" interpretation is that NC2 colluvium is in the age range of about 1–2 ka. Our reevaluation of all data from sites on the Nephi segment favors the younger interpretation. See table 1 for details of age values.*

Evidence of the youngest surface-rupturing earthquake (North Creek paleoearthquake 1: NC1) consists of a colluvial wedge exposed in all three trenches at the site (Hanson and others, 1981). Fault movement during earthquake NC1 displaced mudflow deposits, alluvium, and scarp-derived colluvium from an older earthquake that is capped by a buried soil. Radiocarbon ages from the organic material in the faulted, buried soil A horizon and from charcoal in faulted alluvial-fan deposits provide a maximum time for the earthquake (table 1). These ages indicate that earthquake NC1 is younger than about 1.0–1.5 ka (figure 12; samples WC-12-80-5, WC-12-80-6, and WC-12-80-8), but Schwartz and others (1983) and Schwartz and Coppersmith (1984) estimated that this earthquake occurred within the past 300 to 500 years on the basis of the steep maximum-slope angles of the scarp (report as 40–42° in Harty and others, 1997) and the proximity of the fault scarp to a knickpoint in a small channel in the footwall. This estimate of a few hundred years for the time of the youngest earthquake is consistent with the unvegetated character of the fault scarp at the North Creek site (figure 13). Note that we calibrated the ^{14}C ages from the original sources to the nearest 10 years using OxCal version 4.1.7 (Bronk Ramsey, 2001; 2008) and report the calibrated ages in cal yr B.P. with 2σ uncertainty values. The original, uncalibrated ages are used in the input for all of the OxCal models, so all OxCal models in this report are internally consistent. For information about the OxCal program, see http://c14.arch.ox.ac.uk/embed.php?File=index.html.

The minimum time of the preceding earthquake (NC2) is constrained by ^{14}C ages from charcoal and bulk soil samples from the soil on NC2 colluvium, and in the overlying sediments (Hanson and others, 1981, 1982). Schwartz and Coppersmith (1984) and Hanson and others (1982) relied on two ^{14}C ages of 4.0 ± 0.2 ka and 4.3 ± 1.1 ka (WC-12-80-7; table 1) to define the minimum time since earthquake NC2, but there were ages from several other samples that stratigraphically define a minimum time for earthquake NC2 (WC-12-80-2, WC-12-80-7, and WC-12-80-9 in figure 12; table 1). We dismiss the age for WC-12-80-2 of 0.4 ± 0.5 ka because it is young for its stratigraphic position and has a large uncertainty (figure 12). The remaining ages cluster into two groups: one group at about 1.3–1.7 ka and a second group at about 4.0–4.3 ka. Hanson and others (1982), Schwartz and others (1983), and Schwartz and Coppersmith (1984) favored the older ages because Hanson and others (1981, 1982) considered the younger ages to be contaminated by young carbon. However, it is equally possible that the two older radiocarbon ages are from recycled charcoal fragments and that the younger ages better represent the age of the NC2 colluvium. The younger pair of ages is also consistent with ages of 1.0–1.5 ka from the overlying fan deposits (WC-12-80-5, WC-12-80-6 and WC-12-80-8; table 1). The maximum time for earthquake NC2 is defined by radiocarbon ages from samples WC-12-80-3, WC-12-80-11, and USGSW-4057. The USGSW sample is from charcoal in a burn layer in the North Creek alluvial fan (Bucknam, 1978), which has a rounded age of 5.2 ± 0.6 ka. Sample WC-12-80-3 has two ages, a younger one of 2.2 ka and an older one of 5.1 ka. Based on these ages and the stratigraphic relations, earthquake NC2 could be younger than 2.2 ka, which agrees with our earthquake chronology at Willow Creek.

At North Creek, earthquake NC3 is an inferred earthquake based on a small inset fluvial terrace on the fault footwall and has no minimum age constraints to separate it from earthquake NC2. The only age constraint on earthquake NC3 is that it is younger than the 4.5-ka to 5.2-ka age of the North Creek alluvial-fan deposits into which the terrace is incised.

In summary, previous investigations interpret all three earthquakes at North Creek to be younger than about 5.2 ka, and the two older earthquakes, NC2 and NC3, to have occurred prior to the older ages from sample WC-12-80-7. The most recent earthquake is younger than 1.0–1.3 ka and has a preferred time of 0.3–0.5 ka.

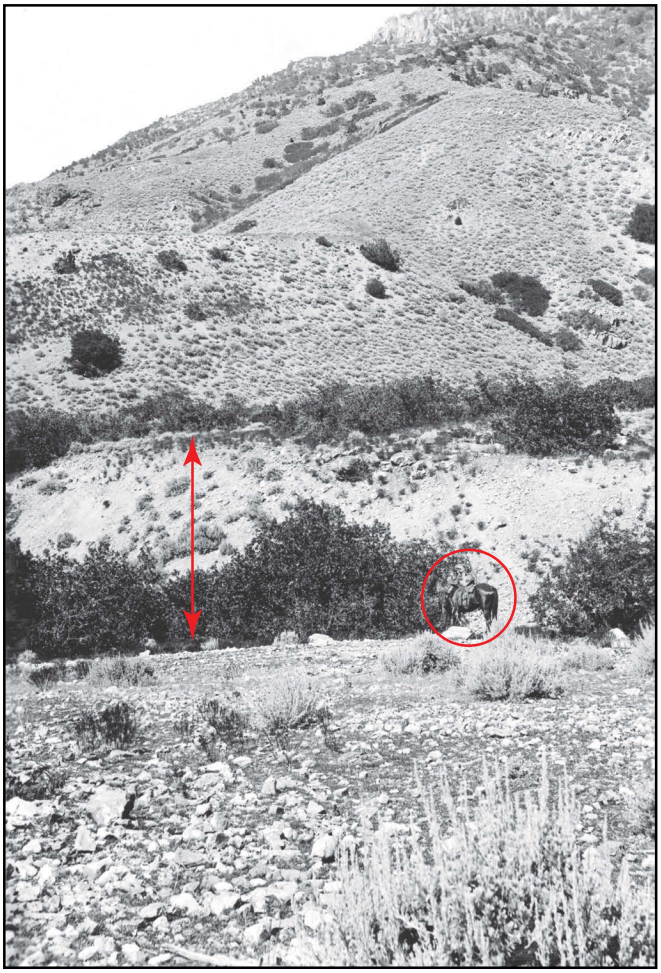

Figure 13. *Photograph by F.B. Weeks showing the fault scarp at the North Creek site along the Nephi segment. The steep, unvegetated slope on the scarp face suggests a young surface rupture on the fault at this site. Circle shows horse and rider for scale. Arrows show approximate 8-m height of youthful fault scarp. Photo is from U.S. Geological Survey Photographic Library, F.B. Weeks photo 82, taken August 9, 1903.*

OxCal Model of Prehistoric Earthquakes at the North Creek Site

To better refine the times of earthquakes at the North Creek site, we developed an OxCal model in a manner similar to that for the Willow Creek site (appendix C). Our model incorporates the stratigraphic evidence and age constraints of two surface-rupturing earthquakes (Hanson and others, 1981, 1982) and of the inferred third earthquake (figure 14).

As previously discussed, the uncalibrated ^{14}C ages from the North Creek study cluster into two broad sets of values (figure 12), and the original interpretations of the North Creek data favored the older set of ages. However, given the new data on earthquake times at Willow Creek, we favor the younger group of ages and developed our OxCal model using these younger values. The North Creek OxCal model (figure 14) indicates earthquake NC1 occurred at 440 ± 460 cal yr B.P., rounded to 0.4 ± 0.5 ka, earthquake NC2 occurred at 1390 ± 300 cal yr B.P., rounded to 1.4 ± 0.3 ka, and earthquake NC3 occurred at 1930 ± 520 cal yr B.P., rounded to 1.9 ± 0.5 ka. The times of these earthquakes are very similar to the earthquake times at Willow Creek. The similar times are especially strong for earthquakes NC2 and NC3, which support our choice of favoring the younger group of ages from the North Creek site (table 4).

Paleoseismology of the Red Canyon Site

In the late 1980s, Jackson (1991) studied the Levan and Nephi segments to test the use of thermoluminescence (TL) dating as a method to determine the times of prehistoric earthquakes. Jackson trenched a 5.5-m-high scarp at Red Canyon near the southern end of the Nephi segment (figure 2), where he identified evidence of three surface-rupturing earthquakes. Jackson used four ^{14}C ages and five TL ages to constrain the times of the earthquakes. His study was one of the first applications of luminescence dating to paleoseismology, and therefore it lacked the refinements of current luminescence analyses. Accordingly, Jackson (1991) specifically stated that his "TL ages should be considered broad age estimates rather than absolute dates."

Jackson mapped three stacked colluvial wedges and a 5-m-wide zone of faulting in his Red Canyon trench (figure 15). He estimated the maximum time of the youngest earthquake (RC1) on the basis of two TL ages and one ^{14}C age from a soil beneath the RC1 colluvial wedge. The rounded TL ages are 1.3 ± 0.5 ka and 1.5 ± 0.4 ka, and the rounded ^{14}C age is 2.9 ± 0.5 ka (table 1). Jackson speculated that the ^{14}C sample was contaminated with old carbon and preferred a time of about 1.2 ka for earthquake RC1.

Evidence for earthquake RC2 is a lenticular colluvial wedge (unit 3, figure 15) that buries a weak soil formed on the colluvial wedge from the preceding earthquake. Two TL ages from the soil A horizon beneath the RC2 colluvial wedge define a maximum time for the earthquake. The rounded TL ages are 1.7 ± 0.2 ka and 7.0 ± 0.8 ka, and the rounded ^{14}C ages are 1.3 ± 0.5 ka and 3.9 ± 0.9 ka. Jackson inferred that the 1.7 ka TL age and the companion 1.3 ka ^{14}C ages are anomalously young because of animal burrowing, and that the 7.0 ka TL age is too old because it may be contaminated by older sheared sediment. He relied on the 3.9 ka ^{14}C age to establish the maximum time for earthquake RC2, and he favored a time interval of 3.0–3.5 ka for the earthquake.

The third earthquake (RC3) is older that the 3.9-ka ^{14}C age because the sample is from the soil that formed on the RC3 colluvial wedge. An additional ^{14}C age from near the base of the RC3 colluvial wedge yielded an overlapping age of 3.6 ± 0.8 ka, supporting the interpretation that earthquake RC3 is older than 3.9 ka.

The maximum time for earthquake RC3 is very poorly constrained; it is younger than the age of the Red Canyon alluvial fan, which has an inferred age of 10–15 ka (Jackson, 1991). Jackson also correlated earthquake RC3 with the oldest earthquake (NC3) at the North Creek site and noted that his preferred time of earthquake RC3 (4.0–4.5 ka) generally agrees with the maximum age constraint of 4.5–5.2 ka for earthquake NC3. Thus, earthquake RC3 is thought to have occurred between 3.9 ka and the 4.5–5.2 ka age of the fan alluvium at North Creek. Jackson preferred a time of 4.0–4.5 ka for earthquake RC3.

OxCal Model of Prehistoric Earthquakes at the Red Canyon Site

Similar to the Willow Creek and North Creek sites, we developed an OxCal model using Jackson's (1991) data to refine the times of earthquakes at Red Canyon (appendix C). Our model incorporates the stratigraphic evidence and age constraints for three surface-rupturing earthquakes (figure 16).

It is worth repeating that Jackson's study was one of the first to use luminescence dating to constrain the times of paleoearthquakes, and since his study, luminescence methodologies and precision have improved considerably. Several of Jackson's ages are stratigraphically out-of-order, and in some instances, co-located ^{14}C and TL ages yielded inconsistent values. Even though these obvious problems reduce our confidence in the accuracy of the Red Canyon OxCal model, the modeling results yield earthquake times that are broadly consistent with the results from North Creek and Willow Creek (table 3).

The OxCal model for Red Canyon indicates earthquake RC1 occurred at 490 ± 540 cal yr B.P. (rounded to 0.5 ± 0.5 ka), earthquake RC2 occurred at 1160 ± 340 cal yr B.P. (rounded to 1.2 ± 0.3 ka), and earthquake RC3 occurred at 4710 ± 2680 cal yr B.P. (rounded to 4.7 ± 2.7 ka) (figure 16, table 4).

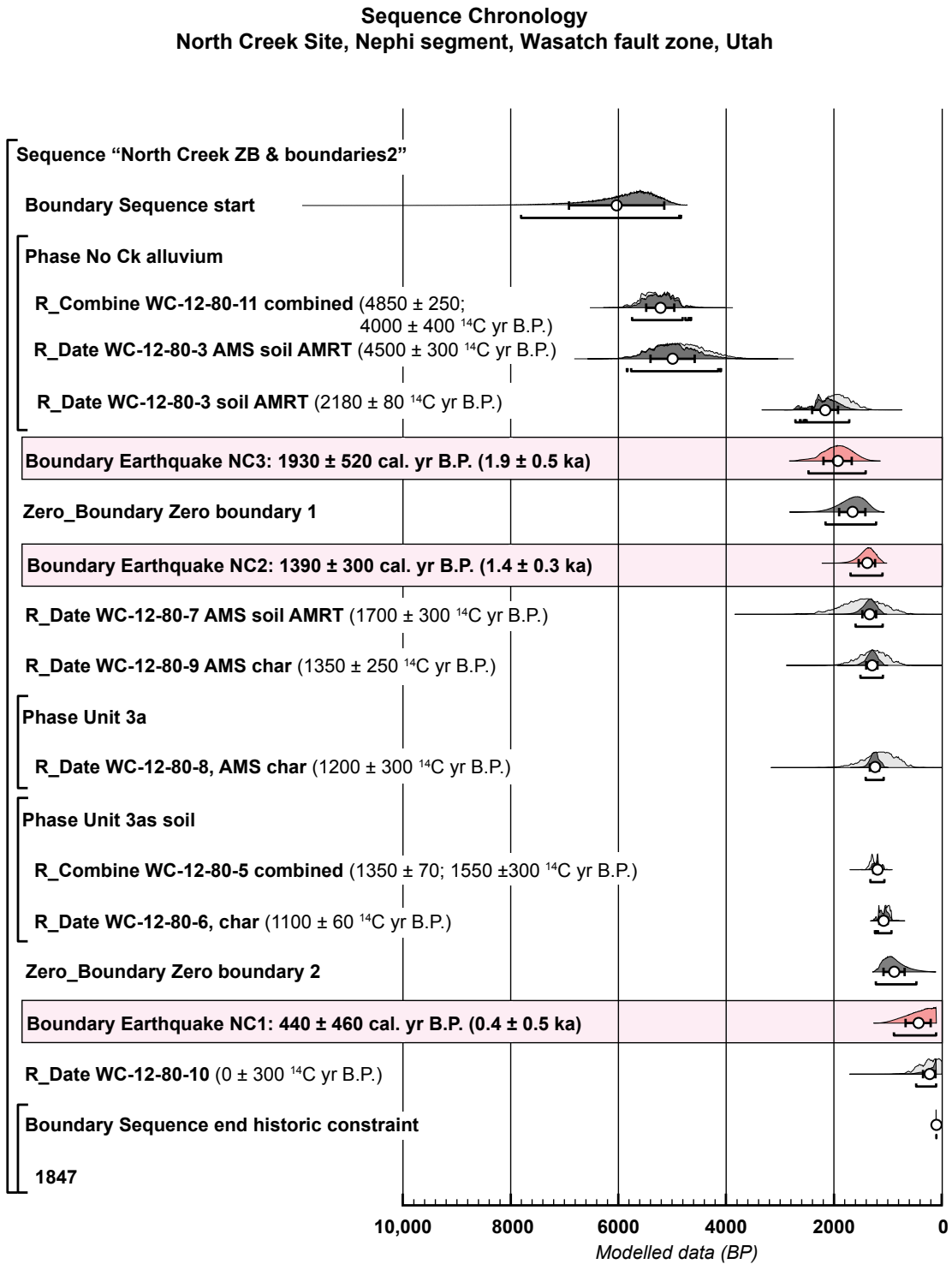

OxCal v4.1.7 Bronk Ramsey (2010); r:5 Atmospheric data from Reimer and others (2009)

Figure 14. *Results of final OxCal model for the North Creek trenches. Model name is "North Creek ZB & boundaries2." It was generated using OxCal v4.1.7 (Bronk Ramsey, 2001, 2008, 2010), and it shows the chronology of depositional phases and surface-faulting earthquakes based on data from the North Creek site reported by Hanson and others (1981, 1982). Radiocarbon ages are referenced to AD 1950. Historic constraint is based on the lack of large earthquakes since European settlement of the Wasatch Front in 1847 (http://historytogo.utah.gov/facts/brief_history/mormonsettlement.html) and in the town of Nephi in 1851 (http://www.uen.org/utah_history_encyclopedia/n/NEPHI.html). Ages are listed in a sequence (in stratigraphic order with no depth constraints) and in one phase (stratigraphic order unknown). Light gray areas of probability density functions (PDFs) are distribution of calibrated radiocarbon ages before modeling, and dark gray areas are PDFs resulting from OxCal modeling (Bayesian analysis) to determine time constraints of specific earthquakes. White dots are weighted means; brackets are 2σ uncertainties. See appendix C for OxCal code.*

Table 4. *Summary of earthquake times from OxCal models and probable correlation of earthquakes on the southern strand of the Nephi segment*[1].

Nephi segment earthquake	North Creek site (NC)	Willow Creek site (WC)	Red Canyon site (RC)	Segment-wide earthquake times	UQFPWG consensus[2]
N1	0.4 ± 0.5 ka (440 ± 460)	0.2 ± 0.1 ka (210 ± 80)	0.5 ± 0.5 ka (490 ± 540)	0.2 ± 0.1 ka (210 ± 90)	≤1.0 ± 0.4 ka
N2	1.4 ± 0.3 ka (1390 ± 300)	1.2 ± 0.1 ka (1220 ± 120)	1.2 ± 0.3 ka (1160 ± 340)	1.2 ± 0.1 ka (1230 ± 100)	3.9 ± 0.5 ka
N3	1.9 ± 0.5 ka (1930 ± 520)	1.9 ± 0.6 ka (1930 ± 560)	ND?	2.0 ± 0.4 ka (2000 ± 390)	>3.9 ± 0.5 ka and <5.3 ± 0.7 ka
N4	ND	4.7 ± 1.8 ka (4700 ± 1760)	4.7 ± 2.7 ka (4710 ± 2680)	4.7 ±1.8 ka (4700 ± 1770)	

[1] Table includes 2σ values for uncertainty in earthquake times. Times are rounded to 100 years and are in ka; specific results from OxCal models in years are shown in parentheses and are in calibrated years before present (BP). ND, not identified at site. Earthquake SQ1 on the northern strand is not included because its correlation with these earthquakes is uncertain; see text for discussion.
[2] Consensus times of earthquakes from the UQFPWG (Lund, 2005).

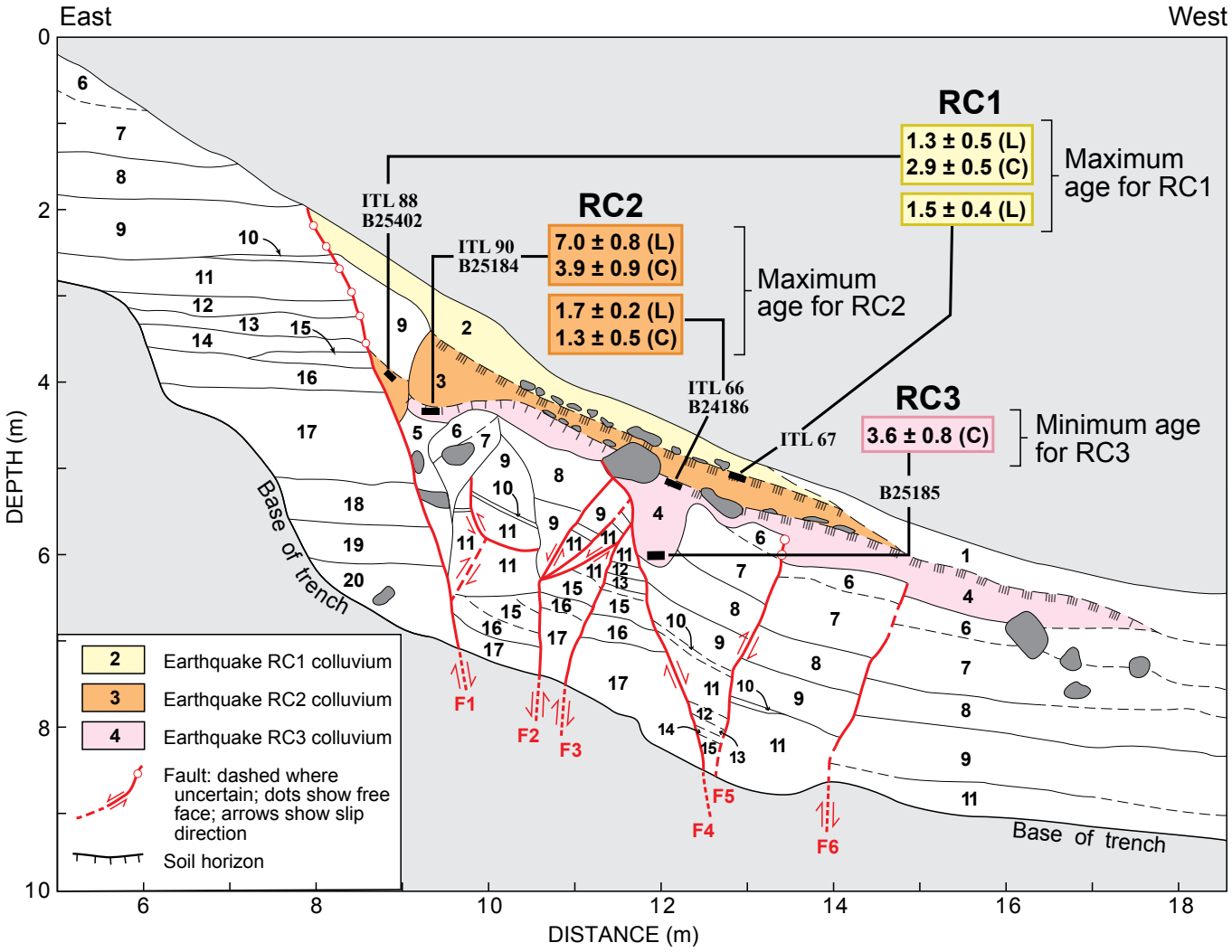

Figure 15. *Trench map showing the stratigraphic relations and locations of radiocarbon (C) and thermoluminescence (L) samples in the Red Canyon trench; modified from Jackson (1991). Numbers label stratigraphic units of Jackson (1991). Units 1–5 are faulting-related colluvial deposits. The alluvial-fan deposits (units 6–20) are inferred to be latest Pleistocene in age (Jackson, 1991). Jackson identified three colluvial deposits (units 2, 3, and 4) interpreted to be associated with three earthquakes that are younger than about 4.0–4.5 ka. "ITL" identifies thermoluminescence sample numbers; "B" identifies radiocarbon sample numbers. Ages shown are in ka, rounded to the nearest century; see table 1 for details. Irregular gray shapes are selected boulders mapped by Jackson.*

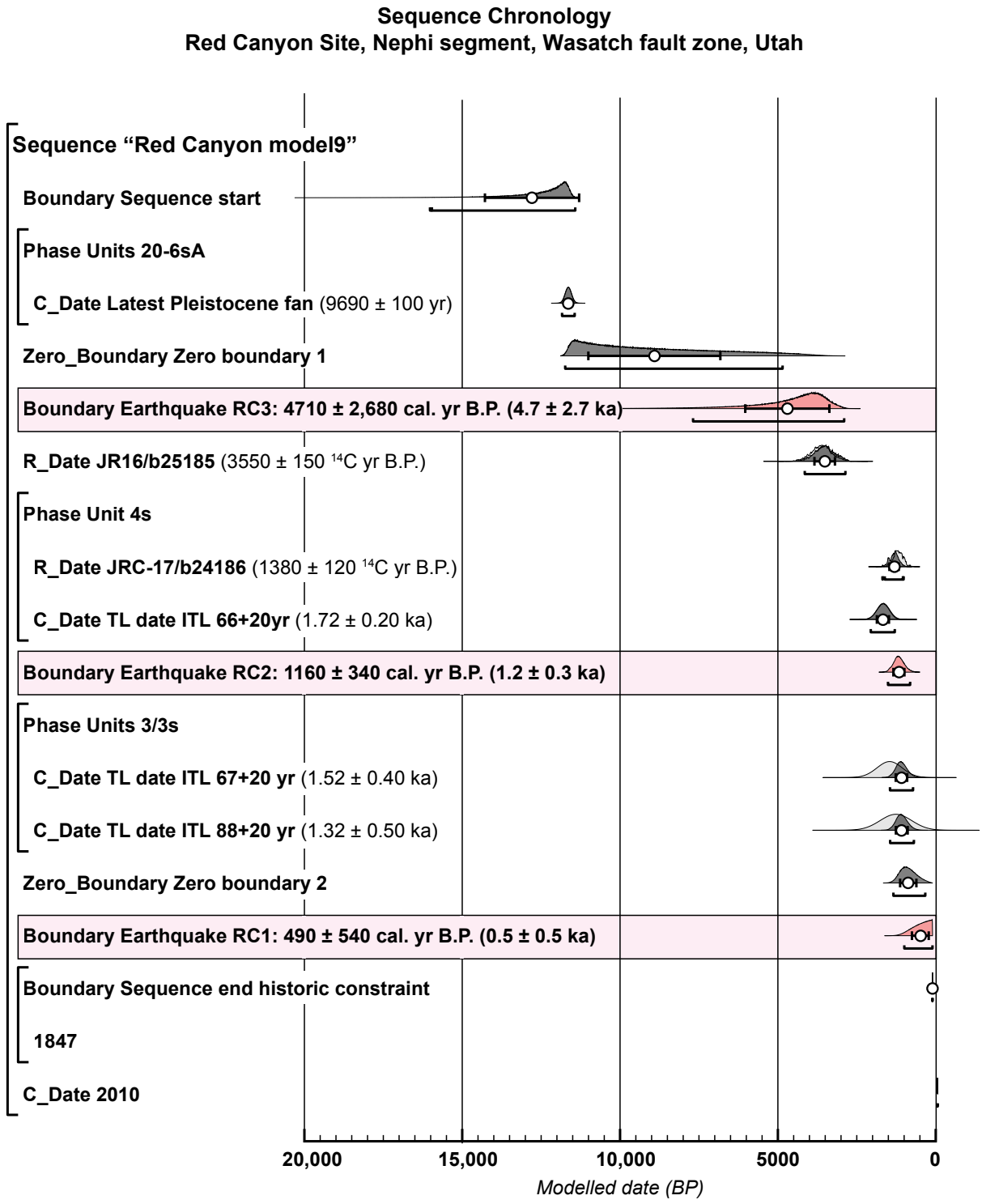

OxCal v4.1.7 Bronk Ramsey (2010); r:5 Atmospheric data from Reimer and others (2009)

Figure 16. *Results of final OxCal model for the Red Canyon trench. Model name is "Red Canyon model9." It was generated using OxCal v4.1.7 (Bronk Ramsey, 2001, 2008, 2010), and it shows the chronology of depositional phases and surface-faulting earthquakes based on data reported by Jackson (1991). Radiocarbon ages are referenced to AD 1950, and luminescence ages are referenced to 2010. Historic constraint is based on the lack of large earthquakes since European settlement of the Wasatch Front in 1847 (http://historytogo.utah.gov/facts/brief_history/mormonsettlement.html) and in the town of Nephi in 1851 (http://www.uen.org/utah_history_encyclopedia/n/NEPHI.html). Ages are listed in a sequence (in stratigraphic order with no depth constraints) and in one phase (stratigraphic order unknown). Light gray areas of probability density functions (PDFs) are the distribution of calibrated radiocarbon and luminescence ages before modeling, and dark gray areas are the PDFs resulting from OxCal modeling (Bayesian analysis) to determine the time constraints of specific earthquakes. White dots are weighted means; brackets are 2σ uncertainties. See appendix C for OxCal code.*

The times of earthquakes RC1 and RC2 correspond well to those of the two youngest earthquakes at Willow Creek and North Creek (table 4), but the correlation of earthquake RC3 with earthquakes at the Willow Creek and North Creek sites is not straightforward because the 2σ uncertainty about the mean time for earthquake RC3 is very large. The large uncertainty results from the poor constraint on the maximum time of earthquake RC3, which is only defined by an estimated latest Pleistocene age for the faulted alluvial fan (figure 16).

The broad time constraints for earthquake RC3 suggest that it may correlate with the oldest inferred earthquake at Willow Creek, WC4, whose age is constrained as younger than 6.2 ka and older than 2.3–2.5 ka. If this correlation is correct, then it implies that no surface rupture at Red Canyon correlates with the WC3 surface rupture (1.9 ± 0.6 ka). This then implies that the WC3 rupture did not extend to the Red Canyon site, which is not unrealistic because Red Canyon is so close to the southern end of the segment.

Fault-scarp Morphology Studies of the Nephi Segment

Little work was done on the Nephi segment following Jackson's 1991 study until DuRoss and Bruhn (2004) evaluated possible rupture scenarios between the northern and southern strands using fault-scarp morphology. Combining their morphological analyses with data from the preceding paleoseismic studies, they developed a preferred scenario in which the timing of earthquakes on the two strands was different, indicating differing rupture histories, at least during the middle and late Holocene. On the southern strand, they preferred times of 1.4 ka and 4.0 ka for the youngest and preceding earthquakes, respectively. On the northern strand, they preferred times of about 0.5 ka and 2.6 ka for the youngest and preceding earthquakes, respectively.

Paleoseismology of the Northern Strand: Santaquin and Spring Lake Sites

DuRoss and others (2008) excavated two trenches across the 3- to 4-m-high scarp near the town of Santaquin. They found evidence of one surface-rupturing earthquake (SQ1) that produced about 3.0 ± 0.2 m of vertical displacement and created a west-facing scarp on an alluvial fan. Fault-scarp mapping indicates that this earthquake ruptured the southern 12 km of the northern strand (DuRoss and others, 2006). Radiocarbon ages on charcoal fragments and their OxCal modeling yield a 2σ time range for this earthquake of 330–550 cal yr B.P., and they preferred an earthquake time of 0.5 ka. Earthquakes older than SQ1 must predate the age of the faulted alluvial-fan sediments exposed in the trench. However, the age of the alluvial fan is difficult to determine as the fan deposits contained both a buried A horizon dated at ~1.5 ka and fragments of reworked (detrital) charcoal from the alluvial-fan sediment (stratigraphically below the buried soil) dated at ~6.9 ka. DuRoss and others (2008) concluded that any earthquakes preceding SQ1 must be older than 1.5 ka and likely older than about 6.9 ka. However, we have less confidence in the 6.9-ka minimum age for any preceding earthquakes because of the potential for an inherited age component to the detrital charcoal sample. DuRoss and others (2008) did not find stratigraphic evidence of a 2.6-ka earthquake on this strand, which was inferred on the basis of DuRoss and Bruhn's (2004) morphological analysis.

Horns and others (2009) excavated a trench across a scarp at the Spring Lake site, which is about 3.3 km northeast of the Santaquin site (figure 2). The Spring Lake trench (SL) is on a separate trace of the northern strand near the boundary with the Provo segment. At Spring Lake, Horns and others (2009) reported evidence of two Holocene surface ruptures and concluded that the earthquakes occurred about 2.5 ka (SL1) and 3.5 ka (SL2) on the basis of ^{14}C ages from organic-rich soils that predate the earthquakes. Using their preferred time of 2.5 ka for earthquake SL1, it is possible that the 500-year-old earthquake at the Santaquin site did not rupture the fault strand at Spring Lake. If accurate, this observation raises important questions about the interaction of individual fault strands on the Nephi and adjacent Provo segments, which we discuss later.

MODELING THE HISTORY OF SURFACE FAULTING ON THE NEPHI SEGMENT

Results from our study at Willow Creek reveal new details about the timing and number of surface-faulting earthquakes on the southern strand of the Nephi segment, and when combined with data from the North Creek and Red Canyon sites, allow us to refine the frequency of surface-rupturing earthquakes on the segment. To fully characterize the segment's faulting history, we developed OxCal models using stratigraphic and chronologic data from the original studies at North Creek and Red Canyon as previously discussed. From these models, we have a more complete temporal perspective of prehistoric ruptures along the southern strand of the Nephi segment.

The next step is to integrate these site-specific models into a segment-wide model (e.g., DuRoss and others, 2011). In our modeling, we assume that the southern strand of the Nephi segment usually ruptures as an independent part of the WFZ and that it is atypical for ruptures to extend beyond the Nephi segment and onto adjacent segments of the fault zone. This assumption is supported by the observation that the estimated vertical displacements from individual earthquakes at each of the four well-studied sites on the Nephi segment (RC, WC, NC, and SQ) range between 1.1–3.2 m (DuRoss, 2008). If we assume that the smallest displacement value of 1.1 m represents the maximum displacement during that earthquake (MD of Wells and Coppersmith, 1994), then using the fault-length

versus magnitude relations of Wells and Coppersmith (1994) for a normal-fault rupture, the inferred rupture length is at least 24 km long, which is the length of the southern strand. If we use 1.1 m as the average displacement (AD of Wells and Coppersmith, 1994), then the inferred rupture length is about 34 km long, which is close to the 42-km length of the entire segment. Other displacement values for the southern strand are even larger, so the inferred rupture lengths would be longer. Thus, based on the smallest displacement values, it is likely that the entire 24-km-long southern strand ruptures during a single large earthquake on the segment. However, the larger vertical displacements raise other questions about possible rupture scenarios that we discuss in a following section.

Integrating Site-Specific Data into a Full-Segment Rupture History

To develop a segment-wide rupture history, we use the site PDFs of earthquakes at each trench site (figures 10, 14, and 16) to correlate earthquakes along the entire segment (figure 17). We excluded the single paleoearthquake at the Santaquin site (SQ1) on the northern strand from the segment PDF because there is significant uncertainty about whether earthquake SQ1 correlates with the youngest earthquake on the Nephi segment or with the youngest earthquake on the Provo segment to the north (discussed later). We also did not include information from the Spring Lake study because it is only published in an abstract, and we do not have enough detailed information to develop an OxCal model. Several permissible correlations exist to link earthquakes between the RC, WC, and NC sites, so to help evaluate the quality of different correlation options, we use the amount of overlap between different site PDFs as a guide (figure 18). An overlap value of zero corresponds to PDFs that have no overlap, whereas a value of 1.0 corresponds to PDFs that fully overlap (DuRoss and others, 2011, after Biasi and Weldon, 2009). Higher overlap values generally suggest a more favorable correlation of the earthquakes; however, the amount of overlap can also be misleading. For example, the overlap value between a well-constrained earthquake (for example, WC1) and a poorly constrained earthquake (for example, NC1) can be low (about 0.3), but when considered within the timeline of earthquakes at both sites, it is clear that earthquakes NC1 and WC1 most likely correlate. We recognize that the amount of overlap in site PDFs offers

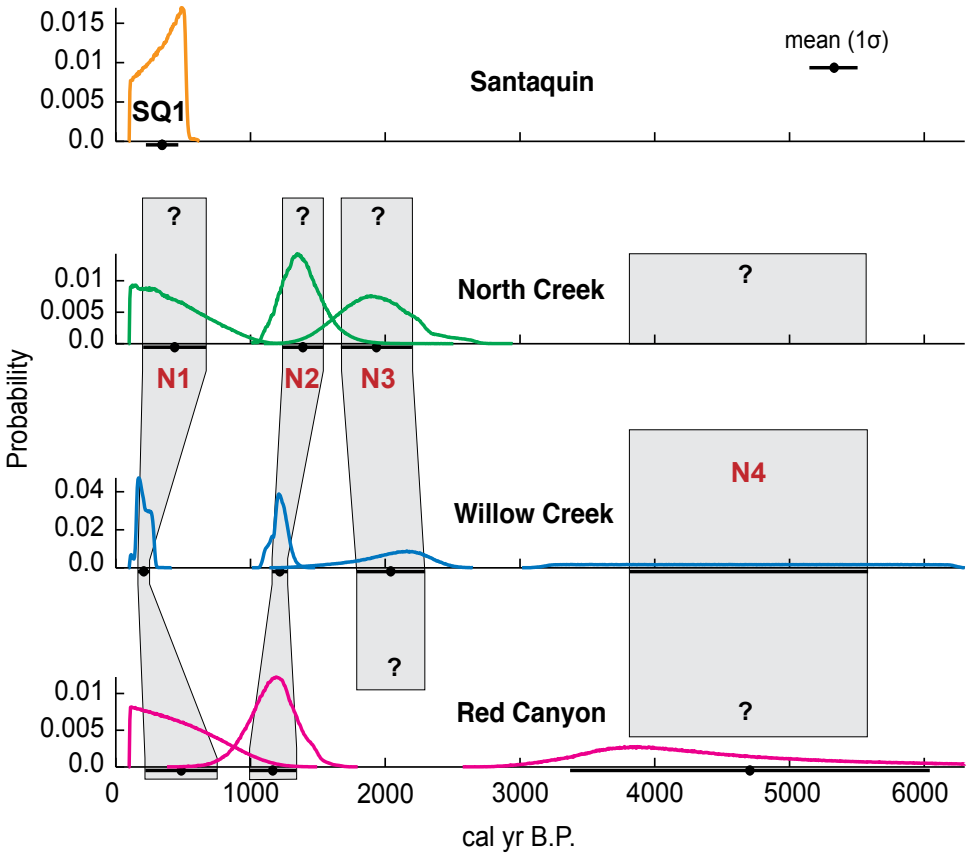

Figure 17. *Correlation of site probability density functions (PDFs) from OxCal models for paleoseismic sites on the Nephi segment showing the preferred correlation of earthquakes between sites. Light-gray areas show how site PDFs correlate to form segment-wide earthquakes N1 to N4. Earthquake N4 is only inferred at Willow Creek from the total stratigraphic displacement of alluvial-fan deposits in the fault footwall. Correlation of the only prehistoric earthquake documented at the Santaquin site (SQ1) is uncertain; this earthquake may correlate with earthquake N1 on the southern strand or with the youngest earthquake on the Provo segment.*

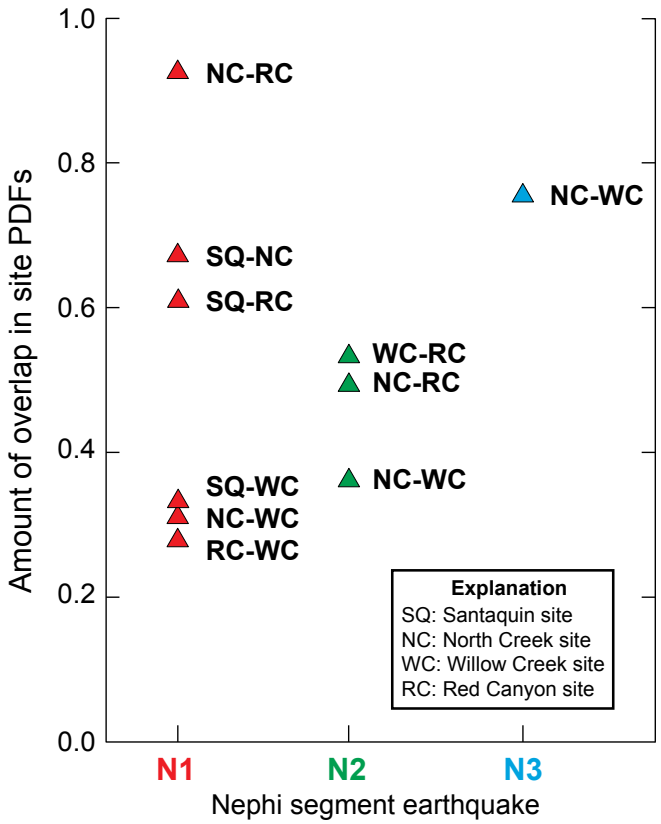

Figure 18. *Plot showing amount of overlap in probability density functions (PDFs) that define the times of earthquakes at pairs of sites on the Nephi segment. An overlap value of 1.0 indicates complete overlap, whereas a value of zero indicates no overlap between PDFs.*

only guidance on correlations, but it is especially helpful in those cases where the overlap value is high such as for earthquakes NC1–RC1 and NC3–WC3.

From our preferred earthquake correlations, we combined the OxCal site PDFs for each earthquake (for example, NC1, WC1, RC1) to yield a segment-wide PDF for each earthquake (DuRoss and others, 2011, after Biasi and Weldon, 2009) (figure 19). We refer to the combined PDFs (which are derived by combining two or more site PDFs) as *segment PDFs*. To create the segment PDF, we first scaled the site PDFs for earthquakes NC1, WC1, and RC1 into bins where the sum of the probabilities for each time bin equals one. We then combined these probabilities into the segment PDF, which defines the time of each documented earthquake on the southern strand of the Nephi segment (for example, N1 in figure 19).

The site PDFs from NC, WC, and RC each contribute to the earthquake times for the entire segment; the shape of each site PDF varies depending on the number and quality of the limiting ages for specific earthquakes, the time of the earthquake, and the vintage of the study (reflecting the evolution in sampling techniques and dating precision). A narrow PDF indicates that the time of an earthquake is well constrained by high-quality limiting ages (for example WC1), whereas a broad PDF results from poorly constrained limiting ages for the earthquake (for example, RC1). Because of the limited amount and variable quality of data on the Nephi segment, we use all of the site data in our analysis, rather than arbitrarily discarding the most broadly shaped PDFs.

To combine the site PDFs into a chronology for the Nephi segment, we use the product PDF method (DuRoss and others, 2011) because it favors the narrowest, most precise PDFs and yields smaller uncertainties in the times of earthquakes versus simply computing the mean of the site PDFs, which yields larger uncertainties in earthquake times. We prefer the product method because it yields final segment PDFs that are most strongly influenced by the narrowest, best-defined PDFs and the amount of overlap in the PDFs from all of the sites. The product method yields segment PDFs with smaller uncertainties (compared to the simple-mean method) and is especially suitable for paleoseismic data sets (such as the WFZ) where the times of earthquakes at some sites are only constrained by broad, overlapping site PDFs (figure 19). For example, the time of the most recent earthquake (N1) on the southern strand is 210 ± 90 yr (2σ) based on the product method versus 380 ± 480 yr based on the mean method. The shift in the mean time of this earthquake to 380 yr and the 480 yr uncertainty is caused by the poor constraints on the maximum time for this earthquake at the Red Canyon and North Creek sites. However, the maximum time for this earthquake is well constrained at the Willow Creek site, so the product method places greater emphasis on the WC maximum time constraint and gives a more precise PDF of 210 ± 90 yr for earthquake N1.

After developing the segment PDFs, we reviewed the PDFs of the OxCal models for each site and the final segment PDFs to determine if the product method may have over-constrained the earthquake times more than is justified by the original geological data. This is a necessary step because the product method can potentially reduce the uncertainties in earthquake times to unrealistically small values in cases where the site PDFs that correspond to the same earthquake (for example, N1) have poor PDF overlap (DuRoss and others, 2011).

Figure 20 and table 3 summarize our preferred times of paleoearthquakes on the southern strand of the Nephi segment. The time of earthquake N1 is 210 ± 90 yr (rounded to 0.2 ± 0.1 ka), earthquake N2 is 1230 ± 100 yr (rounded to 1.2 ± 0.1 ka), and earthquake N3 is 2000 ± 390 yr (rounded to 2.0 ± 0.4 ka). Our poor constraints on the time of earthquake N4 result in a broad PDF and a time of 4700 ± 1770 yr (rounded to 4.7 ± 1.8 ka).

The earthquake times on the southern strand derived from our analysis differ significantly from the consensus times of earthquakes determined by the UQFPWG (table 3; Lund, 2005). The Working Group's preferred time for the youngest surface rupture (earthquake N1) on this strand is ≤ 1.0 ± 0.4 ka, and the Group noted that Hanson and others (1981) preferred a

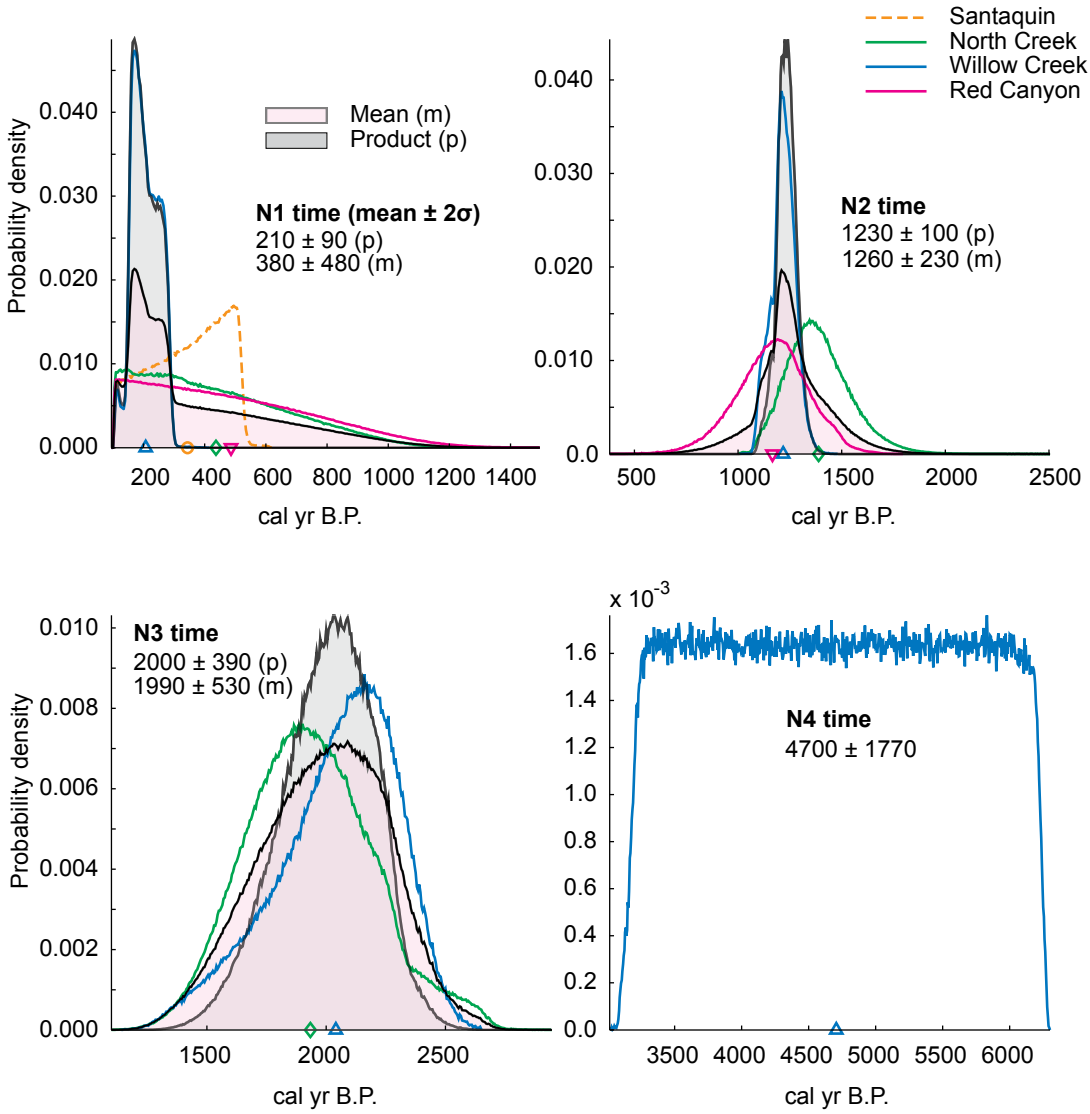

Figure 19. *Plots showing the product of site probability density functions (PDFs) (gray) for individual earthquakes (N1–N3) on the Nephi segment. Pink area shows the simple mean of the site PDFs. Symbols on X-axis show mean value for each plot, which is color-coded to correspond to specific study sites on the segment. The evidence of earthquake N4 is indirect and is based on stratigraphic relations observed only at the Willow Creek site. Colored lines show the site PDFs for individual earthquakes at each site. The product of the site PDFs yields a more precise time of the earthquake compared to the mean of the PDFs. Note differences in vertical scales for each plot. See text for discussion.*

time of 0.4 ± 0.1 ka for this earthquake. Relying on data from the North Creek and Red Canyon sites, the Working Group preferred a time of about 3.9 ± 0.5 ka for earthquake N2, and reported the time of earthquake N3 as older than about 3.9 ± 0.5 ka and younger than 5.3 ± 0.7 ka. With our improved time constraints on earthquakes N1, N2, and N3 at the Willow Creek site, we recommend that the chronology for earthquakes on this strand of the Nephi segment be updated. Furthermore, our recognition of earthquake N4 should be incorporated into the Nephi segment chronology.

Earthquake Recurrence

We computed earthquake recurrence intervals for the southern strand following the method of DuRoss and others (2011), which uses a Monte Carlo simulation to randomly sample the segment PDFs (figure 20). In this method, the site PDFs are divided into five-year time bins and the probability for each time bin is multiplied by 10,000 to yield a dataset that represents the area under the PDF curve. This dataset is then randomly sampled 10,000 times, with each sample determining a recurrence interval between individual earthquakes N1 to N4, that is, the time intervals between N1 and N2, N2 and N3, and N3 and N4. We then plot the cumulative time intervals for each of the 10,000 samples for each earthquake interval (N1–N2, N2–N3, and N3–N4), which yields a PDF of recurrence intervals (figure 21).

The recurrence intervals can be considered in several ways. The simplest way is to only consider the PDF of the time intervals between pairs of individual earthquakes, that is, the inter-earthquake time between N4–N3, N3–N2 or N2–N1 (A, B,

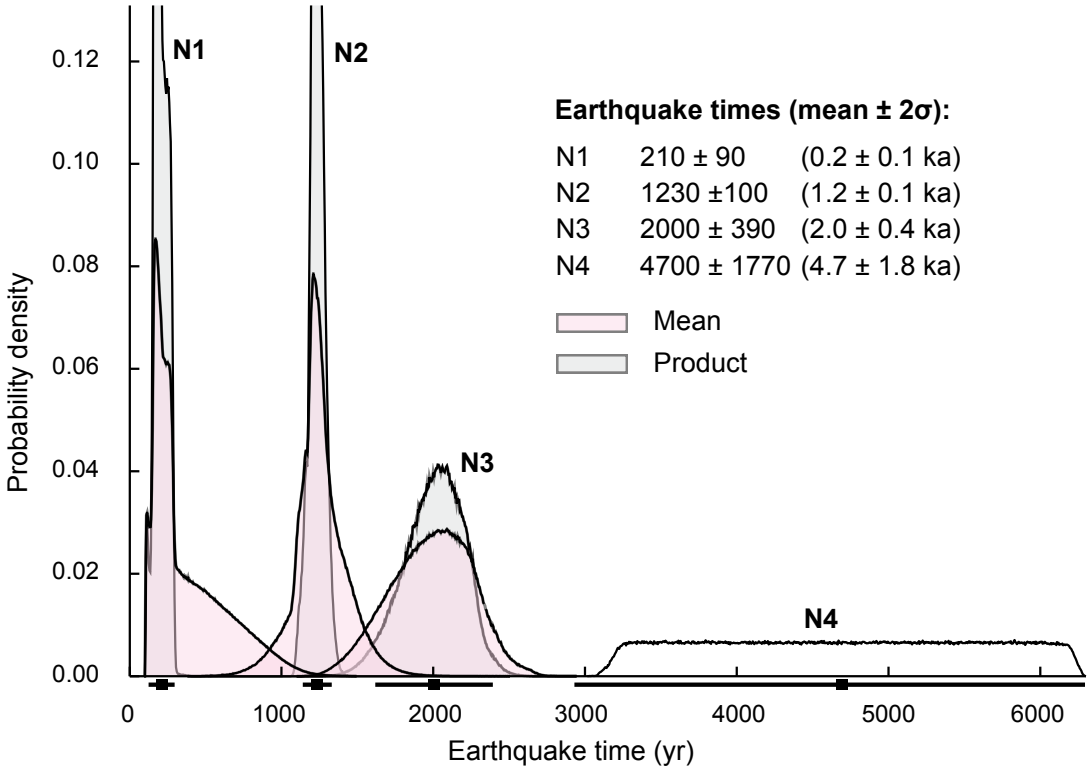

Figure 20. *Chronology of surface-faulting earthquakes on the Nephi segment. Gray probability density functions (PDFs) are the products of site PDFs; pink area shows the simple mean of site PDFs. Earthquake times and uncertainties are based on the product-PDF method. See text for discussion. Vertical scale truncated at 0.13 for clarity.*

C on figure 21). The recurrence interval for N4–N3 has little significance because the time of earthquake N4 is so poorly known.

An alternative way to assess recurrence is to use an average recurrence value that spans multiple earthquake cycles. These cycles are bounded by earthquakes of known age, and recurrence times are defined as *closed recurrence intervals*. Using the times between the individual pairs of earthquakes, we can calculate average closed intervals for the Nephi segment in two ways based on our data. We can calculate a closed mean-recurrence time by using the time between the oldest and youngest earthquakes divided by the number of closed intervals that occurred in the entire time interval. The average recurrence time for the three closed intervals between earthquakes N4 and N1 is 1500 ± 590 yr (D, figure 21), but because the time of earthquake N4 is so poorly known, the significance of this value is limited. A more valid value is the mean recurrence for the two closed intervals between earthquakes N1 and N3, which is 900 ± 200 yr, cited as 0.9 ± 0.2 kyr (E, figure 21). However, this mean recurrence only spans two earthquake cycles, so it is unclear how accurately this value reflects a longer-term recurrence rate that spans many cycles.

We can also compute an open recurrence interval, in which the total time between the oldest earthquake (maximum time of earthquake N4) and the present time is divided by the number of earthquakes that occurred in that time period (F, figure 21). In this case, the calculated mean recurrence time is 1570 ± 20 yr, but this is a minimum value because the open time interval is defined by the present, and an unknown amount of additional time will elapse before the next surface-faulting earthquake. It is important to note that the 20-year uncertainty in this value is anomalously small because it is based on the maximum time of earthquake N4, which is determined by the ^{14}C age of Willow Creek WCN-R1, which has a narrow age range of 6126–6295 cal yr B.P. (table 1). Because the present is tightly defined (no uncertainty) and because the old end of the time range is well determined, the resulting uncertainty in the mean value is very small but meaningless.

Our new Willow Creek data and our combined analysis of data from all three sites on the southern strand yield recurrence values that differ from those of the UQFPWG. The Working Group reported a preferred recurrence value of 2.5 kyr, but assigned broad uncertainty limits with minimum and maximum values of 1.2 kyr and 4.8 kyr, respectively. The large uncertainty reflects the poor constraints on the times of past earthquakes on the Nephi segment prior to our Willow Creek study. With our better-constrained earthquake times and merging the data from all three sites, we now have more robust recurrence values.

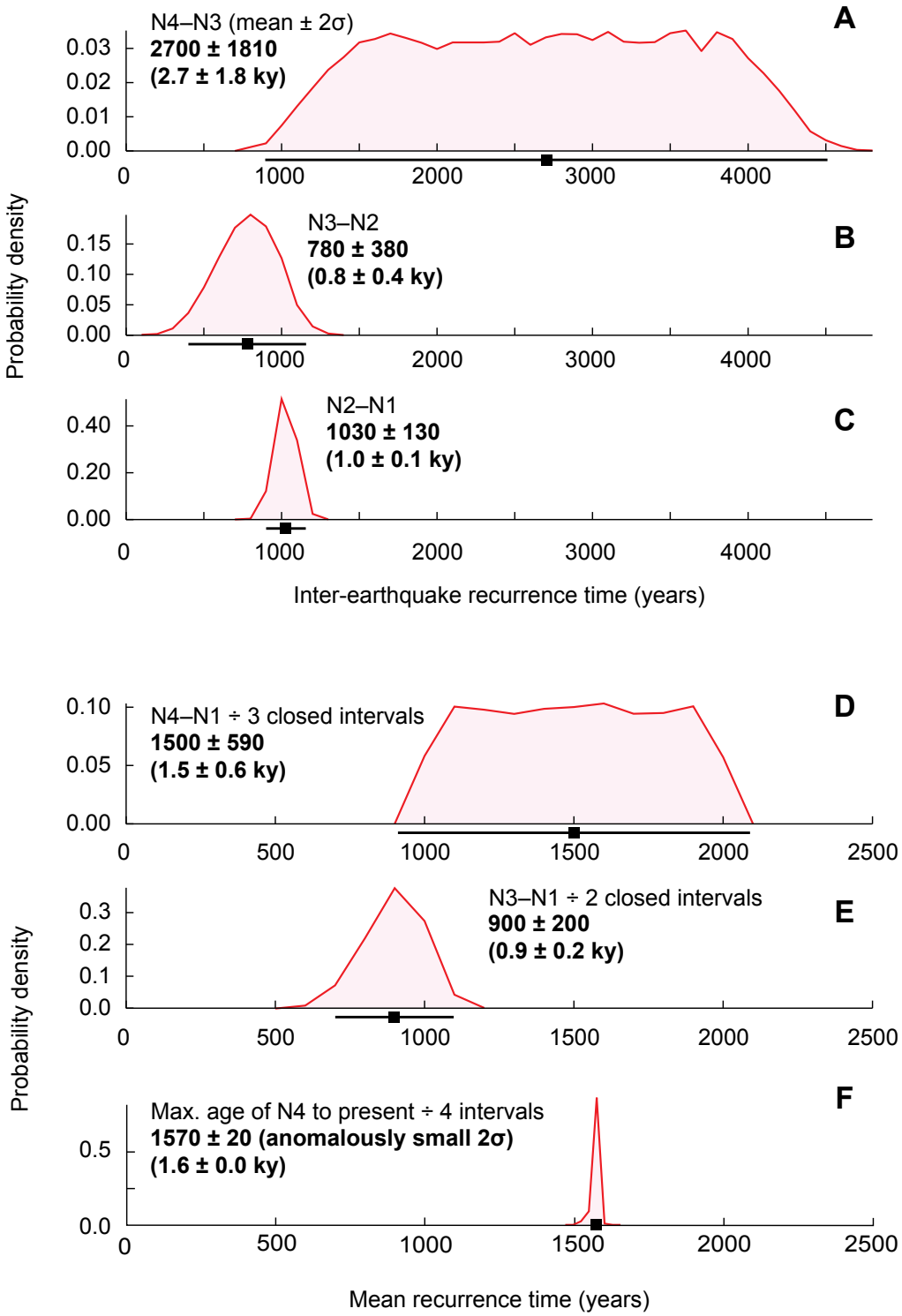

Figure 21. *Individual inter-earthquake (A–C) and mean recurrence times (D–F) for earthquakes on the Nephi segment. Recurrence times between earthquakes are based on Monte Carlo modeling of segment probability density functions (PDFs); see text for details. Closed mean recurrence times (D–E) are based on the elapsed time between the earthquakes divided by the number of inter-earthquake time intervals. Open mean recurrence based on the elapsed time from earthquake N4 to the present, divided by three intervals (including the open interval between the time of earthquake N1 to the present). Individual mean recurrence is based on the average of the three individual-earthquake recurrence PDFs (N4–N3 to N2–N1). Solid box and bar below PDFs indicate mean and 2σ values, respectively. Note differences in vertical scales for each plot.*

DISCUSSION

Rupture Scenarios for Recent Nephi-Segment Earthquakes

The interaction of ruptures on the two strands of the Nephi segment and the adjacent Provo segment is unclear, but information addressing this interaction would be of value in understanding the region's seismic hazard as well as offering insight into the behavior of segment boundaries of normal faults. We have refined the times of late Holocene earthquakes on the southern strand, and the modeled age of 0.5 ± 0.1 ka for the single post-mid-Holocene earthquake on the northern strand (earthquake SQ1; DuRoss and others, 2008) is significantly different than our modeled time of 0.2 ± 0.1 ka for earthquake N1 (figure 22).

More recently as part of the Working Group on Utah Earthquake Probabilities (WGUEP) (Wong and others, 2011; http://geology.utah.gov/ghp/workgroups/wguep.htm), we reanalyzed the dating constraints on earthquake SQ1 and determined that the time of earthquake SQ1 may have a younger mean age and broader uncertainty range of 0.3 ± 0.2 ka (figure 22). Given this reanalysis and the revised southern strand earthquake history, we consider different rupture patterns between these three parts of the fault zone.

First we consider a simultaneous rupture of the southern and northern strands and conclude that the current data indicate that simultaneous rupture of these strands occurs rarely, if at all. PDFs from the original OxCal model for earthquake SQ1 by DuRoss and others (2008) showed only a small amount of overlap between the SQ1 and N1 earthquakes (dashed orange line, figure 22), suggesting that they likely ruptured independently. However, the revised PDF increases the overlap between earthquakes SQ1 and N1 (solid orange line, figure 22), and although such a correlation is permissible, it is not compelling. So on the basis of the paleoseismic data, the youngest earthquakes on the southern and northern strands may correlate, but the fact that earthquakes N2 and possibly N3 and N4 did not rupture at the Santaquin site significantly weakens the case that the northern and southern strands typically rupture together.

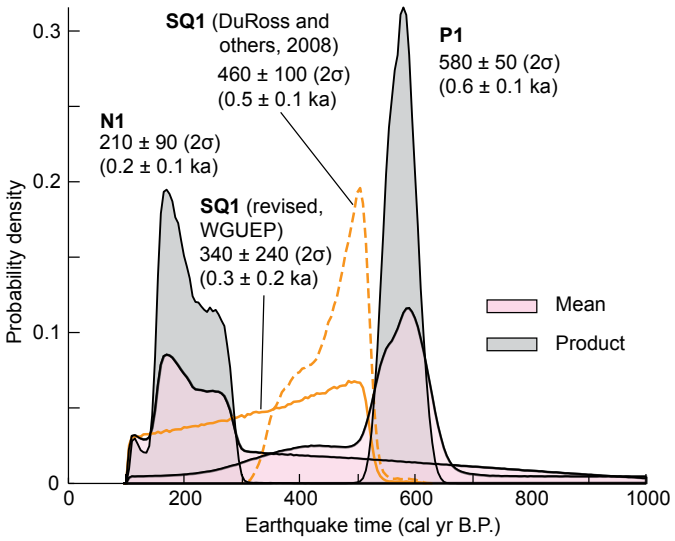

Figure 22. *Probability density function (PDF) plots comparing the time of the youngest earthquake on the southern strand of the Nephi segment (N1). Time of earthquake N1 is compared with the Santaquin site earthquake on the northern strand (SQ1), and the youngest Provo-segment earthquake (P1). The time of earthquake P1 is from Olig (2011), but has been reanalyzed by the WGUEP. See text for discussion.*

Another possible rupture pattern is that the northern and southern strands rupture as independent earthquake sources. The 6- to 7-m-high scarps on the southern strand clearly show that large ruptures have repeatedly occurred here since mid-Holocene time. Empirical relations of fault length versus magnitude suggest that a 25-km-long rupture on the southern strand would be associated with an earthquake of 6.7 or larger (Wells and Coppersmith, 1994). If we use an average displacement of 2.4 m per earthquake (based on data from the WCS trench), then the Wells and Coppersmith empirical relations suggest an earthquake of M 7.1 for a normal fault. Although its length is relatively short compared to the average displacement, an independent rupture on the southern strand would likely generate an earthquake in the range of high magnitude 6 to low magnitude 7.

In contrast, the short, 17-km length of the northern strand does not favor it being an independent seismic source. Empirical relations between fault length, vertical displacement, and rupture length (Wells and Coppersmith, 1994) indicate that a 17-km-long surface rupture would likely be associated with only moderate-sized earthquakes in the range of M 6.5, and M 6.5 earthquakes on normal faults typically produce only about 0.5 m of vertical displacement at the surface. The 3.0 m of vertical displacement from the SQ1 rupture (DuRoss and others, 2008) is much larger than a 0.5-m vertical displacement typical of a 17-km-long fault segment. Furthermore, the Wells and Coppersmith empirical relations suggest that 3.0 m of displacement would be associated with an earthquake in the range of M 6.9–7.1, which in turn, would typically be associated with 40 km or more of surface rupture. From these observations, we conclude that a 3.0-m-high displacement from earthquake SQ1 was likely associated with a surface rupture that was much longer than the 17-km length of the northern strand.

The size of the SQ1 displacement seems to favor a scenario in which the SQ1 rupture was a spillover rupture from the Provo segment. About 70 percent (12.6 km) of the northern strand's length overlaps with the Provo segment (figure 2), so it seems reasonable that these two fault sections could be linked at depth by a relay ramp or a branching fault (Peacock and Sanderson, 1991; Soliva and others, 2008). In this case, the 0.5-ka SQ1 rupture would correlate with the youngest rupture on

the Provo segment. The UQFPWG reported a time of 600 ± 350 cal yr B.P. (0.6 ± 0.4 ka) for the youngest Provo-segment earthquake (Lund, 2005), but more recently, Olig (2011) reported a preferred time of 500 ± 150 yr (0.5 ± 0.2 ka) for the youngest rupture at the Mapleton megatrench site (figure 2), which is 22 km northeast of the Santaquin site. Furthermore, the 3.0-m surface displacement of earthquake SQ1 is closer to the mean displacement per earthquake of 2.9 m for the Provo segment compared to a mean displacement per earthquake of 2.0 m for the Nephi segment (DuRoss, 2008). Additionally, Chang and Smith (2002) modeled the stress changes induced by a scenario Mw 7.1 earthquake on the Provo segment and determined that the scenario earthquake would increase the Coulomb failure stresses on the northern part of the Nephi segment by more than 4 bars, which would enhance the possibility of rupture on the Nephi segment. DuRoss and others (2008) also favor this spillover model to explain the size of the scarp at the Santaquin site.

Conversely, the WGUEP's reevaluation of paleoseismic data from the entire Provo segment suggests that the spillover model may not apply. The reevaluation yields a time of 580 ± 50 cal yr B.P. (0.6 ± 0.1 ka) for earthquake P1, the most recent Provo-segment surface rupture (P1, figure 22). The product PDF for earthquake P1 only overlaps with the revised PDF for earthquake SQ1 between about 530 and 580 cal yr B.P. at a maximum probability density of about 3 percent (figure 22). This small probability in a relative narrow time window does not strongly support a spillover rupture between the Provo segment and northern strand during the last surface rupture. Given these differing observations, it is clear that additional paleoseismic data are needed to help resolve details regarding the interaction of the northern strand with adjacent parts of the WFZ.

Rupture Between Fault Steps

Based on existing paleoseismic data, we cannot yet resolve the interactions of the northern strand with adjacent WFZ segments, so we consider additional information that may provide insight into this matter. The size of steps between adjacent fault strands is widely recognized as a factor affecting whether coseismic ruptures are likely to jump between adjacent faults (Segall and Pollard, 1980; Oglesby, 2005; Wesnousky, 2006, 2008; Soliva and others, 2008). In the case of the Nephi segment, the distance across the steps between the southern and northern strands, and between the northern strand and the Provo segment are about 4 km and 6 km, respectively (figure 2). Wesnousky (2008) reports that historical normal-fault ruptures can cross steps as large as 5–7 km, which suggests that a rupture could potentially jump either of these steps.

The step-over between the Provo segment and northern strand is south of Payson. Quaternary fault scarps on the Provo segment extend southward to the Payson salient (Machette and others, 1992), as far as Peteetneet Creek, which flows in Payson Canyon (figure 2). Here, Paleozoic and Precambrian rocks exposed in 2987-m-high Dry Mountain and Tithing Mountain separate the Provo and Nephi segments (Machette, 1992; Machette and others, 1992). No Quaternary scarps are mapped in the area of Dry Mountain where, if present, they could link the two segments (Machette, 1992). We know of no compelling surface evidence that Quaternary ruptures have extended between the Provo and Nephi segments.

Similarly, there is no strong evidence indicating a connection between Quaternary fault scarps on the northern and southern strands of the Nephi segment. Scarps of the northern strand are east of Santaquin and Santaquin Canyon, and are separated from the southern strand by 2377-m-high ridges of Tertiary, Mesozoic, and Paleozoic bedrock (Harty and others, 1997). Harty and others (1997) show a normal fault in bedrock that trends into the range directly north of Mendenhall Creek that extends northeastward toward the upper reaches of Santaquin Canyon (figure 2). This fault approximately coincides with the down-to-the-north bedrock fault mapped by Sorensen and others (1983). More recently, Solomon (2010a) has mapped surficial deposits in the Santaquin quadrangle and shows a bedrock fault in the same area on which he interprets Quaternary movement. He maps this fault as ending in a large landslide of Quaternary-Tertiary age. However, the fault mapped by Solomon (2010a) has a down-to-the-south sense of slip and is about 500–800 m north of the fault mapped by Sorensen and others (1983). Furthermore, Solomon's surficial geologic maps of the Santaquin (2010a) and adjacent Payson Lakes (2010b) quadrangles show that old landslides are widespread in the areas around Santaquin Canyon and Dry Mountain. Much like near Willow Creek, the hummocky landslide topography makes it difficult to recognize fault traces in these deposits. Thus, bedrock faults may link the northern and southern strands, but the trace (or traces) of any linking faults cross large areas of unstable landslide slopes, which makes it difficult to determine if Quaternary movement has occurred on these fault strands.

The lack of clear evidence that Quaternary scarps connect either the two Nephi-segment strands or the Nephi-Provo segments makes the interaction between these three parts of the fault zone uncertain. Similarly, the revised time for the youngest earthquakes on these three fault sections fails to resolve this issue. Additional paleoseismic data are likely to be the best resource to clarify the interaction of fault strands at this complex segment boundary.

Slip Rates and Earthquake Clustering

Defining a Holocene or longer slip rate for the Nephi segment is more challenging than for other segments of the WFZ because virtually all of the segment's scarps are above the well-dated shorelines of Lake Bonneville, which elsewhere provides a widespread, geomorphic datum that is used to estimate post-latest Pleistocene slip rates (Personius and others, 2012). In the absence of this datum, the lack of Quaternary deposits whose ages are well determined makes it difficult to establish

time constraints on vertical offsets, and thus calculate a long-term slip rate.

Scarps on the Nephi segment offset a variety of alluvial-fan deposits, but the ages of those deposits are only broadly known (Harty and others, 1997; DuRoss and Bruhn, 2004). The best information on the vertical offset and age of faulted deposits comes from the sites of paleoseismic studies, but at those sites, the slip-rate values span only a few thousand years. Still, even in that short time interval, the slip-rate estimates on the Nephi segment span a seven-fold range of values (0.5 mm/yr at Spring Lake to 3.4 mm/yr at Willow Creek South; table 3). In a few places, the scarps have been profiled and the age of the faulted deposits have been estimated using geomorphic or pedologic criteria, but because deposit ages are only estimated, the resulting slip rates have large uncertainty.

At the WCS site where we have a well-documented vertical displacement and a well-determined age for the faulted deposits, the late Holocene slip rate is 2.6–3.4 mm/yr. This is among the highest geologically determined slip rates for multiple earthquakes on the WFZ, but it encompasses a time interval of only 2.5 kyr. Significantly, this high rate is about 21–28 times greater than a mid- to late-Pleistocene slip rate of 0.12 mm/yr estimated at Gardner Creek (table 3), which is only 5.6 km south of Willow Creek. The large difference between our high short-term versus much lower long-term slip rates is best explained by a clustering of earthquakes in the late Holocene. A pattern of earthquake clustering has been suggested for the entire Wasatch fault system by Machette and others (1992), McCalpin and Nishenko (1996), and Friedrich and others (2003), and is also consistent with the observations of Mayo and others (2009), who suggest a broad range of slip rates on the Provo segment over various time intervals since 780 ka based on the analysis of sediments in Timpanogos Cave near American Fork. Earthquake clustering has also been recognized and described for other faults and tectonically similar regions (Swan, 1988; Grant and Sieh, 1994; Crone and others, 1996, 2003; Marco and others, 1996; Rockwell and others, 2000; Dawson and others, 2003; Weldon and others, 2004; Dolan and others, 2007; Ganev and others, 2010).

Nicol and others (2005, 2006) proposed that the first-order control on earthquake recurrence rates (and thus slip rates) is the rate at which a fault system is loaded by the regional strain on time scales of 60 kyr to several Myr. Mouslopoulou and others (2008) built on this work and concluded that rates tend to be more stable for longer time periods ($\geq$ 20 kyr) versus shorter time periods. For the entire Wasatch fault system, the existing data indicate an average geological vertical slip rate for the past 6 kyr of 1.7 $\pm$ 0.5 mm/yr (Friedrich and others, 2003), and a GPS-derived vertical slip rate of 0.9–2.3 mm/yr assuming a 55° dip on the WFZ (Chang and others, 2006), which is distinctly less than our short-term rate from the WCS site. The UQFPWG preferred a slip rate of 1.1 mm/yr for the Nephi segment, but also recognized the large uncertainty in this value by assigning lower and upper limits of 0.5 and 3.0 mm/yr, respectively. Our data from the Willow Creek site yield a well-constrained but unusually high slip rate because of a cluster of late Holocene earthquakes.

The high, steep range front along the Nephi segment provides first-order evidence of sustained, long-term slip on the fault, but this long-term rate is also considerably less than our short-term late Holocene rate. Pennsylvanian-Permian rocks of the Oquirrh Formation in the Nebo-Charleston thrust sheet are exposed on the summit of Mount Nebo (Felger and others, 2004; figure 2) but have been down dropped beneath Juab Valley across the WFZ. The minimum cumulative vertical displacement on the fault zone is on the order of 3.75 km based on the 2.15 km of topographic relief between the summit of Mount Nebo at 3636 m and the 1486 m elevation of Juab Valley near Mona, plus about 1.6 km of basin fill in Juab Valley (Zoback, 1992). If movement on the WFZ began between about 10–17.6 Ma as suggested by Armstrong and others (2003) and Bruhn and others (2005), then the average slip rate during the fault's entire history is about 0.22–0.38 mm/yr, or an order of magnitude less than the Willow Creek latest Holocene rate. The ten-fold disparity between these two rates suggests that the fault's rate of slip varies over time. This is also consistent with the data of Machette and others (1992), who documented a four- to ten-fold increase in the slip rate on the WFZ between 4–5 ka and about 150 to 250 ka. These observations are confirmation of our high short-term rate and are likely indicative of earthquake clustering, which is similar to the conclusion of Friedrich and others (2003) who attributed high Holocene slip rates to clusters of earthquakes on the WFZ.

Significance of Results

Our Willow Creek study confirms the occurrence of three surface-faulting earthquakes on the southern strand of the Nephi segment that are younger than 2.5 ka, and refines the age constraints for those earthquakes. We also have evidence that at least one additional surface rupture (and possibly more) occurred between 2.5 ka and 6.2 ka.

At the Red Canyon site (6.3 km to the south), Jackson (1991) found evidence of only three earthquakes that ruptured an alluvial fan that is thought to be late Pleistocene in age. On the basis of our OxCal analysis, we correlate the two youngest Red Canyon earthquakes with our WC1 and WC2 earthquakes. If the rate of three earthquakes in 2.5 kyr at Willow Creek were sustained throughout the estimated 15-ka age of the Red Canyon alluvial fan (Jackson, 1991), potentially as many as 18 earthquakes could have occurred at Red Canyon since the late Pleistocene, assuming that all ruptures extend to the southern end of the segment. The fact that only three out of a potential 18 earthquakes have ruptured the Red Canyon fan raises the possibility that the frequency of late Holocene surface ruptures at Willow Creek probably is not representative of the frequency of ruptures throughout the latest Pleistocene. Some of the "missing" ruptures at Red Canyon might be attributed to it being closer to the end of the segment, but

if the last two Holocene ruptures reached Red Canyon, then it seems likely that several to many of the 18 "missing" ruptures would have also reached the site. An alternative explanation is that the frequency of earthquakes, and accordingly the slip rate, in the late Holocene is higher than the longer term, latest Pleistocene rate. This explanation of a change in the short-term versus longer-term slip rate is consistent with conclusions of DuRoss and Bruhn (2005) and is echoed by Jackson (1991) who states that "the Nephi segment...was inactive between 15,000 and 4,500 years ago" based on the record at Red Canyon.

Our conclusion that earthquakes have clustered on the Nephi segment and that slip rates have changed over different time periods agrees with the observations of Mattson and Bruhn (2001) and DuRoss and Bruhn (2005) for the Nephi segment, of Machette and others (1992) for the entire WFZ, and of Wallace (1987) for selected faults in the Great Basin. Machette and others (1992) speculated that the rise and fall of pluvial lake cycles may have been an influencing factor in slip-rate changes and that the increased hydrostatic and lithostatic loads caused by the lakes on the fault's hanging wall may have inhibited slip. Recent modeling indicates that these loads can be a factor, and times of high lake levels may correlate with lower slip rates, whereas times of lowering lake levels correlate with times of increased slip rates (Hetzel and Hampel, 2005; Karow and Hampel, 2010).

If lacustrine loading and unloading does affect slip rates on the WFZ, then it seems likely that the impact of this process would be minimal on the Nephi segment because a relatively shallow arm of Lake Bonneville filled Juab Valley for only a few thousand years. The lowest part of Juab Valley is now filled with Mona Reservoir, which has a surface elevation of 1488 m and a maximum depth of about 7 m, so the floor of Juab Valley beneath the reservoir is about 1481 m. Currey (1982) measured the elevation of the Bonneville shoreline at Santaquin at 1558 m, which indicates that the maximum depth of the lake was about 70 m in Juab Valley during the Bonneville highstand (with minor adjustments to this depth because of isostatic effects). The lake in Juab Valley was isolated from the main lake when the water level catastrophically dropped 100 m or more to the Provo shoreline level (Oviatt, 1997; Godsey and others, 2005; Solomon, 2010a; Miller and others, 2013). Oviatt's (1997) hydrograph of the lake indicates that the shallow lake in Juab Valley was connected to the main lake for about 3.5 kyr during the Bonneville highstand and the drop to the Provo level. Given the shallowness of the lake and the relatively short duration of its connection to the main lake, any effects of lacustrine loading on the Nephi segment's slip rate would likely be minor, if any, and probably would not account for an appreciable change in the fault's slip rate. This conclusion is consistent with the modeling of Karow and Hampel (2010), who show that the presence of Lake Bonneville had minimal impact on slip-rate changes on the Nephi segment.

Wallace (1987) proposed a pattern of spatial and temporal clustering of earthquakes and thus changes in slip rates over time spans of thousands to millions of years for faults in the Great Basin. Based on the morphology of Quaternary fault scarps, range-front geomorphology, and fault-generated tilting of bedrock in ranges in Idaho and Nevada, he concluded that seismogenic faults show variations in the occurrence of large-displacement earthquakes and in slip rates at regional and subprovince scales, at the scale of groups of ranges, and within a single range and basin block. Our conclusion about the temporal behavior of faulting on the Nephi segment reinforces his conclusions derived from a province-wide perspective.

In a recent reanalysis of Holocene surface-rupturing earthquakes on the Brigham City segment of the Wasatch fault zone, Personius and others (2012) documented a uniform temporal pattern of earthquakes: between 2.4 ± 0.3 ka and 5.6 ± 0.7 ka, a surface rupture occurred about every 1.1 ± 0.2 kyr. However, they noted that the elapsed time since the youngest earthquake is more than twice the 1.1 kyr recurrence time for the preceding three earthquake cycles. The effect of ruptures on the adjacent Weber segment may have delayed the pending rupture on the Brigham City segment, but their calculations suggest that the segment currently has more than twice the moment accumulated in the three previous earthquake cycles. This non-uniform temporal pattern of earthquakes may be another example of earthquake clustering on the Wasatch fault zone.

Even in plate-boundary settings where steady plate motions may cause strain to accumulate on faults at a more consistent rate, long records of prehistoric earthquakes show intervals of clustering. At the Wrightwood site on the southern San Andreas fault where the paleoseismic history includes 30 earthquakes, Weldon and others (2004) recognized at least one interval of earthquake clustering, similar to what we describe on the Nephi segment. They showed that the short-term slip rate increases to about three times the average rate, and that during the cluster, the slip rate is actually twice the rate for the entire plate boundary.

Earthquake clustering and the associated temporal changes in fault slip rates have significant implications for earthquake hazard assessments. The hazard from a fault or fault segment that is currently within a cluster of activity is higher than the hazard from a fault that is not in a cluster. Unfortunately, our present knowledge of fault behavior is inadequate to determine if a fault segment is currently within or outside a cluster of activity.

Our evidence of the short recurrence interval between recent earthquakes (related to earthquake clustering) could be viewed as indicating high seismic hazard on the Nephi segment. Conversely, if there is an element of time-dependency to large earthquakes on the WFZ (McCalpin and Nishenko, 1996), then the occurrence of the most recent earthquake on

the Nephi segment only a few hundred years ago could be taken to mean that the short-term hazard is low compared to other segments that have not ruptured recently. It is beyond the scope of this publication to explore the implications of clustering and time dependency on hazard assessment, but these issues will continue to be important topics of future research. It is clear that a large earthquake on the WFZ poses a significant hazard to Utah citizens residing along the Wasatch Front, regardless of whether the earthquake ruptures the Nephi or any other segment of the fault zone.

The Nephi-Provo Segment Boundary: Insight into Fault Segmentation

Our evaluation and comparison of the paleoseismic data for the Nephi and Provo segments highlight the complex nature of the boundary between these segments. The paleoseismic evidence indicates that some recent ruptures may have spilled over between the segments whereas others apparently did not. The youngest surface rupture at the Santaquin site may correspond to the youngest rupture on the Provo segment, but the older Provo-segment earthquakes at 1.5 ka, 3.2 ka, 4.7 ka, and 6.1 ka (Olig, 2011) apparently caused little, if any, surface rupture at Santaquin. Because of the large, 12.6-km-long overlap between the northern strand and the Provo segment, it is likely that these two parallel strands of the fault zone converge and ultimately merge at depth in the brittle crust.

The down-dip geometry of these overlapping strands may be similar to that proposed by Doser (1985) for the Red Canyon and Hebgen faults that ruptured in the 1959 Hebgen Lake, Montana, earthquake (figure 23). That earthquake produced large scarps along the shore of Hebgen Lake and on the Red Canyon fault. These two faults are about 5 km apart and bound the Red Canyon fault block as shown by Witkind (1964). Doser (1985) evaluated the seismological data for the two 1959 main shocks and six significant aftershocks that occurred within 24 hours of the sequence. She proposed two configurations of subsurface fault geometry that are consistent with the seismic and geological data, both models favor the Hebgen and Red Canyon faults converging at a depth of about 7–11 km. Given the large along-strike overlap of the northern strand and the Provo segment, it seems plausible that these two faults may have a similar geometric relation at depth. Large earthquakes, such as those we expect to cause rupture on the WFZ nucleate in deeper parts of the brittle crust (Smith and Bruhn, 1984; Doser, 1985), perhaps near depths where these strands might converge. A large earthquake that nucleates at or below the depth of this convergence could potentially cause rupture on one or both strands, depending on the amount of accumulated strain on each strand.

However, the differing paleoseismic histories of the Provo segment and the northern strand of the Nephi segment indicate different levels of independence and interaction across the segment boundary. This boundary may be an example of a "leaky" boundary in which some, but not all propagating ruptures extend through the boundary (Crone and Haller, 1991). If so, it behaves similarly to the boundary between the Brigham City and Weber segments of the WFZ, where the penultimate rupture on the northern Weber segment extended into the southern part of the Brigham City segment (Personius and others, 2012).

At present, details of the interaction between the northern strand and the Provo segment remain unclear. Perhaps frequent ruptures on the Provo segment inhibit the accumulation of strain on the overlapping northern strand, resulting in fewer large, surface ruptures or possibly smaller displacements that are more difficult to recognize at the surface. The distinctly different chronologies of late Holocene earthquakes on the northern and southern strands do not favor a strong link between them; however the northern-strand earthquake chronology prior to 1.5 ka is poorly constrained. The remaining questions about the nature of the Provo-Nephi segment boundary and the histories of earthquakes on the northern and southern strands can only be resolved by acquiring longer histories on both strands, which would offer insight into the nature of segment boundaries on major range-front normal faults and the interaction of ruptures at those boundaries.

CONCLUSIONS

Our new data from the Willow Creek site provide well-defined and narrow bounds on the times of the three youngest earthquakes on the southern strand of the Nephi segment, and refine the time of the youngest earthquake to about 200 years ago. This is the most recent surface rupture on the entire WFZ and occurred about a century or less before European settlers arrived in Utah. Our evidence of the recency of this rupture is consistent with the youthful geomorphic expression of the fault scarp along this section of the segment, including very steep scarp-slope angles (Machette, 1984; Machette and others, 1992) and largely unvegetated scarp faces.

In both trenches at the Willow Creek site, we exposed three scarp-derived colluvial wedges that represent three prehistoric earthquakes (WC1, WC2, and WC3). The three wedges are younger than the 2.4 ± 0.2 ka alluvial fan at the WCS trench site. Stratigraphic relations in the WCN trench indicate that a fourth earthquake (WC4) (and possibly others) occurred prior to 2.5 ka and is younger than the 6.2-ka faulted alluvial fan at the WCN site. Our OxCal modeling of ages from Willow Creek indicate that earthquake WC1 occurred at 0.2 ± 0.1 ka, earthquake WC2 occurred at 1.2 ± 0.1 ka, and earthquake WC3 occurred at 1.9 ± 0.6 ka. Our stratigraphic constraints on the time of earthquake WC4 are extremely poor, so our OxCal model yields a broadly constrained time of 4.7 ± 1.8 ka, which is of limited use.

Our stratigraphic information and age control allow us to accurately determine vertical displacements and a well-con-

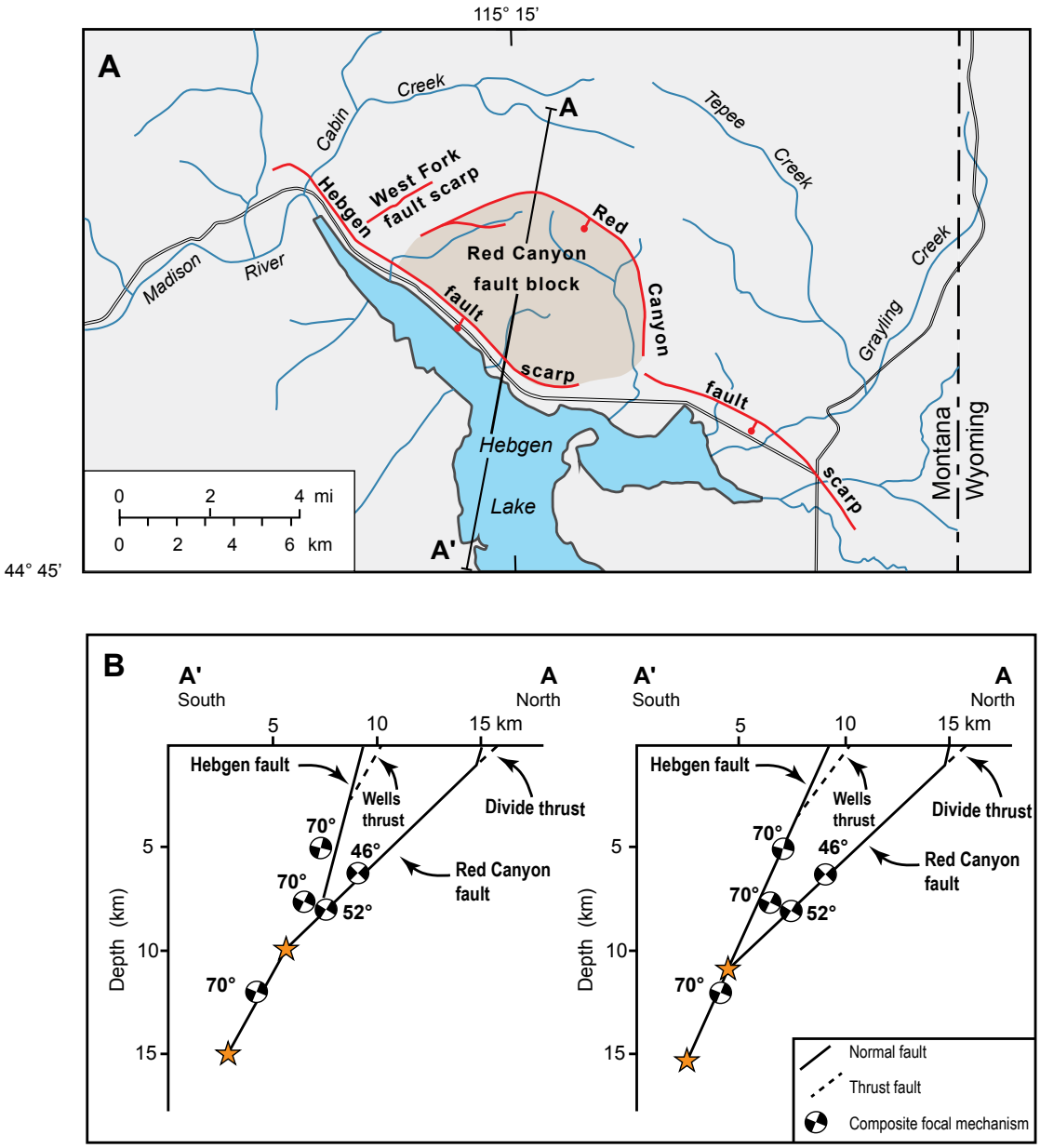

Figure 23. *Fault scarps (A) produced by the 1959 Hebgen Lake, Montana, earthquake (from Witkind, 1964) and cross sections (B) showing possible subsurface geometry of the Hebgen-Red Canyon fault system (from Doser, 1985). The Red Canyon and Hebgen fault scarps are separated by a maximum distance of about 5 km, similar to the separation between the Provo and Nephi segments of the Wasatch fault zone. Doser's proposed fault geometries are based on the locations of two main-shock hypocenters (orange stars) and composite focal mechanisms of aftershocks.*

strained slip rate at the Willow Creek site. Based on the stratigraphic data and fault-scarp profiles from the WCS trench, we estimate that the last three earthquakes produced a net vertical displacement of 7.1 ± 0.2 m, which yields an average of 2.4 m per earthquake. Using a mean age of 2.5 ka for the fan deposits in the WCS trench, the late Holocene slip rate is 2.8 mm/yr, which is considerably higher than previous estimates for the Nephi segment. We recognize that this high rate spans a short time interval compared to other slip-rate estimates for the segment, and we attribute the difference of our high rate and the lower rates to a clustering of earthquakes in the late Holocene.

The Willow Creek results significantly refine the times of late Holocene earthquakes on the southern strand of the Nephi segment, and this result, when combined with our reanalysis of the stratigraphic and chronologic information from previous studies at North Creek and Red Canyon, yields a stronger basis for correlating individual earthquakes between all three sites. Following the methodology described by DuRoss and others (2011), we used OxCal models to develop a segment-wide chronology for the last three surface-rupturing earthquakes on the southern strand of the Nephi segment. The time of earthquake N1 is 0.2 ± 0.1 ka (210 ± 90 yr B.P.), the time of earthquake N2 is 1.2 ± 0.1 ka (1230 ± 100 yr B.P.), and the

time of earthquake N3 is 2.0 ± 0.4 ka (2000 ± 390 yr B.P.). The time of earthquake N4 is poorly constrained because it is based only on stratigraphic evidence from just the Willow Creek site. Using results from the OxCal models, we also calculated new values for the recurrence times of southern-strand earthquakes. Using the two closed intervals between the best-constrained earthquakes (N3–N1), the mean recurrence is 0.9 ± 0.2 kyr.

The cumulative paleoseismic data from all sites on the Nephi segment and from the southern part of the adjacent Provo segment suggest a complex pattern of Holocene surface ruptures. Details of the interaction between the two segments are unclear and require a longer and more complete paleoseismic record for both the northern and southern strands of the Nephi segment in order to make a more rigorous comparison with the history of earthquakes on the Provo segment. Improved knowledge of the behavior of this segment boundary will enhance our ability to generally recognize and understand the segmentation of major range-front normal faults.

ACKNOWLEDGMENTS

We thank Mr. William Tot, Spanish Fork District Ranger of the Uinta-Wasatch-Cache National Forest for the special use permit to excavate our Willow Creek trenches. We also thank Richard L. Dart and David J. Lidke (USGS, Denver) for their enthusiastic assistance and sustained efforts in the field. Also, Susan S. Olig (URS Corporation) provided valuable assistance and advice in interpreting and mapping the trench stratigraphy. Richard W. Briggs (USGS, Denver) developed the digital elevation model of the Willow Creek site shown on figure 5. We thank Ryan D. Gold and Alan R. Nelson (USGS, Denver), and William R. Lund, Steve D. Bowman, Michael D. Hylland, and Kimm Harty (UGS) for valuable, thorough reviews and comments that substantially improved the clarity and presentation of this paper. This work was supported by the U.S. Geological Survey's Earthquake Hazards Program.

REFERENCES

Armstrong, P.A., Ehlers, T.A., Chapman, D.S., Farley, K.A., and Kamp, P.J.J., 2003, Exhumation of the central Wasatch Mountains, Utah—1. Patterns and timing of exhumation deduced from low-temperature thermochronology data: Journal of Geophysical Research, v. 106, no. B3, p. 2172, doi: 10.1029/2001JB001708.

Biasi, G.P., and Weldon, R.J., 2009, San Andreas fault rupture scenarios from multiple paleoseismic records–stringing pearls: Bulletin of the Seismological Society of America, v. 99, no. 2A, p. 471–498.

Black, B.B., Hecker, S., Hylland, M.D., Christenson, G.E., and McDonald, G.N., 2003, Quaternary fault and fold database and map of Utah: Utah Geological Survey Map 193DM, scale 1:500,000, CD.

Bowman, S.D., and Lund, W.R., compilers, 2013, Compilation of U.S. Geological Survey National Earthquake Hazards Reduction Program final technical reports for Utah—Paleoseismology of Utah, Volume 23: Utah Geological Survey Miscellaneous Publication 13-3, 13 p.

Bucknam, R.C., 1978, Northwestern Utah seismotectonic studies, *in* Seiders, W., and Thompson, J., compilers, Summaries of Technical Reports, v. VII: Menlo Park, California, U.S. Geological Survey Office of Earthquake Studies, p. 64.

Bucknam, R.C., and Anderson, R.E., 1979, Estimation of fault-scarp ages from a scarp-height–slope-angle relationship: Geology, v. 7, p. 11–14.

Bruhn, R.L., DuRoss, C.B., Harris, R.A., and Lund, W.R., 2005, Neotectonics and paleoseismology of the Wasatch fault, Utah, *in* Pederson, J., and Dehler, C.M., editors, Interior Western United States: Geological Society of America Field Guide 6, p. 231–250, doi: 10.1130/2005.fld006(11).

Bronk Ramsey, C., 2001, Development of the radiocarbon calibration program: Radiocarbon, v. 43, no. 2A, p. 355–363.

Bronk Ramsey, C., 2008, Depositional models for chronological records: Quaternary Science Reviews, v. 27, p. 42–60.

Bronk Ramsey, C., 2010, OxCal 4.1 Manual: Online, http://c14.arch.ox.ac.uk/oxcalhelp/hlp_contents.html, accessed April 2013.

Chang, W.L., and Smith, R.B., 2002, Integrated seismic-hazard analysis of the Wasatch Front, Utah: Bulletin of the Seismological Society of America, v. 92, no. 5, p. 1904–1922.

Chang, W.L., Smith, R.B., Meertens, C.M., and Harris, R.A., 2006, Contemporary deformation of the Wasatch fault, Utah, from GPS measurements with implications for interseismic fault behavior and earthquake hazard—observations and kinematic analysis: Journal of Geophysical Research, v. 111, B11405, doi:10.1029/2006JB004326.

Crone, A.J., DeMartini, P.M., Machette, M.N., Okumura, K., and Prescott, J.R., 2003, Paleoseismicity of two historically quiescent faults in Australia—Implications for fault behavior in stable continental regions: Bulletin of the Seismological Society of America, v. 93, no. 5, p. 1913–1934.

Crone, A.J., and Haller, K.M., 1991, Segmentation and coseismic behavior of Basin and Range normal faults—examples from east-central Idaho and southwestern

Montana: Journal of Structural Geology, v. 13, no. 2, p. 151–164.

Crone, A.J., Machette, M.N., Bradley, L.A., and Mahan, S.A., 1996, Late Quaternary surface faulting on the Cheraw fault, southeastern Colorado: U.S. Geological Survey Geologic Investigations Map I-2591.

Currey, D.R., 1982, Lake Bonneville—selected features of relevance to neotectonic analysis: U.S. Geological Survey Open-File Report 82-1070, 30 p., 1 plate.

Dawson, T.E., McGill, S.F., and Rockwell, T.K., 2003, Irregular recurrence of paleoearthquakes along the central Garlock fault near El Paso Peaks, California: Journal of Geophysical Research, v. 108, no. B7, p. 2356, doi:10.1029/2001JB001744.

Dolan, J.F., Bowman, D.D., and Sammis, C.G., 2007, Long-range and long-term fault interactions in southern California: Geology, v. 35, p. 855–858, doi: 10.1130/G23789A.1.

Doser, D.I., 1985, Source parameters and faulting processes of the 1959 Hebgen Lake, Montana, earthquake sequence: Journal of Geophysical Research, v. 90, no. B6, p. 4537–4555.

Duller, G.A.T., 2004, Luminescence dating of Quaternary sediments—recent advances: Journal of Quaternary Science, v. 19, no. 2, p. 183–192, doi: 10.1002/jqs.809.

DuRoss, C.B., 2008, Holocene vertical displacement on the central segments of the Wasatch fault zone, Utah: Bulletin of the Seismological Society of America, v. 98, no. 6, p. 2918–2933.

DuRoss, C.B., and Bruhn, R.L., 2004, Active tectonics of the Nephi segment, Wasatch fault zone, Utah, *in* Lund, W.R., editor, Western States Seismic Policy Council Proceedings, Volume of the Basin and Range Province Seismic Hazards Summit II: Utah Geological Survey Miscellaneous Publication 05-2, p. 1–25.

DuRoss, C., McDonald, G., and Lund, W., 2006, Holocene paleoseismic activity on the Nephi segment of the Wasatch fault zone, Utah: Seismological Research Letters, v. 77, no. 2, p. 273.

DuRoss, C.B., McDonald, G.N., and Lund, W.R., 2008, Paleoseismic investigation of the northern strand of the Nephi segment of the Wasatch fault zone, Santaquin, Utah—Paleoseismology of Utah, Volume 17: Utah Geological Survey Special Study 124, 33 p., 1 plate.

DuRoss, C.B., Personius, S.F., Crone, A.J., Olig, S.S., and Lund, W.R., 2011, Determining segment earthquake times from site paleoseismic data—an approach to integrating paleoseismic data applied to the Weber segment of the Wasatch fault zone, Utah: Bulletin of the Seismological Society of America, v. 101, no. 6, p. 2765–2781, doi: 10.1785/0120110102.

Felger, T.J., Machette, M.N., and Sorensen, M.L., 2004, Provisional geologic map of the Mona quadrangle, Juab and Utah Counties, Utah: Utah Geological Survey Open-File Report 428, 1 plate, scale 1:24,000.

Friedrich, A.M., Wernicke, B.P., Niemi, N.A., Bennett, R.A., and Davis, J.L., 2003, Comparison of geodetic and geologic data from the Wasatch region, Utah, and implications for the spectral character of Earth deformation at periods of 10 to 10 million years: Journal of Geophysical Research, v. 108, no, B4, p. 2199, doi:10.1029/2001JB000682.

Ganev, P.N., Dolan, J.F., Blisniuk, K., Oskin M., and Owen, L.A., 2010, Paleoseismologic evidence for multiple Holocene earthquakes on the Calico fault—implications for earthquake clustering in the eastern California shear zone: Lithosphere, v. 2, no. 4, p. 287–298, doi:10.1130/L82.1.

Gilbert, G.K., 1928, Studies of Basin-Range structure: U.S. Geological Survey Professional Paper 153, 92 p.

Godsey, H.S., Currey, D.R., and Chan, M.A., 2005, New evidence for an extended occupation of the Provo shoreline and implications for regional climate change, Pleistocene Lake Bonneville, Utah, USA: Quaternary Research, v. 63, p. 212–223, doi:10.1016/j.yqres.2005.01.002.

Grant, L.B., and Sieh, K., 1994, Paleoseismic evidence of clustered earthquakes on the San Andreas fault in the Carrizo Plain, California: Journal of Geophysical Research, v. 99, no. B4, p. 6819–6841.

Hanson, K.L., Swan, F.H., III, and Schwartz, D.P., 1981, Study of earthquake recurrence intervals on the Wasatch fault, Utah, Sixth semi-annual technical report, July 1981: San Francisco, Woodward-Clyde Consultants, report for the U.S. Geological Survey, Contract No. 14-08-0001-16827, 22 p. (Available *in* Bowman, S.D., and Lund, W.R., compilers, 2013, Compilation of U.S. Geological Survey National Earthquake Hazards Reduction Program Final Technical Reports for Utah: Utah Geological Survey Miscellaneous Publication 13-3, DVD.)

Hanson, K.L., Swan, F.H., III, and Schwartz, D.P., 1982, Study of earthquake recurrence intervals on the Wasatch fault, Utah, Seventh semi-annual technical report, May 12, 1982: San Francisco, Woodward-Clyde Consultants, report for the U.S. Geological Survey, Contract No. 14-08-0001-19842, 26 p. (Available *in* Bowman, S.D., and Lund, W.R., compilers, 2013, Compilation of U.S. Geological Survey National Earthquake Hazards Reduction Program Final Technical Reports for Utah: Utah Geological Survey Miscellaneous Publication 13-3, DVD.)

Harty, K.M., Mulvey, W.E., and Machette, M.N., 1997, Surficial geologic map of the Nephi segment of the Wasatch fault zone, eastern Juab County, Utah: Utah Geological Survey Map 170, 14 p., 1 pl., scale 1:50,000.

Hetzel, R., and Hampel, A., 2005, Slip rate variations on normal faults during glacial-interglacial changes in surface loads: Nature, v. 435, p. 81–84.

Horns, D.M., Rey, K.A., Barnes, C.S., McShinsky, R.D., and Palmer, M., 2009, New constraints on the timing of prehistoric earthquakes on the northernmost part of the Nephi segment of the Wasatch fault, Utah: Geological Society of America Abstracts with Program, v. 41, no. 6, p. 42.

Hylland, M.D., and Machette, M.N., 2008, Surficial geologic map of the Levan and Fayette segments of the Wasatch fault zone, Juab and Sanpete Counties, Utah: Utah Geological Survey Map 229, scale 1:50,000, 37 p. pamphlet.

Jackson, M.E., 1991, The number and timing of Holocene paleoseismic events on the Nephi and Levan segments, Wasatch fault zone, Utah—Paleoseismology of Utah, Volume 3: Utah Geological Survey Special Study 78, 23 p.

Karow, T., and Hampel, A., 2010, Slip rate variations on faults in the Basin-and-Range Province caused by regression of late Pleistocene Lake Bonneville and Lake Lahontan: International Journal of Earth Science, v. 99, p. 1941–1953, doi: 10.1007/s00531-009-0496-3.

Lienkaemper, J.J., and Bronk Ramsey, C., 2009, OxCal—versatile tool for developing paleoearthquake chronologies—a primer: Seismological Research Letters, v. 80, no. 3, p. 431–434.

Lund, W.R., 2005, Consensus preferred recurrence-interval and vertical slip-rate estimates—Review of Utah paleoseismic–trenching data by the Utah Quaternary Fault Parameters Working Group: Utah Geological Survey Bulletin 134, 109 p.

Machette, M.N., 1984, Preliminary investigation of late Quaternary slip rates along the southern part of the Wasatch fault zone, central Utah, *in* Hays, W.W., and Gori, P.L., editors, Proceedings of Conference XXVI—a workshop on Evaluation of Regional and Urban Earthquake Hazards and Risk in Utah: U.S. Geological Survey Open-File Report 84-763, p. 391–406.

Machette, M.N., 1992, Surficial geologic map of the Wasatch fault zone, eastern part of Utah Valley, Utah County and parts of Salt Lake and Juab Counties, Utah: U.S. Geological Survey Miscellaneous Investigations Map I–2095, scale 1:50,000.

Machette, M.N., Crone, A.J., Personius, S.F., Mahan, S.A., Dart, R.L., Lidke, D.J., and Olig, S.S., 2007, Paleoseismology of the Nephi segment of the Wasatch fault zone, Juab County, Utah—preliminary results from two large exploratory trenches at Willow Creek: U.S. Geological Survey Scientific Investigations Map SIM–2966, 2 oversize sheets.

Machette, M.N., Personius, S.F., and Nelson, A.R., 1992, Paleoseismology of the Wasatch fault zone—a summary of recent investigations, conclusions, and interpretations, *in* Gori, P.A., and Hays, W.W., editors, Assessing regional earthquake hazards and risk along the Wasatch Front, Utah: U.S. Geological Survey Professional Paper 1500, Chapter A, p. A1–A72.

Marco, S., Stein, M., Agnon, A., and Ron, H., 1996, Long-term earthquake clustering—a 50,000-year paleoseismic record in the Dead Sea graben: Journal of Geophysical Research, v. 101, no. B3, p. 6179–6191.

Mattson, A., and Bruhn, R.L., 2001, Fault slip rates and initiation age based on diffusion equation modeling—Wasatch fault zone and eastern Great Basin: Journal of Geophysical Research, v. 106, no. B7, p. 13,739–13,750.

Mayo, A.L., Bruthans, J., Tingey, D., Kadlec, J., and Nelson, S., 2009, Insights into Wasatch fault vertical slip rates using the age of sediments in Timpanogos Cave, Utah: Quaternary Research, v. 72, p, 275–283, doi: 10.1016/j.yqres.2009.04.006.

McCalpin, J.P., 2009, Paleoseismology (2nd edition): Amsterdam, Elsevier Publishing, 613 p.

McCalpin, J.P., and Nishenko, S.P., 1996, Holocene paleoseismicity, temporal clustering, and probabilities of future large (M > 7) earthquakes on the Wasatch fault zone, Utah: Journal of Geophysical Research, v. 101, no. B3, p. 6233–6253.

Miller, D.M., Oviatt, C.G., and McGeehin, J.P., 2013, Stratigraphy and chronology of Provo shoreline deposits and lake-level implications, Late Pleistocene Lake Bonneville, eastern Great Basin, USA: Boreas, v. 42, no. 2, p. 342–361 (published online: 25 Oct 2012, doi: 10.1111/j.1502-3885.2012.00297.x)

Mouslopoulou, V., Walsh, J.J., and Nicol, A., 2008, Fault displacement rates on a range of timescales: Earth and Planetary Science Letters, v. 278, p. 186–197, doi: 10.1016/j.espl.2008.11.031.

Nelson, A.R., 1992, Lithofacies analysis of colluvial sediments—an aid in interpreting the recent history of Quaternary normal faults in the Basin and Range Province, western United States: Journal of Sedimentary Petrology, v. 62, no. 4, p. 607–621.

Nicol, A., Walsh, J., Berryman, K., and Villamor, P., 2006, Interdependence of fault displacement rates and paleoearthquakes in an active rift: Geology, v. 34, no. 10, p. 865–868, doi: 10.1130/G22335.1.

Nicol, A., Walsh, J.J., Manzocchi, T., and Morewood, N., 2005, Displacement rates and average earthquake recurrence intervals on normal faults: Journal of Structural Geology, v. 27, p. 541–551, doi:10.1016/j.jsg.2004.10.009.

Oglesby, D.D., 2005, The dynamics of strike-slip step-overs with linking dip-slip faults: Bulletin of the Seismologi-

cal Society of America, v. 95, no. 5, p. 1604–1622, doi: 10.1785/0120050058.

Olig, S.S., 2011, Extending the paleoseismic record of the Provo segment of the Wasatch fault zone, Utah: U.S. Geological Survey, National Earthquake Hazards Reduction Program Final Technical Report, award no. 02HQGR0109, 100 p., 19 plates, online, http://earthquake.usgs.gov/research/external/reports/02HQGR0109.pdf.

Ostenaa, D., 1984, Relationships affecting estimates of surface fault displacements based on scarp-derived colluvial deposits: Geological Society of America Abstracts with Programs, v. 16, no. 5, p. 327.

Oviatt, C.G., 1997, Lake Bonneville fluctuations and global climate change: Geology, v. 25, no. 2, p. 155–158.

Peacock, D.S.P., and Sanderson, D.J., 1991, Displacements, segment linkage, and relay ramps in normal fault systems: Journal of Structural Geology, v. 13, no. 6, p. 721–733.

Personius, S.F., DuRoss, C.B., and Crone, A.J., 2012, Holocene behavior of the Brigham City segment—implications for forecasting the next large-magnitude earthquake on the Wasatch fault zone, Utah, USA: Bulletin of the Seismological Society of America, v. 102, no. 6, p. 2265–2281, doi: 10.1785/0120110214.

Puseman, K., and Cummings, L.S., 2005, Separation and identification of charcoal and organics from bulk sediment samples for improved radiocarbon dating and stratigraphic correlations, *in* Lund, W.R., editor, Proceedings volume—Basin and Range Province Seismic Hazards Summit II: Utah Geological Survey Miscellaneous Publication 05-2, p. 32.

Reimer, P.J., Baillie, M.G.L., Bard, E., Bayliss, A., Beck, J.W., Blackwell, P.G., Bronk Ramsey, C., Buck, C.E., Burr, G.S., Edwards, R.L., Friedrich, M., Grootes, P.M., Guilderson, T.P., Hajdas, I., Heaton, T.J., Hogg, A.G., Hughen, K.A., Kaiser, K.F., Kromer, B., McCormac, F.G., Manning, S.W., Reimer, R.W., Richards, D.A., Southon, J.R., Talamo, S., Turney, C.S.M., van der Plicht, J., and Weyhenmeyer, C.E., 2009, IntCal09 and Marine09 radiocarbon age calibration curves, 0–50,000 years cal BP: Radiocarbon, v. 51, no. 4, p. 1111–1150.

Rockwell, T.K., Lindvall, S., Herzberg, M., Murbach, D., Dawson, T., and Berger, G., 2000, Paleoseismology of the Johnson Valley, Kickapoo, and Homestead Valley faults—clustering of earthquakes in the eastern California shear zone: Bulletin of the Seismological Society of America, v. 90, no. 5, p. 1200–1236.

Schwartz, D.P., and Coppersmith, K.J., 1984, Fault behavior and characteristic earthquakes—examples from the Wasatch and San Andreas fault zones: Journal of Geophysical Research, v. 89, no. B7, p. 5681–5698.

Schwartz, D.P., Hanson, K.L., and Swan, F.H., III, 1983, Paleoseismic investigations along the Wasatch fault zone—an update, *in* Gurgel, K.D., editor, Geologic excursions in neotectonics and engineering geology in Utah: Utah Geological and Mineral Survey Special Study 62, p. 45–48.

Segall P., and Pollard, D.D., 1980, Mechanics of discontinuous faults: Journal of Geophysical Research, v. 85, no. B8, p. 4337–4350.

Smith, R.B., and Bruhn, R.L., 1984, Intraplate extensional tectonics of the eastern Basin-Range—inferences on structural style from seismic reflection data, regional tectonics, and thermal-mechanical models of brittle-ductile deformation: Journal of Geophysical Research, v. 89, no. B7, p. 5733–5762.

Soliva, R., Benedicto, A., Schultz, R.A., Maerten, L., and Micarelli, L., 2008, Displacement and interaction of normal fault segments branched at depth—implications for fault growth and potential earthquake rupture size: Journal of Structural Geology, v. 30, p. 1288–1299, doi: 10.1016/j.jsg.2008.07.005.

Solomon, B.J., 2010a, Interim geologic map of unconsolidated deposits in the Santaquin quadrangle, Utah and Juab Counties, Utah: Utah Geological Survey Open-File Report 570, scale 1:24,000, 29 p. pamphlet.

Solomon, B.J., 2010b, Interim geologic map of unconsolidated deposits in the Payson Lakes quadrangle, Utah County, Utah: Utah Geological Survey Open-File Report 571, scale 1:24,000, 29 p. pamphlet.

Sorensen, M.L., Korzeb, S.L., and Nubert, J.T., 1983, Mineral resource potential map of the Birdseye, Nephi, and Santaquin roadless areas, Juab and Utah Counties, Utah: U.S. Geological Survey Miscellaneous Field Studies Map MF-1574, scale 1:62,500.

Swan, F.H., 1988, Temporal clustering of paleoseismic events on the Oued Fodda fault, Algeria: Geology, v. 16, no 12, p. 1092–1095.

Wallace, R.E., 1987, Grouping and migration of surface faulting and variations in slip rates on faults in the Great Basin Province: Bulletin of the Seismological Society of America, v. 77, no. 3, p. 868–876.

Weldon, R., Scharer, K., Fumal, T., and Biasi, G., 2004, Wrightwood and the earthquake cycle—what a long recurrence record tells us about how faults work: GSA Today, v. 14, no. 9, doi: 10.1130/1052-5173(2004)014<4:WATECW>2.0.CO;2.

Wells, D.L., and Coppersmith, K.J., 1994, New empirical relationships among magnitude, rupture length, rupture width, rupture area, and surface displacement: Bulletin of the Seismological Society of America, v. 84, no. 4, p. 974–1002.

Wesnousky, S.G., 2006, Predicting the endpoints of earthquake ruptures: Nature, v. 444, p. 358–360, doi: 10.1038/nature05275.

Wesnousky, S.G., 2008, Displacement and geometrical characteristics of earthquake surface ruptures—issues and implications for seismic-hazard analysis and the process of earthquake rupture: Bulletin of the Seismological Society of America, v. 98, no. 4, p. 1609–1632, doi: 10.17580/0120070111.

Wheeler, R.L., and Krystinik, K.B., 1988, Segmentation of the Wasatch fault zone, Utah—summaries, analyses, and interpretations of geological and geophysical data: U.S. Geological Survey Bulletin 1827, 47 p.

Witkind, I.J., 1964, Reactivated faults north of Hebgen Lake: U.S. Geological Survey Professional Paper 435-G, p. 37–50.

Wong, I., Lund, W., DuRoss, C., Arabasz, W., Pechmann, J., Crone, A., Luco, N., Personius, S., Petersen, M., Olig. S., and Schwartz, D., 2011, The Working Group on Utah Earthquake Probabilities (WGUEP)—background and goals [abs.]: Seismological Research Letters, v. 82, no. 2, p. 345.

Zoback, M.L., 1992, Superimposed late Cenozoic, Mesozoic, and possible Proterozoic deformation along the Wasatch fault zone in central Utah, *in* Gori, P.A., and Hays, W.W., editors, Assessing regional earthquake hazards and risk along the Wasatch Front, Utah: U.S. Geological Survey Professional Paper 1500, Chapter E, p. E1–E20.

APPENDICES

APPENDIX A

PALEO RESEARCH INSTITUTE TECHNICAL REPORT 05-41

Examination of Bulk Soil for Radiocarbon Datable Material from the Willow Creek Trenches, Wasatch Fault, Utah

by Kathryn Puseman

Paleo Research Institute
Golden, Colorado

Paleo Research Institute Technical Report 05-41
Prepared For
U.S. Geological Survey Geologic Hazards Team Denver, Colorado
July 2005

INTRODUCTION

A total of six bulk soil samples from stratigraphic horizons in trenches excavated across the Nephi segment of the Wasatch fault, Utah, were floated to recover organic fragments suitable for radiocarbon analysis. These samples were recovered from two trenches: Willow Creek North (WCN) and Willow Creek South (WCS). Botanic components and detrital charcoal were identified, and potentially radiocarbon datable material was separated. After initial examination of the samples was complete, charred material was selected and submitted for AMS radiocarbon dating to the Graphite Laboratory at Lawrence Livermore National Laboratory, Livermore, California.

METHODS

The bulk samples were floated using a modification of the procedures outlined by Matthews (1979). Each sample was added to approximately 3 gallons of water. The sample was stirred until a strong vortex formed, which was allowed to slow before pouring the light fraction through a 150 micron mesh sieve. Additional water was added and the process repeated until all visible macrofloral material was removed from the sample (a minimum of five times). The material that remained in the bottom (heavy fraction) was poured through a 0.5-mm mesh screen. The floated portions were allowed to dry.

The light fractions were weighed, then passed through a series of graduated screens (US Standard Sieves with 4-mm, 2-mm, 1-mm, 0.5-mm and 0.25-mm openings to separate charcoal debris and to initially sort the remains. The contents of each screen were then examined. Charcoal pieces larger than 1 mm in diameter were broken to expose a fresh cross section and examined under a binocular microscope at a magnification of 70x. The remaining light fraction in the 4-mm, 2-mm, 1-mm, 0.5-mm, and 0.25-mm sieves was scanned under a binocular stereo microscope at a magnification of 10x, with some identifications requiring magnifications of up to 70x. The material that passed through the 0.25-mm screen was not examined. The coarse or heavy fractions also were screened and examined for the presence of botanic remains. Remains from both the light and heavy fractions were recorded as charred and/or uncharred, whole pieces and/or fragments. Individual detrital charcoal/wood samples also were broken to expose a fresh cross-section and examined under a binocular microscope at a magnification of 70x.

Macrofloral remains, including charcoal, were identified using manuals (Martin and Barkley 1961; Core, et al. 1976; Panshin and Zeeuw 1980; Petrides and Petrides 1992) and by comparison with modern and archaeological references. The term "seed" is used to represent seeds, achenes, caryopses, and other disseminules. Because charcoal and possibly other botanic remains were to be sent for radiocarbon dating, clean laboratory conditions were used during flotation and identification to avoid contamination. All instruments were washed between samples, and samples were protected from contact with modern charcoal.

DISCUSSION

The Willow Creek trench site is located at an elevation of about 5700 feet at the foot of the Wasatch Mountains. Local vegetation consists of sagebrush (*Artemisia*), maple (Acer), and Gambel's oak (*Quercus gambellil*), while willows (*Salix*) grow adjacent to drainage channels. Higher elevations in the drainage basin support spruce (*Picea*) and pines (*Pinus*).

Four samples were examined from the Willow Creek South trench (Table A1–1). Sample WSC-R1 from Unit 2 contained several small fragments of charred undiagnostic central pith from small, woody twigs (Table A1–2, Table A1–3). These charcoal fragments weighed 0.006 g and were submitted for AMS radiocarbon analysis. The sample also contained a few uncharred rootlets from modern plants, two insect chitin fragments, and six snail shells, as well as a small amount of rock/gravel.

Numerous small fragments of charred central pith weighing 0.011 g also were present in sample WCS-R2 from Unit 3-1 A. These charred fragments were sent for AMS radiocarbon analysis. In addition, the sample contained a few uncharred rootlets from modern plants, an insect chitin fragment, a few rodent fecal pellets, a few snail shells, and a small amount of rock/gravel.

Sample WCS-R4 from Unit 3-14 yielded fragments of *Quercus* charcoal weighing 0.064 g that were submitted for AMS radiocarbon dating. A few uncharred rootlets from modern plants and a small amount of rock/gravel also were present.

Sample WCS-R6 contained two pieces of Acer charcoal weighing 0.007 g that were submitted for AMS radiocarbon analysis. Two small fragments of Asteraceae charcoal weighing 0.002 g, a piece of conifer charcoal weighing less than 0.001 g, and charred undiagnostic central pith weighing 0.004 g also were present. In addition, the sample contained an uncharred Asteraceae seed, a moderate amount of uncharred rootlets from modern plants, a piece of dried sap/resin, several insect chitin fragments, numerous snail shells, a few worm casts, an abundance of rock/gravel, and a few sclerotia. Sclerotia are commonly called "carbon balls." They are small, black, solid or hollow spheres that can be smooth or lightly sculpted. These forms range from 0.5 to 4 mm in size. Sclerotia are the resting structures of mycorrhizae fungi, such as *Cenococcum graniforme*, that have a mutualistic relationship with tree roots. Many trees are noted to depend heavily on mycorrhizae and may not be successful

without them. "The mycelial strands of these fungi grow into the roots and take some of the sugary compounds produced by the tree during photosynthesis. However, mycorrhizal fungi benefit the tree because they take in minerals from the soil, which are then used by the tree" (Kricher and Morrison 1988:285). Sclerotia appear to be ubiquitous and are found with coniferous and deciduous trees including *Abies* (fir), *Juniperus communis* (common juniper), *Larix* (larch), *Picea* (spruce), *Pinus* (pine), *Pseudotsuga* (Douglas fir), *Acer pseudoplatanus* (sycamore maple), *Alnus* (alder), *Betula* (birch), *Carpinus caro Jiniana* (American hornbeam), *Carya* (hickory), *Castanea dentata* (American chestnut), *Corylus* (hazelnut), *Crataegus monogyna* (hawthorn), *Fagus* (beech), *Populus* (poplar, cottonwood, aspen), *Quercus* (oak), *Rhamnus fragula* (alder bush), *Salix* (willow), *Sorbus* (chokecherry), and *Tilia* (linden). These forms originally were identified by Dr. Kristiina Vogt, Professor of Ecology in the School of Forestry and Environmental Studies at Yale University (Trappe 1962; McWeeney 1989:229-230).

Samples WCN-R3 and WCN-R6 were recovered from the Willow Creek North trench. Sample WCN-R3 from Unit C2 contained two fragments of Asteraceae charcoal weighing 0.003 g that were submitted for AMS radiocarbon analysis. These charcoal fragments might represent sagebrush, although the fragments were too small for a positive identification. Two charred fragments of undiagnostic central pith weighing less than 0.001 g also were present. In addition, the sample contained a moderate amount of uncharred rootlets from modern plants, eight insect chitin fragments, and a moderate amount of rock/gravel.

Small fragments of undiagnostic central pith also were present in sample WCN-R6 from Unit 3-1. These pith fragments weighed less than 0.001 g; therefore, they were not sent for AMS dating. A few uncharred rootlets from modern plants, five insect chitin fragments, and a moderate amount of rock/gravel were the only other remains to be recovered.

SUMMARY AND CONCLUSIONS

Flotation of bulk samples from the Willow Creek trenches excavated across the Nephi segment of the Wasatch fault, Utah, resulted in recovery of charcoal that was submitted for AMS radiocarbon analysis. Several samples contained fragments of charred central pith from small, woody twigs. The central pith consists of parenchyma, which does not contain diagnostic elements. These fragments of charred central pith were sent for dating from samples WCS-R1 and WCS-R2. Oak charcoal in sample WCS-R4, maple charcoal from sample WCS-R6, and charcoal from a woody member of the sunflower family, possibly sagebrush, in sample WCN¬R3 also were submitted for AMS radiocarbon analysis. Recovery of insect chitin fragments, rodent fecal pellets, and worm casts reflects limited subsurface disturbance from insect, rodent, and earthworm activity.

Table A1–1. Provenience data for samples from the Willow Creek trenches, Nephi segment, Wasatch fault.

Sample No.	Trench Unit	Provenience/ Description	Analysis
WCS-R1	2	Bulk soil from Willow Creek South Trench	FloaUCharcoal 10 prior to C-14 analysis
WCS-R2	3-1A	Bulk soil from Willow Creek South Trench	FloaUCharcoal 10 prior to C-14 analysis
WCS-R06	2 (?)	Bulk soil from Willow Creek South Trench	FloaUCharcoal 10 prior to C-14 analysis
WCS-R4	3-14 (fan)	Bulk soil from Willow Creek South Trench	FloaUCharcoal 10 prior to C-14 analysis
WCN-R3	C2	Bulk soil from Willow Creek North Trench	FloaUCharcoal 10 prior to C-14 analysis
WCN-R6	3-1 (Deb. Fl)	Bulk soil from Willow Creek North Trench	FloaUCharcoallD prior to C-14 analysis

Table A1–2. Macrofloral remains from the Willow Creek trenches, Nephi segment, Wasatch fault.

Sample No.	Identification	Part	Charred		Uncharred		Weights/ Comments
			W	F	W	F	
WCS-R1	Liters Floated						0.15 L
Unit 2	Light Fraction Weight						1.17 g
	FLORAL REMAINS:						
	Rootlets					X	Few
	CHARCOAL/WOOD:						
	Undiagnostic central pith from woody twigs**	Charcoal		24			0.006 g
	NON-FLORAL REMAINS:						
	Insect Rock/Gravel Snail shell					2 X 6	Few
WCS-R2	Liters Floated						0.15 L
Unit 3-1A	Light Fraction Weight						9.27 g
	FLORAL REMAINS:						
	Rootlets					X	Few
	CHARCOAL/WOOD:						
	Undiagnostic central pith from woody twigs**	Charcoal		70			0.011 g
	NON-FLORAL REMAINS:						
	Insect Rock/Gravel Rodent fecal pellet Snail shell	Chitin			 X 2	1 X 1	Few
WCS-R6	Liters Floated						2.10 L
Unit 2 (?)	Light Fraction Weight						5.77 g
	FLORAL REMAINS:						
	Asteraceae Rootlets Sap/Resin Sclerotia	Seed		 X	1	 X 1 	 Moderate Few

W = Whole
F = Fragment
X = Presence noted in sample
g = grams
L = Liters

Table A1–2. (Continued)

Sample No.	Identification	Part	Charred		Uncharred		Weights/ Comments
			W	F	W	F	
WCS-R6	CHARCOAL/WOOD:						
Unit 2 (?)	*Acer"**	Charcoal		2			0.007 g
	Asteraceae	Charcoal		4			0.002 g
	Conifer	Charcoal		1			<0.001 g
	Undiagnostic central pith from woody twigs	Charcoal		20			0.003 g
	Unidentified ≥ 1 mm	Charcoal		X			0.004 g
	NON-FLORAL REMAINS:						
	Insect ≥ 0.5 mm	Chitin				22	
	Rock/Gravel					X	Numerous
	Snail shell ≥ 0.5 mm				271	24	
	Snail shell < 0.5 mm					X	Few
	Worm casts				X	X	Few
WCS-R4	Liters Floated						<0.10 L
Unit 3-14 (fan)	Light Fraction Weight						0.52g
	FLORAL REMAINS:						
	Rootlets					X	Few
	CHARCOAL/WOOD:						
	*Quercus***	Charcoal		10			0.064 g
	NON-FLORAL REMAINS:						
	Rock/Gravel					X	Few
WCN-R3	Liters Floated						1.00 L
Unit C2	Light Fraction Weight						3.32g
	FLORAL REMAINS:						
	Rootlets					X	Moderate
	CHARCOAL/WOOD:						
	Asteraceae**	Charcoal		2			0.003 9
	Undiagnostic central pith from woody twigs	Charcoal		2			<0.001 9
	NON-FLORAL REMAINS:						
	Insect	Chitin				8	
	Rock/Gravel					X	Moderate

W = Whole
F = Fragment
X = Presence noted in sample
g = grams
L = Liters

TABLE A1–2 (Continued)

Sample No.	Identification	Part	Charred		Uncharred		Weights/ Comments
			W	F	W	F	
WCN-R6	Liters Floated						0.60 L
Unit 3-1 (Deb. Fl)	Light Fraction Weight						1.08 g
	FLORAL REMAINS:						
	Rootlets					X	Few
	CHARCOAL/WOOD:						
	Undiagnostic central pith from woody twigs	Charcoal		2			<0.001 g
	NON-FLORAL REMAINS:						
	Insect Rock/Gravel	Chitin				5 X	 Moderate

W = Whole
F = Fragment
X = Presence noted in sample
g = grams
L = Liters

Table A1–3. Index of macrofloral remains recovered from Willow Creek trenches, Nephi segment, Wasatch fault.

Scientific Name	Common Name
FLORAL REMAINS:	
Asteraceae	Sunflower family
CHARCOAL/WOOD:	
Acer	Maple, Box elder
Asteraceae	Sunflower family
Conifer	Cone-bearing, gymnospermous trees and shrubs, mostly evergreens, including the pine, spruce, fir, juniper, cedar, yew, and cypress
Undiagnostic central pith from woody twigs	Central pith from small, woody twigs; consists of parenchyma with no diagnostic elements

REFERENCES CITED

Core, H. A., W. A. Cote and A. C. Day, 1976, *Wood Structure and Identification*. Syracuse University Press, Syracuse, New York.

Kricher, John C., and Gordon Morrison, 1988, *A Field Guide to Ecology of Eastern Forests*. Houghton Mifflin Company, Boston and New York.

Martin, Alexander C., and William D. Barkley, 1961, *Seed Identification Manual*. University of California, Berkeley, California.

Matthews, Meredith H., 1979, Soil Sample Analysis of 5MT2148: Dominguez Ruin, Dolores, Colorado. Appendix B. In *The Dominguez Ruin: A McElmo Phase Pueblo in Southwestern Colorado*, edited by A. D. Reed. Bureau of Land Management Cultural Resource Series. vol. 7. Bureau of Land Management, Denver, Colorado.

McWeeney, Lucinda, 1989, What Lies Lurking Below the Soil: Beyond the Archaeobotanical View of Flotation Samples. *North American Archaeologist* 10(3):227-230.

Panshin, A. J., and Carl de Zeeuw, 1980, *Textbook of Wood Technology*. McGraw-Hill Book, Co., New York, New York.

Petrides, George A., and Olivia Petrides, 1992, *A Field Guide to Western Trees*. The Peterson Field Guide Series. Houghton Mifflin Co., Boston.

Trappe, James M., 1962, Fungus Associates of Ectotrophic Mycorrhizae. In The Botanical Review. U.S. Department of Agriculture, Washington, D.C.

APPENDIX B

PALEOSEISMOLOGY OF THE NEPHI SEGMENT OF THE WASATCH FAULT ZONE, JUAB COUNTY, UTAH—PRELIMINARY RESULTS FROM TWO LARGE EXPLORATORY TRENCHES AT WILLOW CREEK

U.S. Geological Survey Scientific Investigations Map SIM-2966
2007

by M.N. Machette, A.J. Crone, S.F. Personius, S.A. Mahan, R.L. Dart, D.J. Lidke, and S.S Olig

OPEN PDF

APPENDIX C

CODE FOR OXCAL MODELS AT THE RED CANYON, WILLOW CREEK, AND NORTH CREEK SITES

Luminescence ages are referenced to 2010 when the OxCal models were constructed, and their ages are modeled by subtracting the luminescence age from 2010. For example, a luminescence age of 1720 ± 90 yr is included in the model as (290, 90), and a luminescence age of 3150 ± 210 yr is included as (-1140, 210).

The models include *C_Date* for luminescence ages, *R_Date* for radiocarbon ages, and Boundary for undated events (paleoearthquakes). *Delta_R* accounts for the bulk-soil residence time following DuRoss and others (2011). These components are arranged into ordered sequences based on the relative stratigraphic positions of the samples. The sequences may contain phases, or groups where the relative stratigraphic ordering information for the individual radiocarbon ages is unknown. The models are presented in reverse stratigraphic order, following the order in which the ages and events are evaluated in OxCal.

Red Canyon (see Jackson [1991] for map of trench and details of radiocarbon and luminescence ages).

```
Plot()
 {
  Sequence("Red Canyon model 9")
  {
   Boundary("Sequence start");
   Phase("Units 20-6sA")
   {
    C_Date("Latest Pleistocene fan", -9690, 100);
   };
   Zero_Boundary("Zero boundary 1");
   Boundary("Earthquake RC3");
   Delta_R("MRT correction Jackson1", 200, 200);
   R_Date("JR16/b25185", 3550, 150);
   Phase("Unit 4s")
   {
    Delta_R("MRT correction Jackson2", 100, 100);
    R_Date("JRC-17/b24186", 1380, 120);
    C_Date("TL date ITL 66+20yr", 290, 200);
   };
   Boundary("Earthquake RC2");
   Phase("Units 3/3s")
   {
    C_Date("TL date ITL 67+20 yr", 490, 400);
    C_Date("TL date ITL 88+20 yr", 690, 500);
   };
   Zero_Boundary("Zero boundary 2");
   Boundary("Earthquake RC1");
   Boundary("Sequence end historic constraint", 1847);
   C_Date("2010", 2010, 0);
  };
 };
```

Willow Creek (see Machette and others [2007] for map of trenches and details of radiocarbon and luminescence ages).

```
Plot()
 {
  Sequence("Willow Creek master9 (w/WC4)")
  {
   Boundary("Sequence start");
   R_Date("WCN-R1", 5420, 35);
   Date("Earthquake WC4");
   Phase("Holocene fan deposits")
   {
    R_Combine("WCS fan ages")
    {
     R_Date("WCS-R4", 2970, 35);
     R_Date("WCS-R5", 3000, 35);
    };
    C_Date("WCS-L2", -560, 170);
    C_Date("WCS-L4", -490, 190);
    C_Date("WCS-L1", -310, 170);
   };
   Boundary("Earthquake WC3");
   Zero_Boundary("Zero boundary 1");
   C_Date("WCN-L3", 770, 80);
   Boundary("Earthquake WC2");
   Phase("CW2")
   {
    R_Date("WCN-R3", 1280, 35);
    C_Date("WCN-L2", 970, 70);
    R_Date("WCN-R4", 730, 35);
   };
   Phase("Post CW2 sediment and soil")
   {
    R_Date("WCN-R7", 330, 30);
    R_Date("WCS-R3", 310, 45);
    R_Date("WCS-R2", 230, 35);
    R_Date("WCS-R7", 205, 35);
   };
   Boundary("Earthquake WC1");
   Phase("CW1")
   {
    R_Date("WCS-R1", 210, 35);
   };
   Boundary("Sequence end historic constraint", 1847);
  };
 };
```

North Creek (see Hanson and others [1981, 1982] for maps of trenches and details of radiocarbon ages).

```
Plot()
 {
  Sequence("North Creek ZB & boundaries2")
  {
   Boundary("Sequence start");
   Phase("No Ck alluvium")
   {
    R_Combine("WC-12-80-11 combined")
    {
     R_Date("WC-12-80-11 Bucknam char", 4850, 250);
     R_Date("WC-12-80-11 AMS char", 4000, 400);
    };
    Delta_R("MRT correction1", 200, 200);
    R_Date("WC-12-80-3 AMS soil AMRT", 4500, 300);
    R_Date("WC-12-80-3 soil AMRT", 2180, 80);
   };
   Boundary("Earthquake NC3");
   Zero_Boundary("Zero boundary 1");
   Boundary("Earthquake NC2");
   Delta_R("MRT correction2", 200, 200);
   R_Date("WC-12-80-7 AMS soil AMRT", 1700, 300);
   Delta_R("MRT correction3", 0, 0);
   R_Date("WC-12-80-9 AMS char", 1350, 250);
   Phase("Unit 3a")
   {
    R_Date("WC-12-80-8, AMS char", 1200, 300);
   };
   Phase("Unit 3as soil")
   {
    R_Combine("WC-12-80-5 combined")
    {
     R_Date("WC-12-80-5, char", 1350, 70);
     R_Date("WC-12-80-5 AMS char", 1550, 300);
    };
    R_Date("WC-12-80-6, char", 1100, 60);
   };
   Zero_Boundary("Zero boundary 2");
   Boundary("Earthquake NC1");
   R_Date("WC-12-80-10", 0, 300);
   Boundary("Sequence end historic constraint", 1847);
  };
 };
```